APPLICATIONS OF PRESTRESSED AFRP BARS IN CONCRETE RAILROAD TIES

A Thesis

by

RYAN D. POSLUSZNY

Submitted to the Office of Graduate and Professional Studies of
Texas A&M University
in partial fulfilment of the requirements for the degree of

MASTER OF SCIENCE

Committee Chair,	Stefan Hurlebaus
Committee Members,	John B. Mander
	Gary T. Fry
	Anastasia Muliana
Head of Department	Robin Autenrieth

December 2016

Major Subject: Civil Engineering

ABSTRACT

Since the 1970's, concrete railroad ties have become more and more prominent in the railroad industry. Their improved durability and increased safety over traditional timber ties has paved the way for new and more efficient concrete ties to be developed. Prestressing with steel strands was a key design aspect in providing the strength the ties needed to overcome the tonnage seen in heavy haul lines spread across the United States and the world. A major flaw seen with these concrete ties is deterioration due to environment or fatigue loading under the connected rail. This deterioration can lead to a change in gauge of the track structure which can then cause derailment of trains. A second issue found in concrete ties that was not found in timber is the electrical conductivity. Timber is a highly insulating material while concrete possesses insulating and conductive properties based on the amount of moisture present. This is an issue because track structures use the steel rails to carry electrical signals to detect the presence of a train within a signaled block. During construction, the steel strands may come into contact with the embedded steel shoulders on both sides of the tie, therefore creating a direct circuit that needs to be insulated from the steel rails.

Aramid fiber-reinforced polymer bars have shown promise, as an electrical non-conductive material, to fix the problem of false signaling due to electrical shorts. AFRP is a composite material made of Kevlar fibers bound in a polymer resin. This material has a tensile strength of approximately 200 ksi and has been investigated for use as a replacement for steel in such structures as concrete bridge girders and decks. The objective of this research is to design and test new concrete railroad ties utilizing AFRP as the prestressing material. Four of these ties were constructed and tested for strength following the guidelines provided by the American Railroad Engineering and Maintenance-of-way Association (AREMA). Bending tests at the rail seat section and center section of the tie were performed to prove strength adequacy, and electrical resistivity tests were performed to prove insulation from the current in the rails. The AFRP ties showed to have over twice the electrical resistance of their steel counterparts

with 2.42 MΩ of resistance compared to 1.11 MΩ. The strength comparison proved inconclusive, for although the ties did not fail, they did not meet AREMA cracking requirements for strength. A major factor that was seen was in the method of testing AREMA provides; through improved testing procedures, AFRP shows to be very promising as a full replacement of steel as prestressing reinforcement for concrete railroad ties.

DEDICATION

This thesis is dedicated to Steve and Jody Posluszny, my parents. Without your constant support and push, I never would have accomplished this tremendous goal. Thank you for all you love, trust, and support throughout my research project and my entire academic career.

ACKNOWLEDGEMENTS

I would like to thank Dr. Stefan Hurlebaus for his commitment to me and the completion of this project. Serving as my committee chair, he provided guidance and assistance in design, construction, and analysis for the project. I would also like to thank Dr. John Mander for both serving on my committee and greatly assisting me in designing the railroad ties, along with providing guidance and experience in construction of the ties as well. Finally, I wish to thank Dr. Gary Fry and Dr. Anastasia Muliana for serving on my committee and supporting my research.

I especially would like to acknowledge Dr. Kyle Wieghaus for his exceptional support; helping me obtain all of my materials, designing the prestressing bed, with all aspects of construction, and providing guidance when needed most. I also would like to express my thanks and gratitude to all other student workers employed by the Texas A&M Transportation Institute for their help in the final construction of the ties.

I wish to recognize the American Association of Railroads (AAR) for their support and funding of my research project and for securing a donation of eight railroad ties, and Pandrol for donating the fasteners necessary to construct the ties of my own.

TABLE OF CONTENTS

Page

LIST OF FIGURES

Page

LIST OF TABLES

Page

1. INTRODUCTION

1.1 Project Motivation

Concrete ties were first used on North American railroads in the 1890's by the Reading Company in Pennsylvania (Hanna 1979). The ties were standard reinforced concrete, which showed no major improvement to the traditional timber ties in use. With the development of prestressed concrete structures in the mid 1900's and increased cost of timber due to World War II, railroad companies began to research and experiment with prestressing steel in concrete railroad ties. It was not until the 1960's that prestressed concrete railroad ties began to be manufactured and installed in the United States with more than 900,000 continuous ties installed on the FEC Railway in 1966 (White 1984). However, with much higher capital required to build these ties, production has been slow.

The primary incentive for the use of concrete railroad ties over traditional timber ties comes from their extended design life; lasting 50 years compared to 20 for timber. Also with concrete ties being substantially heavier than timber, the track holds its alignment better and thus requires less maintenance. These advantages have led to a higher demand for concrete railroad ties, and the railroad industry has begun to demand more out of the tie's strength and durability to meet ever-growing transportation needs. With approximately 160,000 miles of heavy haul track hauling 1.7 trillion ton-miles annually, the United States has one of the most extensive system of railroads in the world (AAR 2013). These high loads cause significant stress on the rail ties which may lead to increased maintenance and higher cost. However, it is important to note that prestressed concrete railroad ties are far more advantageous compared to its timber counterpart in terms of strength and durability, yet there are issues that need to be investigated and improved if they are to reach full potential.

One such issue is the electrical conductivity of concrete rail ties and how it affects signaling. Standard track systems use a direct current (DC) circuit to signal the presence of a train within that circuit block which notifies, via signaling, other trains to

not enter that section of track. A power source sends current through the rail to a relay point which then sends the signal back to the power source along the opposite rail. When no train is present the relay is energized and displays a “clear” signal. As a train enters the circuit, the steel wheels and axle short circuit the current causing the relay to become de-energized which displays a “stop” signal. Figure 1 shows the track circuit with both energized, and de-energized relays. The problem occurs when the insulator pad isolating the steel shoulders from the rail fails allowing the current to enter the concrete and create a connection between the two rails. This connection creates a false short circuit causing the relay to de-energize. By having a relay de-energized, the track sees a major loss in capacity and must spend money to repair the problem tie once it is detected.

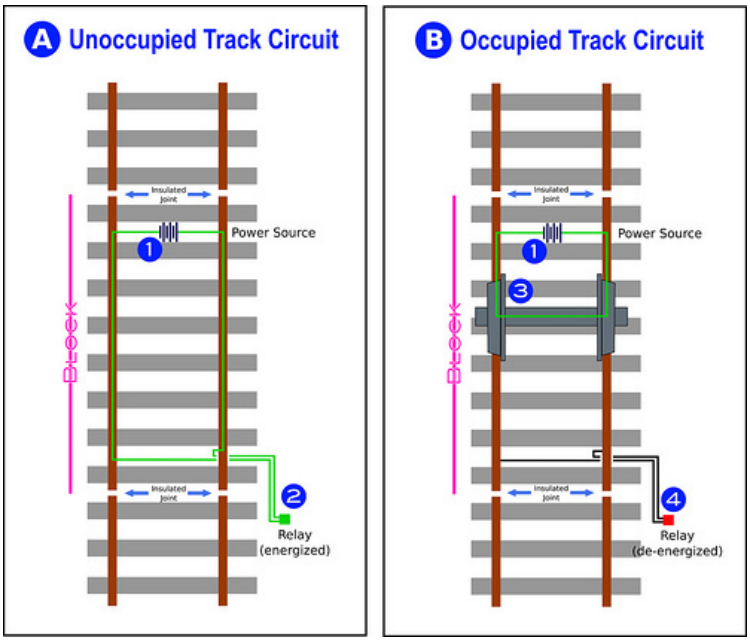

Figure 1: Track circuit system: (1) Power source, (2) Energized relay, (3) Wheel and axel of train, (4) De-energized relay (Johnson 2010)

Another issue is the corrosion and deterioration of concrete ties which has been shown to be a primary cause of failure. Corrosion of the prestressing steel may occur

when water seeps into cracks in the tie and oxidizes the metal within. Freeze-thaw cycles accelerate water penetration and corrosion as well. The American Railway Engineering and Maintenance-of-Way Association (AREMA) has stated that a tie has failed if cracked under service load conditions, and therefore requires maintenance. If left unchecked and unrepaired, train derailment may occur. Figure 2 shows a pair of concrete ties after derailment of the Metro-North train in New York City. The National Transportation Safety Board (NTSB) reported that the accident was caused by excessive track gauge resulting from tie deterioration. The tie deterioration was determined to have resulted from fouled ballast and cracks allowing water penetration and corrosion (NTSB 2014). Derailment may have been avoided if the track was more regularly inspected and the ties and fastenings had the required durability to reduce deterioration. Also note in Figure 2 the steel tie bar would automatically prohibit trains from running as the system would fail-safe to stop. Consequently manual, tablet, train operations would be needed which markedly reduces operational effectiveness.

Figure 2: Cracked concrete rail ties with gauge holding bar installed post-accident (NTSB)

One promising material is Aramid Fiber-Reinforced Polymer (AFRP), a composite tendon that exhibits non-corrosive and electrically non-conducting properties,

which has recently been investigated as a replacement for steel in prestressed concrete structures. These structures are mainly found in locations where corrosion and weather induced deterioration is of prime concern, i.e. bridge decks and girders, marine structures, etc. Similarly, concrete railroad ties supported on ground and constantly exposed to weather could benefit from this material. With the noncorrosive nature of AFRP, the ties could experience more cracks before deemed failed by AREMA and therefore support a larger train load and require less frequent maintenance. Also, the non-conducting property of AFRP eliminates the possibility of a false negative signal. If sufficient insulation is provided between the steel shoulders between both rails, it may be possible to build concrete ties without the need for the insulator pads decreasing the initial cost, but more importantly preventing sources of deterioration at the rail seat. There currently are three major types of Fiber-Reinforced Polymer bars that are used in concrete structures: Glass, Carbon, and Aramid. Aramid is the chosen FRP bar because Carbon does not exhibit the desired electrical insulation that Aramid does, and Glass has shown to creep more than Aramid in prestressed applications.

1.2 Project Objectives

The objectives of this research are to (1) develop a series of design layouts that meet ACI, AREMA, and physical requirements using prestressed AFRP bars in an existing concrete railroad tie, (2) construct new ties using the designed layouts, (3) test the structural performance of the ties in both the laboratory and in the field, and (4) examine the reduction of conductivity between the fastenings within the tie. Overall, the purpose of this research is to create a new concrete railroad tie that, if the insulator pads fail, will not lead to a short circuit of the track signaling system.

These objectives are expected to benefit the railroad industry through increased safety and reliability of the track over its life span. This is due to the enhancement in durability and serviceability expected from the use of AFRP. Along with increased safety, total cost of track is expected to decrease due to the decreased cost from maintenance and replacing ties with corroded steel prestressing strands. Finally, with the

conductivity reduced between the fastenings, it is expected that insulating pads can be removed thus decreasing initial costs and improving longevity of the ties as well.

1.3 Project Significance

Increased use of concrete railroad ties and the growing importance of the railroad transportation system has led to a need for better ties that last longer, require less maintenance, and are more durable. Due to the corrosive nature of steel prestressing tendons, cracking in the tie is of primary concern. AREMA (2014) states that once noticeable cracking occurs in a concrete tie, maintenance must be performed and replacement soon after. Replacing a single concrete tie is laborious and time intensive which greatly adds to the cost of the replacement. To add to the problem, steel is a strong conductor of electricity and with rails carrying a current used in the signaling system, the steel tendons can cause a short circuit of the system falsifying the signal. Therefore, designing a new tie using non-corrosive, electrically non-conducting material is pertinent if the concrete railroad tie is to continuously improve and be more widely used in North America.

While research has been conducted on improving the durability of concrete railroad ties, no entity has gone as far as to replace the prestressing steel with another material entirely. By having the steel completely replaced with AFRP tendons, the need to repair and replace the ties can reduce significantly. It allows for the tie to crack lightly while still maintaining strength and removes the concern of steel corrosion within the tie, and it does not conduct electricity which would insulate the tie and prevent inaccurate signals. A major concern in the use of AFRP is the pre-tensioning system that will be used. Proper anchorage is required due to a stress concentration that can occur at the anchor during prestressing which can cause premature failure in the tendon. Usage of a 1.9 in. diameter by 18 in. long hollow steel pipe filled with grout was found to be the most effective anchorage system for the prestressing operation (Medina 2012).

1.4 Research Approach

Laboratory experimentation is the primary approach that will be taken in conducting this research. After careful review of past and on-going experiments involving AFRP as a material and applied in concrete structures, study on the design and manufacture of concrete railroad ties takes place. A commonly used concrete railroad tie is selected as the original specimen to base the research off. LB Foster CXT's 505S-50 tie, Figure 3, was chosen due to its extensive use in long line heavy-haul track for Union Pacific Railroad. It was assumed this tie would undergo 75 MGT annual tonnage at a speed of 60 mph while spaced at 24 in. on center. That information along with charts and graphs provided by Chapter 30 of the AREMA manual are to be used in calculating the service moments on the tie which it will be designed for.

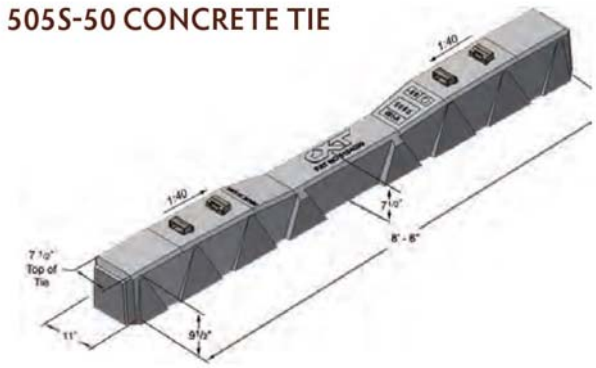

Figure 3: 3D model of concrete railroad tie

A series of designs were then created using traditional prestressed concrete design guides and calculations but instead of using steel, AFRP was the prestressed material. Transfer and service loading stresses were considered in the calculations on the number of strands, the location of the strands, and the prestressing load applied to the strands. The designs chosen for construction used the least amount of AFRP, are within allowable prestress range, and met all physical constraints needed for construction.

These designs are then tested in accordance with AREMA concrete railroad tie strength testing requirements. The ties will be deemed adequate if they meet said requirements and prove to be more electrically insulating than its steel counterpart.

1.5 Thesis Organization

This thesis contains eight main chapters including the introduction to the research, Chapter 1. Chapter 2 comprises of a look into the current knowledge on concrete railroad ties and applications of prestressed AFRP bars through a literature review. Chapter 3 covers the design process including the selection of the final layout of AFRP bars that will be used in construction. Chapter 4 describes the construction of the ties: fabricating the molds, stressing the AFRP, and pouring the concrete. Chapter 5 presents an overview of the experimental program involving the testing set up and instrumentation. Chapter 6 compares the experimentally tested ties reinforced with AFRP to the theoretical analysis based on the design parameters of Chapter 3 and as built conditions. Chapter 7 compares the experimental data from Chapter 6 to theoretical data of steel reinforced ties in a comprehensive AFRP to steel comparison. Finally, Chapter 8 summarizes the work done and draws conclusions from the experiments; along with a brief look into future research that can be done using the data presented in this thesis and recommendations on how to improve further testing.

2. LITERATURE REVIEW

2.1 Concrete Railroad Ties

Venuti (1980) detailed the history of concrete railroad ties; why they became used, how they were designed, fabricated, and installed, and how they're currently being used on modern railroads. He states that concrete railroad ties began becoming popular in the 1950's in post-World War II Europe due to the destruction of the railroads during the war and the rising cost of wood. America took notice and began developing its own set of codes and specifications in the late 1970's. These ties were designed to hold a wheel load of 40,000 lb which is then factored to account for the dynamics effects of the moving train. It was also discovered that pretensioning the ties with strands or wires improved their strength by setting an eccentricity off the centroid of the concrete balancing out positive bending moments at the rail seat and negative moments at the center of the tie. Fabrication of the ties was relatively efficient to begin with by being able to cast ties on a daily basis: approximately 2 hours for the initial set, 10 hours for curing via steam or hot oil, and 6 hours for demolding, cleaning, prestressing, and casting the next tie. Installing the ties was mostly a process of replacement of wood ties and track with the concrete ties and a welded rail track. Due to the success of the concrete ties, a set of specifications were developed by the American Railway Engineering Association (AREA), now known as American Railway Engineering and Maintenance Association (AREMA), and ACI Committee 545. These specifications contain limits on the positive and negative bending moments, load resistance of 3 million cycles of downward force, and bond development of the pretensioning tendons. With these specifications, a concrete tie design life is expected to be 50 years.

A concrete tie installed in a rail system typically has two major locations of concern within its geometry that affects its strength and durability. These locations are at the rail seat and the center of the tie as shown in Figure 4. AREMA states that the top and bottom of the tie must be tested for strength at both locations. These checks represent positive and negative bending moments within the tie. However, Zeman et al.

(2009) states that the primary cause of failure in concrete rail ties is rail seat abrasion (RSA). This occurs when moisture becomes present under the rail seat and the tie sees high volume of heavy-axle loads. The deterioration of the rail seat can lead to a differential in the gauge of the rail which then can cause further damage to the tie or derailment of the train. If no RSA is present, then next mode of failure is corrosion of the prestressing steel resulting in greater loss of prestressing forces and overall strength of the tie.

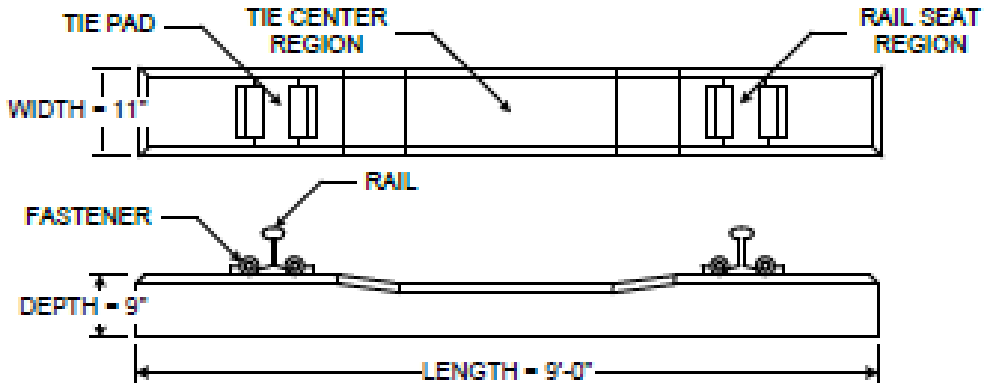

Figure 4: Typical concrete rail tie plan and profile view

There has been noted distress in concrete ties only a few years after installation along the eastern coast of the United States. After investigation, this distress was caused by delayed ettringite formation (DEF) (Mielenz et al. 1995). This was caused by large amounts of sulfate in the cement used in the mix. Mielenz used a scanning electron microscopy to located ties with DEF so they can be removed and replaced. DEF causes cracking within the ties which can lead to the concrete loosing anchorage to the prestressing steel. During the investigation, field engineers took note of patterns and irregularities found in the track. These patterns showed engineers that the cause of DEF was only due to the concrete mix difference, not environmental or loading conditions.

Research has been conducted on concrete rail ties to improve durability and overall performance in order to lower the total cost and make their use economical. Mindess, et al. (1991) explored the use of mixing fibers into the concrete mix itself to increase impact resistance of the tie. Three different concrete mixes were developed from a single matrix: a plain concrete mix with no fibers, corrugated steel fibers at 0.57% by volume, and mono-filament polypropylene fibers at 0.15% by volume. Using 9.5 mm diameter steel prestressing strands, several ties were made for each concrete matrix and tested using a static load applied directly to the rail and impact loads applied at varying heights. Failure was typically initiated with cracking at the bottom of the tie under the load, and failure occurred with slippage of the prestressing strands. It was determined that including fibers within the concrete matrix did increase the toughness and durability of the tie by being able to resist a larger peak load and absorb more energy prior to failure. However, there is no indication of corrosion resistance and electrical conductivity improvements.

Donovan (1997) performed research into the development of concrete railroad ties in order to increase their durability. This was done by evaluating several tie designs, concrete mixes, and material sources. Four different tie designs were reviewed and tested according to AREMA guidelines: 9, 3/8 in. strand LB Foster CXT; 8, 3/8 in. strand LB Foster CXT; 8, 3/8 in. strand Rocla; and 24, 5 mm strand Canadian National. The CXT ties were shown to have the highest strength at the most reasonable cost. With the tie design chosen, Donovan reviewed and selected a possible source of aggregate to be used in the concrete mix. Aggregate producers were compared using a series of tests: Alkali Silica Reactivity (ASR), freeze-thaw cycles, abrasion resistance, and shape. Of 11 producers, only 3 passed all the tests. With the aggregate selected, the mix design was established using multiple factors including type of cement, use of plasticizers and fly ash, air entrainment, and method in which it is cured. This research provided an optimized concrete railroad tie, but it was for one specific purpose, a short line railroad in Nevada. A durable, corrosion resistant design needs to be established for more general use.

Jimenez and LoPresti (2004) reviewed the performance of four different materials of rail tie: wood, concrete, plastic, and steel. All testing of these ties occurred at the TTCI testing facility in Pueblo, CO. Plastic ties were developed by TieTek, Inc. and US Plastic Lumber in an attempt to create a lighter and stronger tie compared to wood. During laboratory testing, it was found that although cut spike removal required less force than wood, uplift of the rail has not been an issue. For full scale testing, two zones were set up at the TTCI facility: one with plastic ties intermixed with wood and the other with consecutive plastic ties. This testing revealed that spike uplift was a problem and temperature had a much greater effect than expected. During a 100°F change in temperature the plastics ties experienced a 0.24 in. growth in the gauge length while timber ties typically see 0.016 in. Overall, the plastic ties performed just as well as timber ties but with an obvious increase in cost meaning this is not a feasible solution.

One of the primary causes for this research is the electrical resistance of the concrete railroad tie. With wet concrete being a type of semi-conductor and steel being a high conductor of electricity (Sengul 2009), issues with corrosion and false signaling can be more prevalent than anticipated. Performing electrical resistivity tests are becoming more popular as a quality control check for concrete. Laysse et al. (2015) performed several tests to determine the electrical resistivity of concrete to show correlation with chloride penetration and durability. Two of the tests performed were a uniaxial test and a four-probe test also called a Wenner test, Figure 5. It was found that the uniaxial test is best performed on concrete in labs as another cylinder test similar to standard compression tests, while the Wenner test is best done in the field. They concluded that concrete with a higher resistivity is more corrosion resistant, and that the higher resistivity will prevent rapid chloride penetration (RCP). However, the problem occurs with attempting to mitigate the corrosion caused by lack of resistivity.

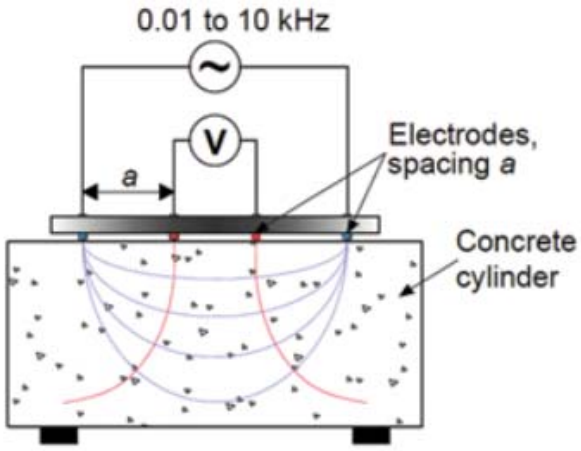

Figure 5: Four-point or Wenner probe test (Layssi 2015)

Monfore (1968) studied the effect of admixtures, within the concrete railroad ties, on concrete resistivity as a means of insulating the concrete itself outside of the use of insulator pads between the rail and the tie. Moisture proved to be the primary cause of electrical conductivity and would cause the ties to behave like common electrolytes when exposed to an electrical current. However, when oven dried at 105 °C the resistivity increases by nearly 10 million ohm-cm. Several admixtures were tested within the concrete matrix: ammonium phosphate, hydroxyacetic acid, hydroxyethyl cellulose, and calcium chloride. Each was mixed in a cement paste of variable ratios and cured as 4 in. cubes which underwent the resistivity test. Although resistivity of the concrete increased with the use of admixtures, it was not enough to counter the effect of water on and in the cured concrete. Through this research, concrete resistivity was determined to be a factor in the rate of corrosion on embedded steel which poses a problem for the embedded fasteners within the concrete railroad tie.

2.2 Concrete Tie Testing Procedures

To structurally test the concrete ties, three different tests are performed. A vertical load test, repeated (fatigue) load test, and ultimate load test.

2.2.1 Vertical Load Test

The first set of testing done on the tie is a vertical load test which follows the guidelines of AREMA Chapter 30.4.9.1.4 *Rail Seat Vertical Load Test,* Chapter 30.4.9.1.6 *Center Negative Bending Moment Test*, and Chapter 30.4.9.1.7 *Center Positive Moment Test*. These tests are performed at both the rail seat section and the center of the tie for they are the critical sections in the tie for bending moment. First, the test is performed at the rail seat in the positive moment direction using a 3-point bending apparatus shown in Figure 6. The vertical load is placed 30 in. from the center of the tie and supported on two rubber strips located 2.25 in. from the center line of the load. The applied load is calculated from Equation 1.

$$P = \frac{2M}{\frac{2X}{3} - 2.25"} \tag{1}$$

where P = the vertical load; M = the design positive rail seat moment; and X = the distance from the load center to the edge of the tie. If under the applied load the tie shows no noticeable cracking after 3 minutes, the tie is deemed adequate. The tie is simply supported and rests on 2” x 1” rubber pads placed on top of rockers located two thirds of the distance from the center line of the vertical load to the edge of the tie following the diagram of Figure 6. The load is then applied through a plate resting on 1” x ½” rubber strips. AREMA calls for 50A durometer scale hardness to be used as the rubber material.

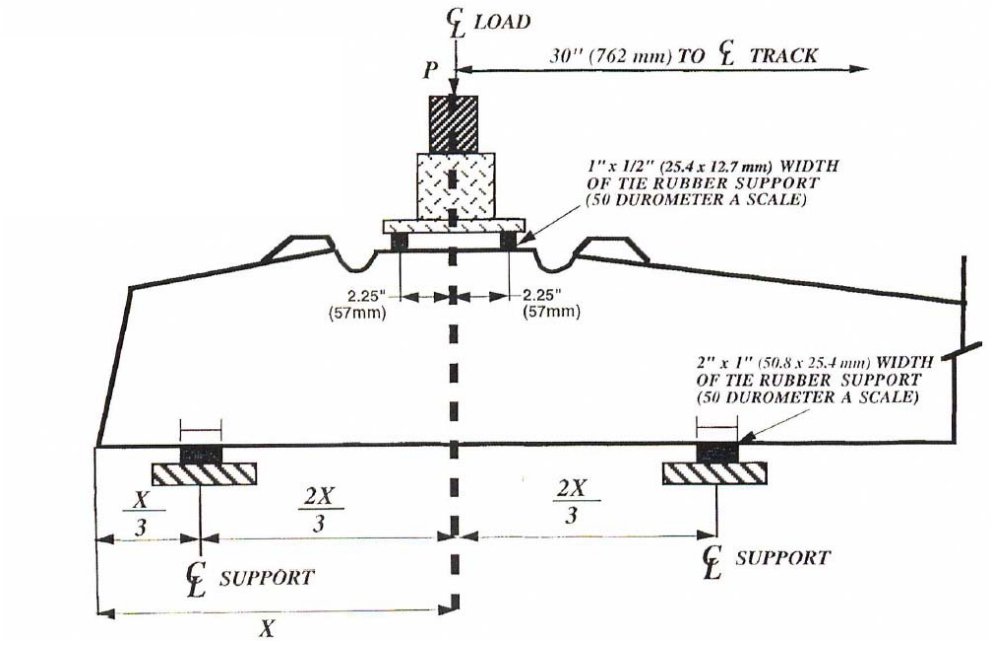

Figure 6: Vertical load test at the rail seat in the positive moment direction (AREMA 2014)

This test is repeated for the rail seat but in negative moment direction as shown in Figure 7. Here the strips supporting the applied load are located 3.0 in. off the center line while the bottom supports are still located the same distance as with the positive moment. Equation 1 is adjusted appropriately by replacing 2.25 in. with 3.0 in. to achieve the desired applied load for this test. This load is applied for 3 minutes and deemed adequate if no visible cracking occurs.

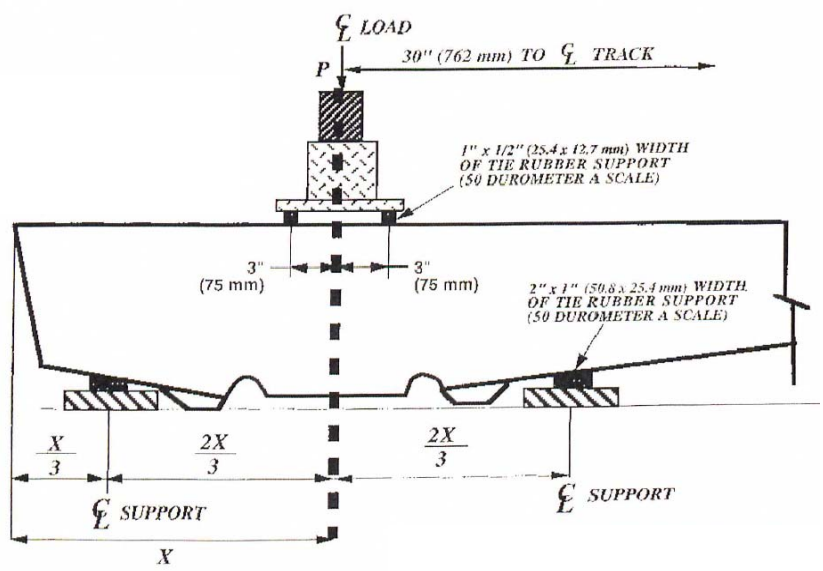

Figure 7: Vertical load test at the rail seat in the negative moment direction (AREMA 2014)

Next, the process is repeated but for the center of the tie and follows the instructions in AREMA Chapter 30.4.9.6-7. Figure 8 shows the set up for testing the center of the tie under negative and positive bending moments respectively. The actuator load is again supported on two 1" x ½" rubber strips located 3 in. off the center line of the tie, and the tie is resting on two 2"x1" rubber pads sitting on rockers spaced 30 in. off the center line of the applied load. Due to the symmetry between the two load cases, the equation for finding the necessary applied load is the same for both positive and negative and shown in Equation 2

$$P = \frac{2M}{27"} \tag{2}$$

where P = the applied load and M = the service moment for the negative and positive moments respectively.

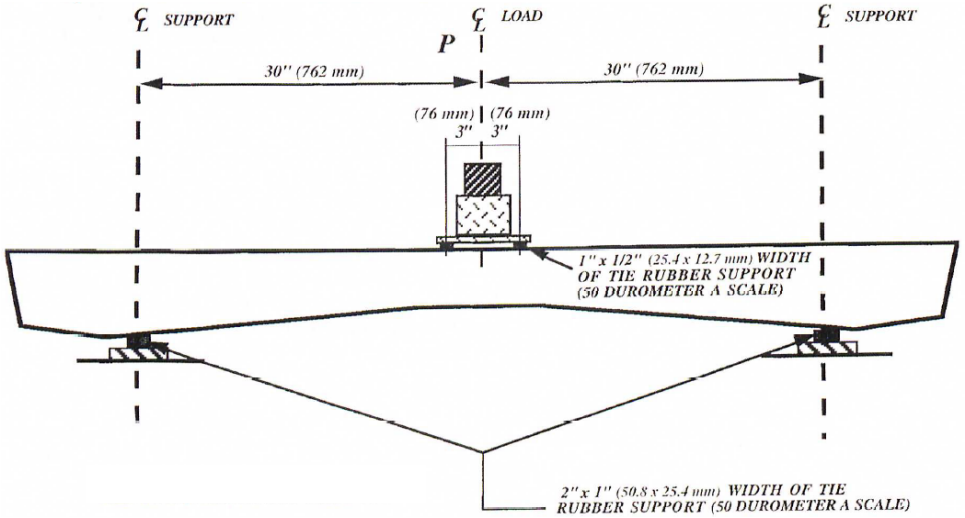

(a)

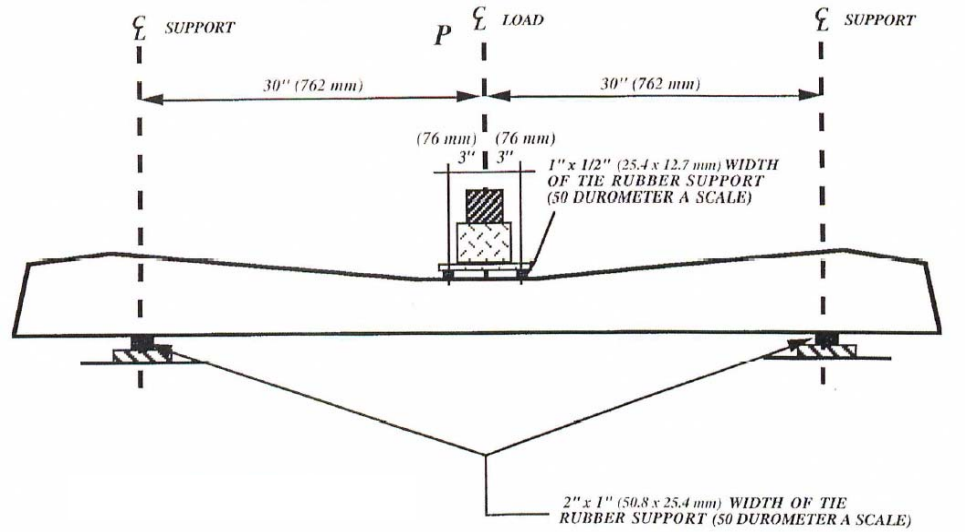

(b)

Figure 8: Vertical Load test at center section for (a) negative moment test and (b) positive moment test

2.2.2 Repeated Load Test

The repeated load test is intended to simulate fatigue loading on the tie. Set up for this test follows AREMA Chapter 30.4.9.1.5 *Rail Seat Repeated-Load Test*; therefore it is only performed at the rail seat and in the positive moment direction as laid out in Figure 9 and following the support setup of Figure 6. When performing the repeated load test, the cracking load, P_c, is found first. In this instance the cracking load is defined as

the load in which a crack has formed and propagated from the tension face to the outermost layer of reinforcement. From there, the load is released down to 4 kips and where it then begins to cycle from that load to $1.1P_c$. Approximately 3 million cycles are counted at a rate of no more than 10 Hz. Once the repetition of load is complete, a static load of $1.5P_c$ is applied at the same location. If no tendon slippage above 0.001 in, concrete compression, shear cracking, or tendon rupture occurs then the tie is deemed adequate under fatigue loading.

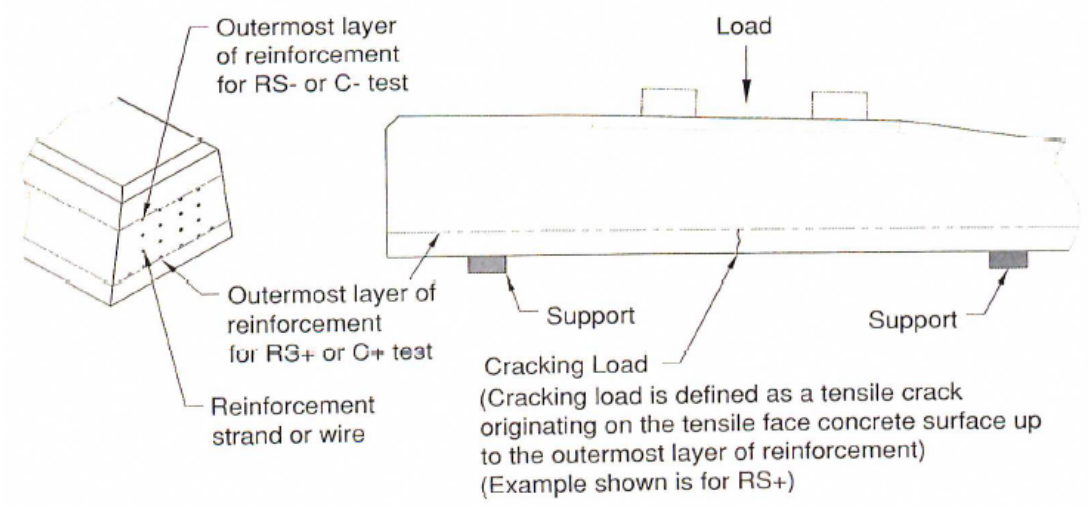

Figure 9: Repeated load test set up (AREMA 2014)

2.2.3 Ultimate Load Test

The ultimate load test is designed to determine the failure load and mode of the ties and follows AREMA Chapter 30.4.9.1.8 *Bond Development, Tendon Anchorage, and Ultimate Load Test*. A static load of $1.5P_c$, as defined in the previous section, is applied to an uncracked positive rail seat section and the bottom layer of reinforcement is checked for tendon slippage. If less than 0.001 in. of slippage occurs then the tie meets bond requirements and can then be loaded until failure. Once failure occurs, the tendon slippage, maximum load, and failure mode are documented. It is expected that the failure

mode of the ties reinforced with AFRP to be tendon rupture based on prior experiments involving bending moment tests of beams prestressed with AFRP (Gar 2013).

2.3 AFRP Material Properties

Medina (2011) performed detailed analysis on the properties of Arapree® AFRP bars including tensile tests, creep-rupture tests, and relaxation tests. Through the process of testing the tensile strength of the AFRP, the appropriate anchorage was developed to best be used for this material as it undergoes prestress. The use of 1.9 in. diameter, 18 in. long steel pipes were used to house the bars and they were then filled with Shepler's Shep Rock^{TM} quick setting grout. This type of anchor allowed for proper development length so that there were minimal stress concentrations at the anchor and more accurate results could be determined.

2.3.1 Ultimate Strength

Tensile tests for the AFRP were done using six specimens in the set up shown in Figure 10 and averaging their strengths to determine the typical tensile strength. Modulus of elasticity was also determined by plotting the stress-strain diagram found for each specimen. The results of the stress-strain diagrams for all six specimens are shown in Figure 11. It should be noticed that there is no clearly defined yield point as there is with steel. This means that when applying prestress to AFRP, no more than 50% of the ultimate stress shall be applied through the jack (ACI 440.4R). The numerical values for the ultimate stress, strain, and modulus of elasticity or shown in Table 1 and are used to calculate the necessary prestressing load to use on the AFRP. Based on the results present, the ultimate strength of AFRP is 212 ksi with an ultimate strain of 0.0209 in/in leading to a modulus of elasticity of 10231 ksi. With the modulus of elasticity of steel being 29000 ksi, it is evident that the AFRP has approximately one-third of the elasticity to that of steel.

Figure 10: Tensile test of AFRP bars (Medina 2012)

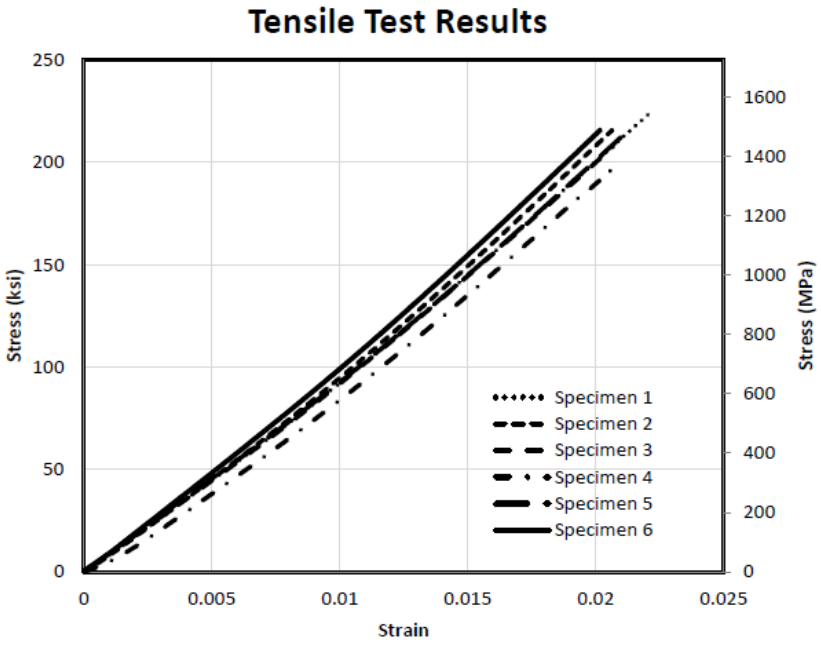

Figure 11: Results from 6 tensile tests of AFRP bars (Medina 2011)

Table 1: Test summary for tensile test of AFRP (Medina 2011)

Specimen	Ultimate Load (kips)	Ultimate Stress (ksi)	Ultimate Strain	Modulus of Elasticity (ksi)
1	27.39	224	0.0222	10189
2	26.30	215	0.0206	10500
3	25.29	207	0.0207	10071
4	24.01	196	0.0207	9819
5	25.31	212	0.0210	10092
6	26.31	215	0.0202	10717
Average	25.86	212	0.0209	10231

2.3.2 Creep-Rupture

To further determine the desired prestressing load required for the AFRP bars, a creep-rupture test was performed also by Medina (2011). Both short and long term creep analysis was considered during experimentation. Short-term creep testing consisted of prestressing six AFRP bars to 80 and 85% of ultimate (3 for each stress level) and locked into place similar to the tensile test set up. It was quickly discovered that the tendons would rupture within a few hours of being stressed showing that the prestressing load plays a significant role in the creep of the tendons (Gar 2012); therefore when conducting long-term creep tests, the stresses were lowered to 50% and 60% respectively. These specimens were also encased in concrete to better recreate real-world conditions for prestressed AFRP applications as seen in Figure 12. It was seen that the specimens stressed to 50% of the ultimate yielded the best results showing a 4% increase in strain of a 1000 hour period of time with no rupture of slippage occurring (Gar 2012). However, the specimens stressed to 60% of the ultimate did not fare so well, two had experienced slippage in the anchor at 150 hours and 350 hours respectively while the third did not slip until 550 hours, long enough to go through the two phases of creep: primary and secondary. Figure 13 shows the increase in strain for the three bars stressed to 50% and the location of the primary and secondary creep phase and Figure 14 shows it for the bars stressed to 60%.

Figure 12: Creep-rupture test set-up (Medina 2011)

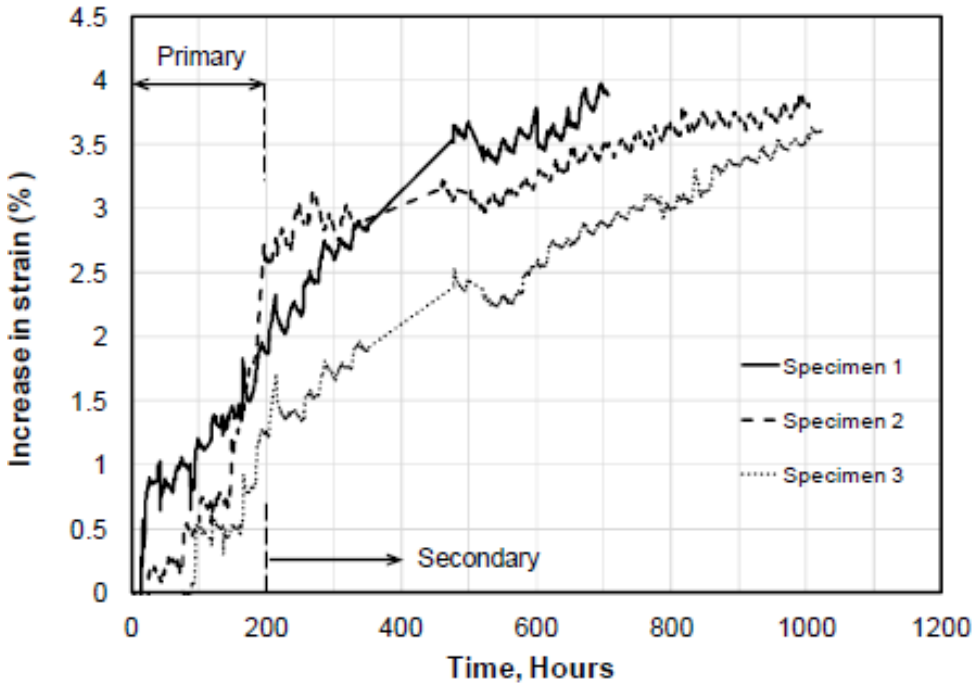

Figure 13: Strain increase due to creep for AFRP prestressed to 50% of ultimate (Gar 2012)

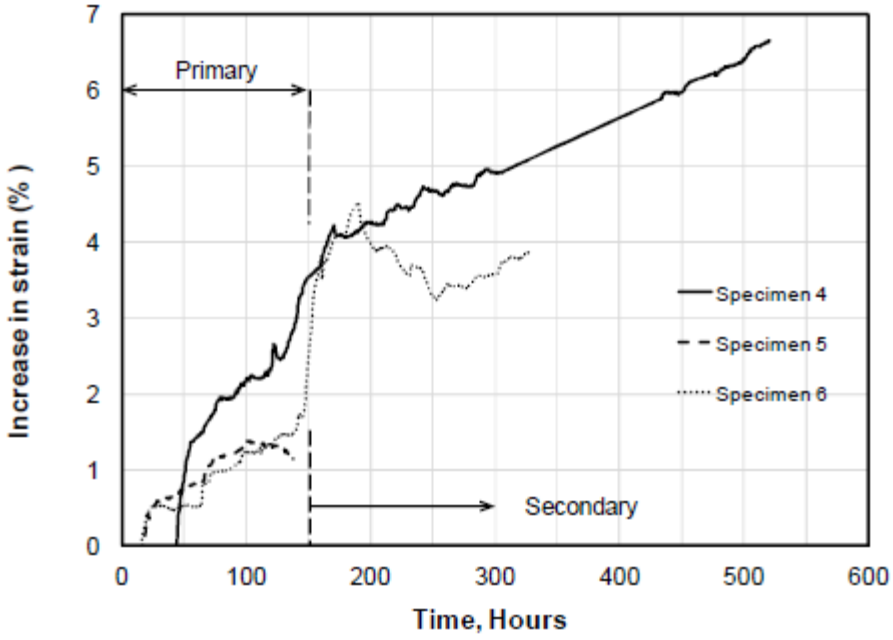

Figure 14: Strain increase due to creep for AFRP prestressed to 60% of ultimate load (Gar 2012)

Based on the results from the creep-rupture test here, increasing the prestressing load from 50% to 60% can increase the long-term strain increase from 4% to 6%. This indicates that a prestressing load of 50% of ultimate shall be used in prestressed concrete applications such as prestressed concrete railroad ties.

2.3.3 Relaxation

Relaxation tests were also performed to reinforce the idea of limiting the allowable prestress to only 50% of the ultimate stress of the AFRP bars. The set up for the relaxation test is similar to that of the long-term creep test with the prestressed AFRP being cast into individual concrete blocks as shown in Figure 12. The total relaxation was calculated by finding the total loss after 1000 hours and subtracting the loss due to creep and slippage. Each was measured using strain gauges and LVDTs respectively. It was seen that at 50% prestress, the AFRP relaxed approximately 7.5% yet it relaxed 9.7% at 60% prestress (Gar 2012). This once again shows that the more prestress applied to the bars, the more losses will occur. Therefore, the total loss that can be predicted in

50% prestressed AFRP due to the combined effects of creep and relaxation is 11.5%. This confirms the assumption of a 20% total loss in prestressing AFRP.

2.4 Prestressed AFRP Applications

A fast growing solution to the corrosion problem is the introduction of Fiber-Reinforced Polymer (FRP) bars. There are three main types of FRP bars currently in use today: Aramid (AFRP), Carbon (CFRP), and Glass (GFRP). AFRP bars have shown to be the more applicable material due its greater deflection and curvature under prestressed applications compared to carbon, and greater strength and moment capacity compared to glass (Gar 2013). Current research of the use of AFRP bars in prestressed concrete structures primarily focused on bridge girders and decks. Due to the environmental similarities seen by both railroad ties and bridge girders, the success of AFRP in concrete railroad ties should reveal similar results.

Most research involving prestressed FRP tendons is through the use of concrete beams. McKay and Erki (1992) demonstrated this by prestressing three similar concrete beams with AFRP bars on the bottom and conventional steel on the top, Figure 15. The AFRP bars were prestressed to 80% of the ultimate strength. Each beam was subjected to a different loading condition: beam 1 was loaded to near ultimate, released, and loaded again until failure; beam 2 was loaded until cracking then set under a cyclic loading of 4 Hz and failed after 1.96 million cycles; and beam 3 was loaded in the same fashion as beam 2 but with a more consistent cycle of loading to minimize elastic recovery. The results of this experiment showed the AFRP having a higher relaxation than steel at 10-20% over 50 years, yet near equal fatigue strength under service conditions to that of steel. Another major finding was found that AFRP should be used in fully prestressed applications to prevent the need for rod fretting which leads to a decrease in bond strength decreasing the capacity of the concrete beam.

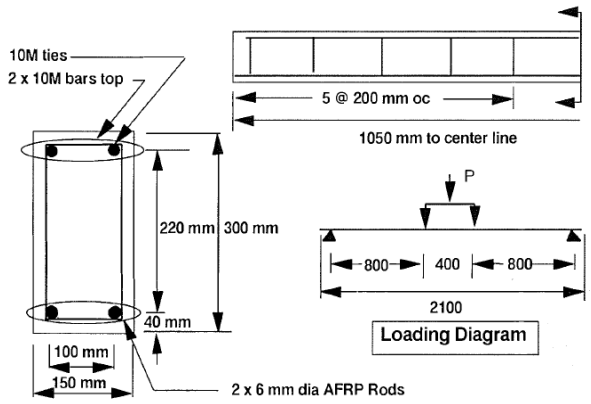

Figure 15: Dimensions and loading pattern for concrete beams (McKay 1992)

Lutch (2009) researched an optimal layout design for concrete ties by using combinations of concrete strengths, prestressing loads, and prestressing materials. Four different concrete compressive strengths were used in the project: 7, 9.5, 12, and 15 ksi. For each concrete strength, three different prestressing materials were used: 0.21 in. diameter wire; 0.25, 0.3125, and 0.375 in. diameter 7-wire strands; and 0.25 and 0.3125 in. diameter CFRP. A CXT 505S-50 tie was used as the basis for the optimization design and posed to be the basis for this proposed thesis project as well. Following the guidelines set by ACI 440, the committee on the application of FRP in concrete, a tie using 0.25 in. diameter CFRP resulted in having the highest flexural capacity for high strength concrete. Although this project shows the best resemblance of the proposed research, it is only a theoretical application with no physical testing performed.

Gar et al. (2013) used prestressed AFRP in an AASHTO Type 1 I-girder in composite with a conventional bridge deck and compared to conventional prestressed steel girder with the same decking as seen in Figure 16. Both experimental and a finite element analysis were performed resulting in a 5%-7% error in the prediction of cracking moments and material failure. Gar demonstrated that pre-tensioned AFRP both meets serviceability requirements and maintains adequate flexural strength. It was seen that the curvature at failure was approximately 18 times greater than the curvature at cracking, yet the mode of failure was tendon rupture in the tension face. This increase in

curvature showed that although the tendons may fail suddenly in rupture, there is sufficient ductility present to provide appropriate warning prior to failure. Deflection of the girder was also measured during the load testing. It was found that the AFRP girder deflected half the allowable under service loading and half the deflection of a comparable prestressed steel girder at failure see in Figure 17. This is due to the higher ductility of steel after yielding compared to AFRP. However, this research does not review the corrosion resistance of the AFRP girder in comparison to the prestressed steel girder and how it affects serviceability.

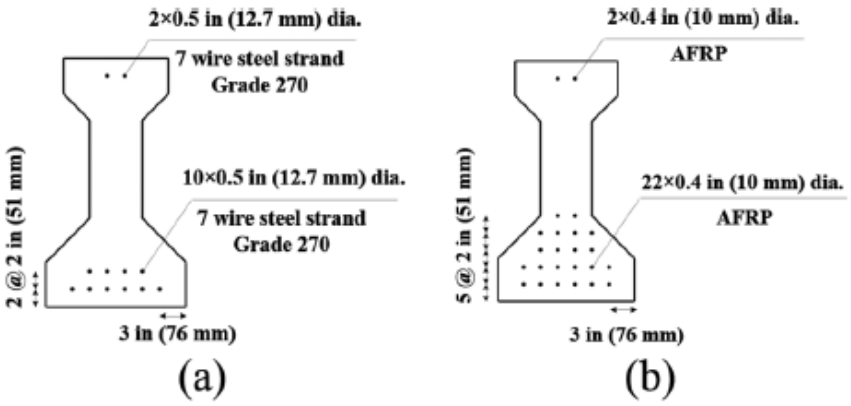

Figure 16: Prestressing layouts of Type-1 girder (a) is prestressing steel and (b) is prestressed AFRP (Gar 2013)

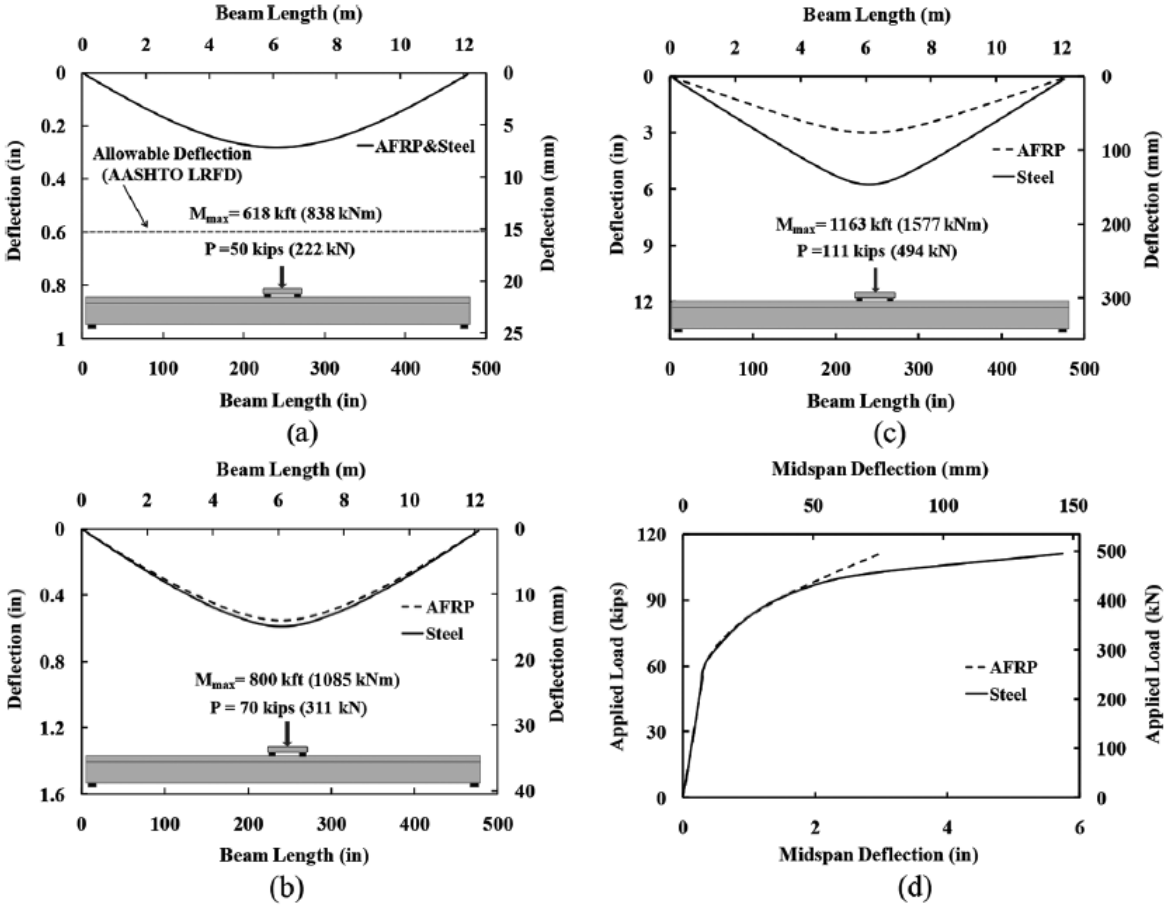

Figure 17: Deflection graphs of (a) at service, (b) post-cracking, (c) at failure, and (d) with respect to load (Gar 2013)

Gar (2012) also considered the use of prestressed AFRP bars on a two-way bridge deck with precast panels. The deck consisted of two 18’ x 7’-10” panels at 8 in. think, and prestressed with AFRP bars spaced about 5 in. on center in the direction of traffic and reinforced with AFRP bars spaced about 6 in. on center in the transverse direction. The entire deck was supported on three reinforced beams equally spaced with equal tributary areas for each as shown in Figure 18. The deck was loaded with a factored HS20 truck load equating to approximately 22.5 tons and was applied through a steel plate representative of the tire footprint. This load was applied to seven locations on the deck as shown in Figure 18 and cracking patterns were observed. It was found that

the deck resisted the maximum factored wheel loads in all locations. Failure was governed by flexure, the tandem axle load governed the flexural failure, and shear requirements were met. It was also discovered that although AFRP bars are a brittle material with no clear yield point, the deck underwent noticeable deformation before failure due to the low modulus of elasticity of AFRP, about 1/3 that of steel as seen in Figure 19.

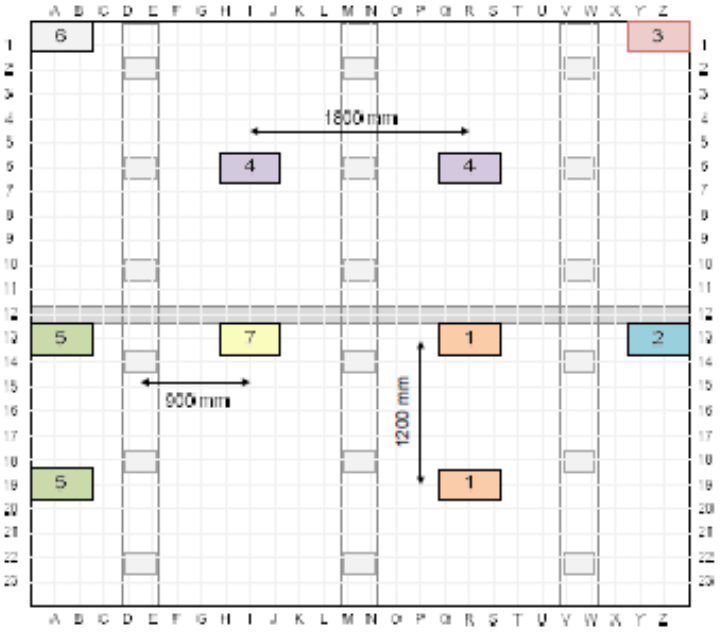

Figure 18: Loading plan of AFRP bridge deck (Gar 2012)

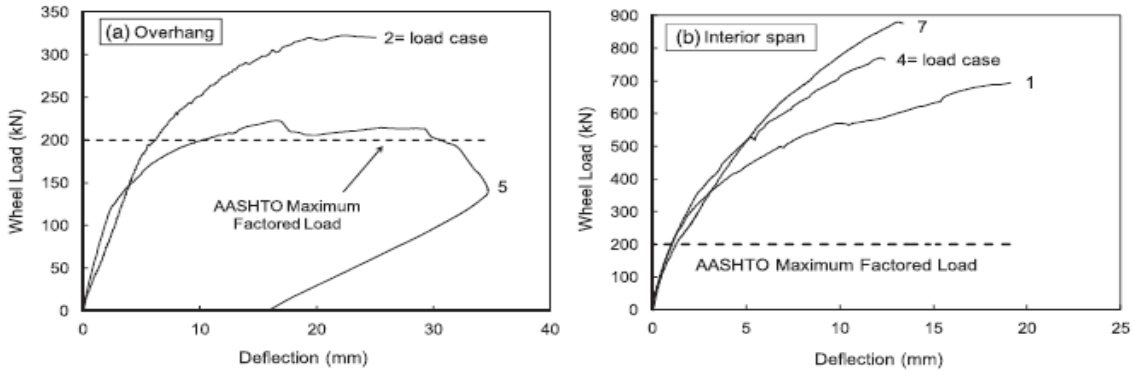

Figure 19: Load-deflection graphs for loads on the overhang (left), and interior panels (right) (Gar 2012)

Based on the previous work described above, the following research questions arise:

1. As the bond length of AFRP strands is relatively large when compared to the steel strands presently used in prestressed concrete railroad ties, how will this affect the performance of AFPR prestressed ties?
2. Given the small cross section of concrete railroad ties, how can the AFRP bars, which have a larger diameter than their steel counterparts, fit into that congested space while still meeting quantities necessary for strength adequacy and allowing proper anchorage?
3. How does the resistivity between the Pandrol shoulders that are used for fastening the rails compare for AFRP versus steel prestressed tie systems?

3. DESIGN OF PRESTRESSED CONCRETE RAILROAD TIES WITH AFRP

3.1 Introduction

This section reviews the design process for a new class of prestressed concrete railroad tie using prestressed AFRP to replace the conventional steel strands. Firstly, an in-depth look into the current status of material properties of AFRP is conducted to determine what the limits are for its use. Next, a detailed outline of the tie itself is analyzed to determine the required section properties design. This project used a LB Foster CXT 505S-50 concrete tie that is primarily used by Union Pacific Railroad Company on their main heavy haul tracks. Using the AREMA 2014 manual for concrete tie design, the service moments were calculated based on the annual tonnage, average speed, and tie spacing. Using these moments as checks, transfer and service limit state design was explored for determining the most efficient location of the centroid of the AFRP tendons. Once an acceptable range of successful eccentricities were found, a series of layouts were modeled to meet strength requirements. These layouts were limited not only by strength needs and spacing within the tie cross section, but anchorage space limited the center spacing of the AFRP tendons to a 2 in. minimum. After all constraints were considered, a final design was selected for construction and testing.

3.2 Concrete Tie Properties

There are several different parts of the concrete tie that are involved in its design including location of the critical sections and the cross section at those points, amount of loss experienced in prestressing, and material used in the concrete. The critical sections are points in the tie where stress is maximized based on the loading applied. For concrete railroad ties, the critical sections are at the rail seat section and under positive moment (i.e. the top of the tie is in compression while the bottom is in tension), and at the center of the tie under negative moment (AREMA 2014). These are the service moments that occur when the wheels of a train are directly on top of the tie and will be calculated later. The CXT 505S tie, the subject of this investigation, has a typical positive moment

capacity of 381 kip-in at the rail seat and a negative moment capacity of 224 kip-in at the center (LB Foster). This capacity will be attempted to be matched by the newly designed tie.

3.2.1 Tie Cross Sections

The dimensions properties for the CXT 505S tie were provided by the manufacturer and compared to the work of Lutch (2009). These dimensions are shown in Figure 20 and summarized in Appendix B. Due to the non-standard shape of the tie, the cross section was broken up into six sections of rectangles and triangles for ease of calculation. The extra area on the side of the cross section is not considered for it is a shear key used solely for lateral resistance which is not covered in the scope of this research.

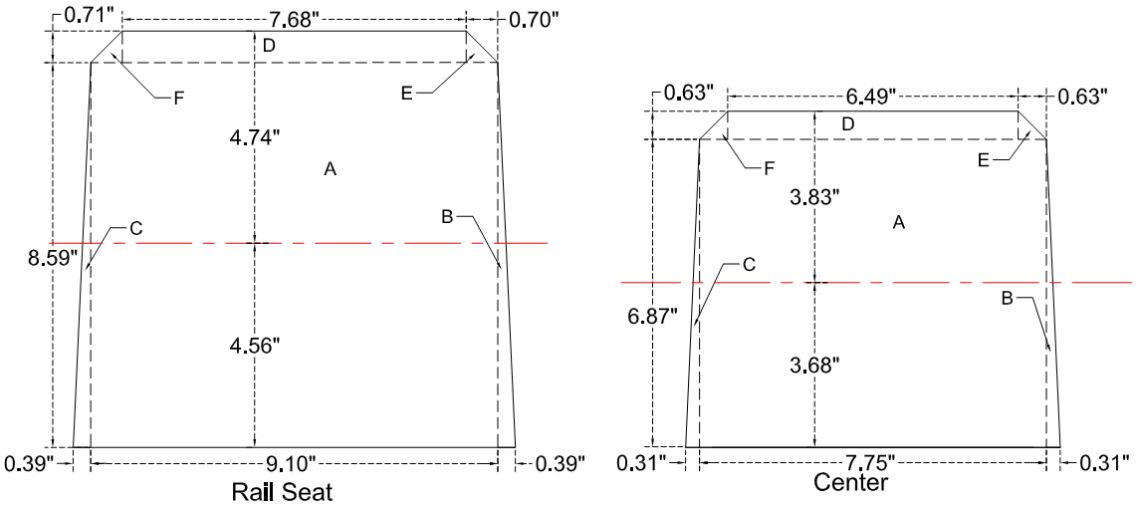

Figure 20: Cross section of tie at rail seat and center sections

The reason the center section is of smaller area and thus lower neutral axis is due to the bending moment critical sections as discussed previously. By changing the depth of the tie throughout the length, it allows for an altering neutral axis and, with the use of straight pretensioned steel strands, an altered eccentricity. This then can utilize the tension in the strands to resist both positive moment and negative moments simultaneously at the critical points. This concept is employed in determining the location of the AFRP strands; having the centroid below the rail seat neutral axis, yet above the center neutral axis. By having two eccentricities both above and below the cross section neutral axis, a sign convention was established which will also create consistency in the stress calculations. For this project, any eccentricity below the neutral axis is defined as positive, while an eccentricity above the neutral axis is negative. Compression stresses are defined as negative and tensile stresses as positive.

3.2.2 Concrete Properties

When designing a new cross tie with AFRP, it is important to use current properties of concrete for continuity and error limitation. Typical manufactured CXT 505S ties are composed of 8000 psi strength concrete with a 4500 psi minimum transfer strength. However, with speed being of great importance when manufacturing these ties, typical 28-day strengths can reach much higher values that can range from 9000 to 11000 psi (Lutch 2009). This fact was considered in the design process for the new ties to help keep the total number of tendons low assists in keeping the initial cost low. AREMA have set forth guidelines for concrete mix design. However, mix proportions were provided for this research by CXT.

The concrete used by CXT is a self-consolidating concrete (SCC) that contains a plasticizer to maintain workability while decreasing the water/cement ratio. Table 2 shows the mix provided by CXT including type of material and its weight per cubic yard. The mix also includes an air entrained admixture to assist in preventing freeze-thaw damage. Air entrained concrete is typically seen in exterior structural concrete in areas where freeze-thaw cycles are regular and have shown to cause damage to the concrete.

Table 2: Concrete mix design used by LB Foster CXT for the 505S tie

Material	Size/Type	Weight / yd^3
Cementitious Material	Type III Portland Cement	650 lb.
	Class F Fly Ash (30%)	195 lb.
Aggregate	Blended Sand	875 lb.
	#57 Coarse	1015 lb.
	#8 (3/8") Pea Gravel	760 lb.
Water	-	242 lb.
Admixtures	Sika Air 360	10 oz.
	Sika 2110 HRWR	90 oz.

3.3 Service Load Calculations

AREMA provides a guide to calculating the design moments based on the length of the ties and their center to center spacing. Appendix B walks through that process using the 8'-6" long CXT 505S-50 tie at a 24 in. center to center spacing. For this research, CXT provided design moments required by the primary client of the 505S-50 tie and are shown in Table 5.

Table 3: Applied service moments

Moments		
Positive Moment @ RS =	378	kip-in
Negative Moment @ RS =	-176	kip-in
Negative Moment @ C =	-230	kip-in
Positive Moment @ C =	140	kip-in

3.4 Limit States

This project was designed with two limit states in mind: transfer and service. These limit states follow the guidelines and requirements set by the American Concrete Institute (ACI). However, the prestressing limits are followed by ACI 440.4R, the report on prestressed design of concrete using FRP tendons. It states that AFRP stressing is not

to exceed 50% of the ultimate load during jacking, and 40% immediately following transfer. This low limit is based on the failure mode of AFRP, rupture. For this research, a prestressing load of 11 kips was used because that is 45% of the ultimate load: sufficient to counter the losses and service loads seen on the ties. Assuming 20% prestress loss, a design load of 8.8 kips was adopted for the service load calculations.

3.4.1 Transfer

Transfer occurs when the applied prestress force is released onto the freshly manufactured early age concrete ties. This action typically occurs 16-24 hours after the concrete is poured, or when the concrete strength reaches 60% of its specified strength. In standard beam design, critical sections for transfer strength are at the top or bottom edges of the ends of the beam, depending on the eccentricity. For the concrete railroad ties, strength at the top of the center is more important being that the tie does not have a consistent cross section. As a double check, stresses under the rail seat are also calculated to ensure no cracking occurs. The stress is calculated by summing the total initial load over the cross sectional area in question and the stress due to the moment caused by the eccentricity of the load. Equation 3 depicts the stress calculation with F_i being the initial force, A being the cross section area, e being the eccentricity, and S_x being the section modulus.

$$\sigma = -\frac{F_i}{A} \pm \frac{F_i e}{S_x} \tag{3}$$

The sign of the stress (whether it is compressive or tensile) depends on the location of the AFRP centroid in relation to the cross section neutral axis. If the location in question is in the tension face, the eccentric load created a tensile stress and is positive, yet if it is in the compression face, a negative stress is found. Figure 21 shows the stress blocks at the rail seat and center sections of the tie during manufacturing. Note that there is not scaling in this figure as to what the actual stresses are. They are also upside-down because that is how they will be cast to match the process by the manufacturer. Once calculated, the stress values are compared to the ACI (2011)

required transfer stress conditions. The tension limit is $\sigma_t \leq 3\sqrt{f'_{ci}}$ while the compression limit is $\sigma_c \geq -0.6 f'_c$.

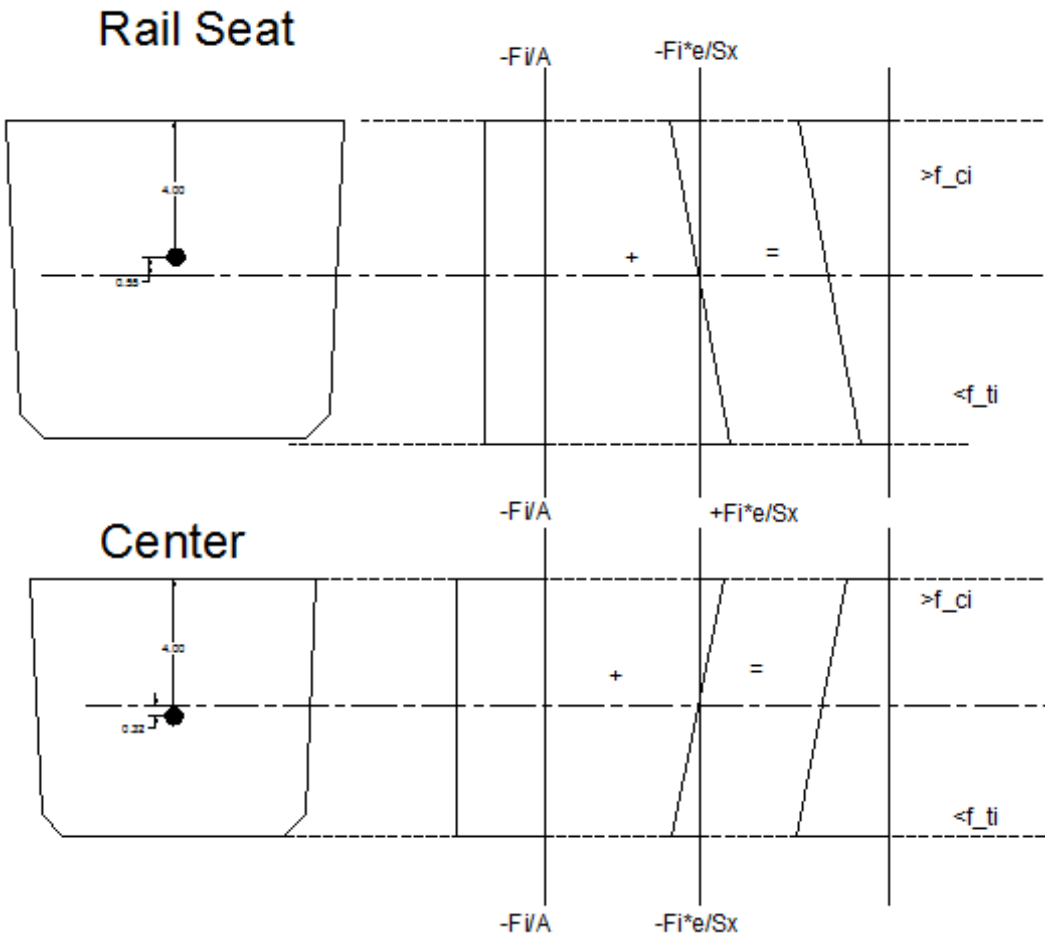

Figure 21: Stress blocks at transfer during manufacturing

3.4.2 Service

The second limit state considered is the service limit. This occurs when the tie is placed in the rail system and begins to see the live loading of trains passing over it. As trains pass over the tie two moment conditions occur: Positive moment at the rail seat with negative moment at the center, and negative moment at the rail seat with positive

moment at the center. The greater of the two is when positive moment at the rail seat and negative moment at the center occur, for this is when the wheels are directly over the tie and its load is being transferred straight down. Adding service moments the total stresses are

$$\sigma = -\frac{F}{A} \pm \frac{Fe}{S_x} \pm \frac{M}{S_x} \tag{4}$$

To more accurately represent the loads during the service time of a tie, prestress losses must be accounted for. Losses of 22% are typically found in the final design of ties (Kaewunruen 2011), but for this research an assumed loss of 20% is used to account for elastic shortening, creep and relaxation, and anchor slippage. Therefore a new axial load is used for the stress calculations, F is now $0.8F_i$. This then changes the stress block to that shown in Figure 22. For the service limit state, the tensile limit becomes $\sigma \leq 7.5\sqrt{f'_c}$ and the compressive limit becomes $\sigma \geq -0.6f'_c$ (ACI 318-11). By having a concrete strength of 8 ksi, the tensile limit under service becomes 0.671 ksi and the compression limit is 4.8 ksi. However, one of the ideas behind using AFRP over steel in a concrete tie is that it should allow the tie to crack slightly before being considered failed. The lack of cracks in the tie is to prevent as much water penetration as possible to protect the steel within from corroding. If AFRP does not corrode, there may be some minor cracking permitted because the resulting water infiltration should have little or no effect on the strength of the tie itself.

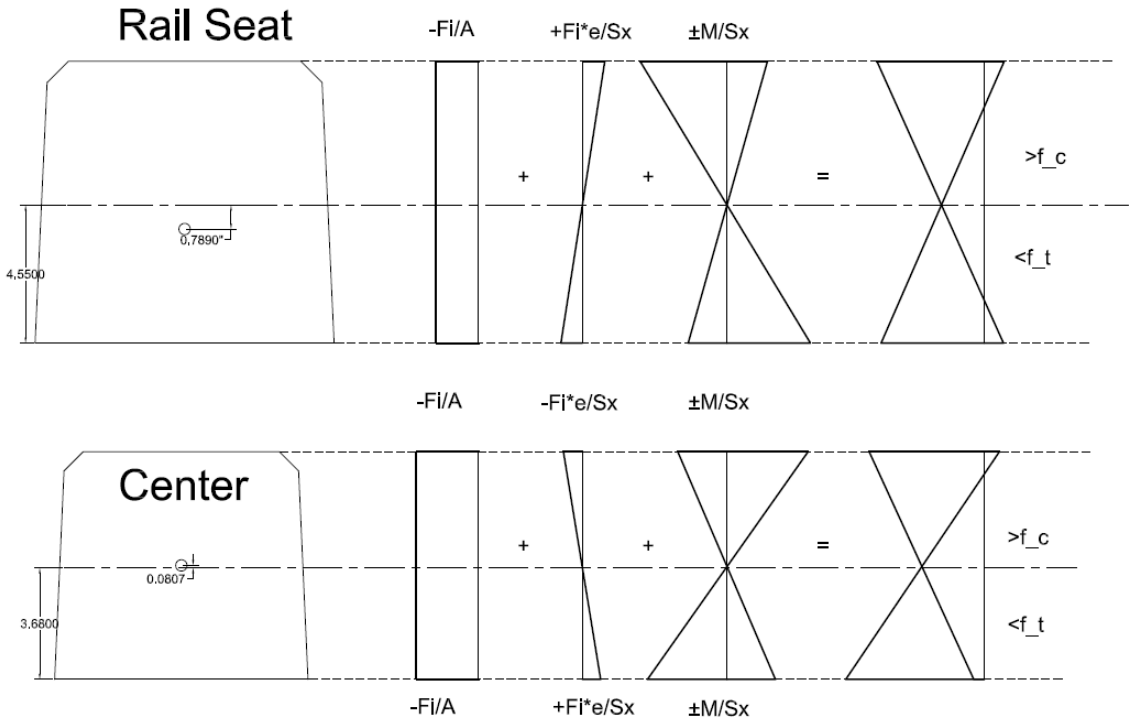

Figure 22: Service stresses on rail seat and center sections

3.5 Design Options

3.5.1 Prestressing Load

After considering all the limit states needed to complete the design, a series of tables were created to determine the centroid of the AFRP strands, the eccentricity caused by the centroid, the transfer stress checks, and the service load checks. Medina (2011) and Gar (2012) concluded that Arapree AFRP strands have a tensile strength of approximately 203 ksi, and with a diameter of 0.39 in. (10 mm), the ultimate load for AFRP is 24.25 kips. ACI 440.4R states that the jacking stress for AFRP is to not exceed $0.5f_{pu}$ however, Gar (2012) was able to stress the strands up to 60% of ultimate using a different anchoring system. This anchoring system uses 1.9 in. diameter steel pipes with 0.5 in. thick walls and is 18 in. long. AFRP was then placed through the center of the pipe and held by plastic stoppers. A quick setting, expansive grout called Shep Rock was

then used to fill the pipe and lock the AFRP strands into place. The 18 in. length was sufficient for transferring the prestressing load effectively from the AFRP to the grout and therefore to the concrete and the grout was sufficient to prevent pull out of the strands. A transfer length of 50 bar diameters (20 in.) has been reported for Arapree AFRP bars, but for this research an effective length of 10 in. is deemed the appropriate to reach the plastic section of the specimen (Ehsani et al. 1997 and Gar 2012).

Even though this new anchor can allow up to 60% jacking stress (14 kips) to be applied to the prestress, there were still some breakages that occurred prestressing operations. Therefore, a lower initial prestressing load of 11 kips was used. That load was used as the transfer load in the design checks, and with the 20% assumed loss, 8.8 kips was the service load to which the design was based.

3.5.2 AREMA Based Design

This section focuses on the design options that strictly meet the basic AREMA load requirements deemed acceptable for this research. These loads are based off a 24 in. tie spacing, 75 annual MGT, and 60 mph speed. Design moments were calculated in Appendix B. A systematic search for an appropriate layout was made to efficiently use the AFRP while maintaining spacing and stress requirements. The spacing requirements used are based on AREMA specifications and anchorage necessities. A 0.75 in. cover, as specified by AREMA, was needed on all sides of the tie, and a minimum of 2 in. was needed between the strands to allow the 1.9 in. diameter anchor to fit on the adjacent strands. With those criteria in mind and the desire to have the AFRP centered between the neutral axes of the rail seat and center sections, three layouts were found and are shown in Appendix B. These layouts are based around a grid and staggered idea to ease the prestressing and maintain symmetry about the vertical axis of the cross section.

Determining how many strands were needed per row and their location was an iterative process between finding appropriate spacing for a simple layout, calculating the centroid, and checking transfer and service stresses. AFRP centroids were calculated using Equation 5. Where n is the number of strands per row, A_{AFRP} is the cross section

area of each AFRP strand (0.12 in^2), and y is the height above the bottom for each row. Figure 23 and the table in Appendix B show the basic layout of a tie used in the design process and the method of calculating the centroid. A key item that is needed to be considered in the tie design and strand placement are embedded shoulders used to fasten the steel rail to the tie. The 505S tie uses Pandrol® Safelok III fasteners which were donated to the project as a means to best represent full functioning ties used by the industry. These embedded shoulders are approximately spaced 3 in. on center, are ¼ in. thick, and extend 3.5 in. into the concrete.

$$centroid = \frac{\sum n\, A_{AFRP}\, y}{\sum nA_{AFRP}} \tag{5}$$

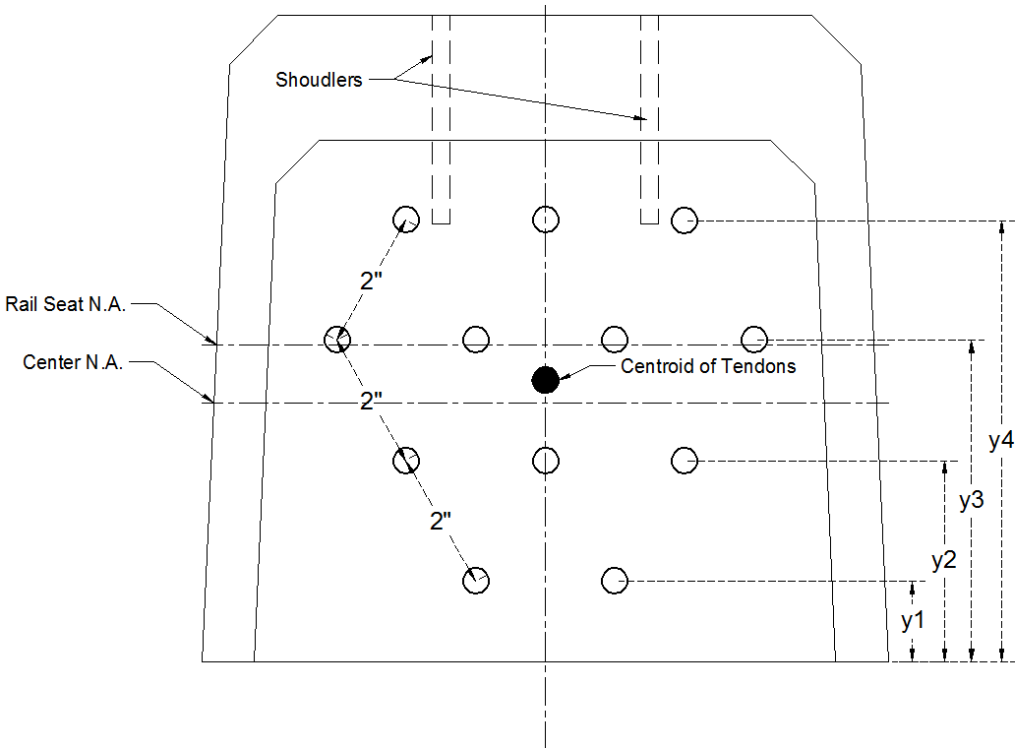

Figure 23: Basic model to base design

When the ties are put into service they are done so in the orientation as they are stored so there is only one stage to consider. However, because external moments are now applied, stresses at both the top and bottom of the tie exist under each moment case. The four moment cases are of that prescribed by AREMA: positive at the rail seat, negative at the rail seat, negative at the center, and positive at the center. Therefore, top and bottom stresses for each of the four moments must be checked under service stresses.

The primary limiting factor was tension at the top of the rail seat under negative moment. This occurred because of the combine stress of the eccentric moment plus the applied moment at the location with the greatest area. That stress forced changes in the location of the strands to decrease that eccentricity to decrease the tension at the rail seat. The other area of concern was the bottom of the center under positive stress for the same reasons; tensile stresses from the eccentric load and applied moment would over compensate the axial compression.

3.5.3 Final Design

After several iterations and adjusting the applied moments to meet manufacturer specifications, a final design was adopted which met all spacing and cover requirements. The solution utilizes 8 ksi strength concrete; and 11 kips of initial prestress per strand. Figure 24 shows this final layout with locations of each layer in relation to the bottom of the tie and their spacing off the centerline of the cross section. Also included in the layout are approximate size and position of the embedded steel shoulders which also played an important role in the geometrical constraints.

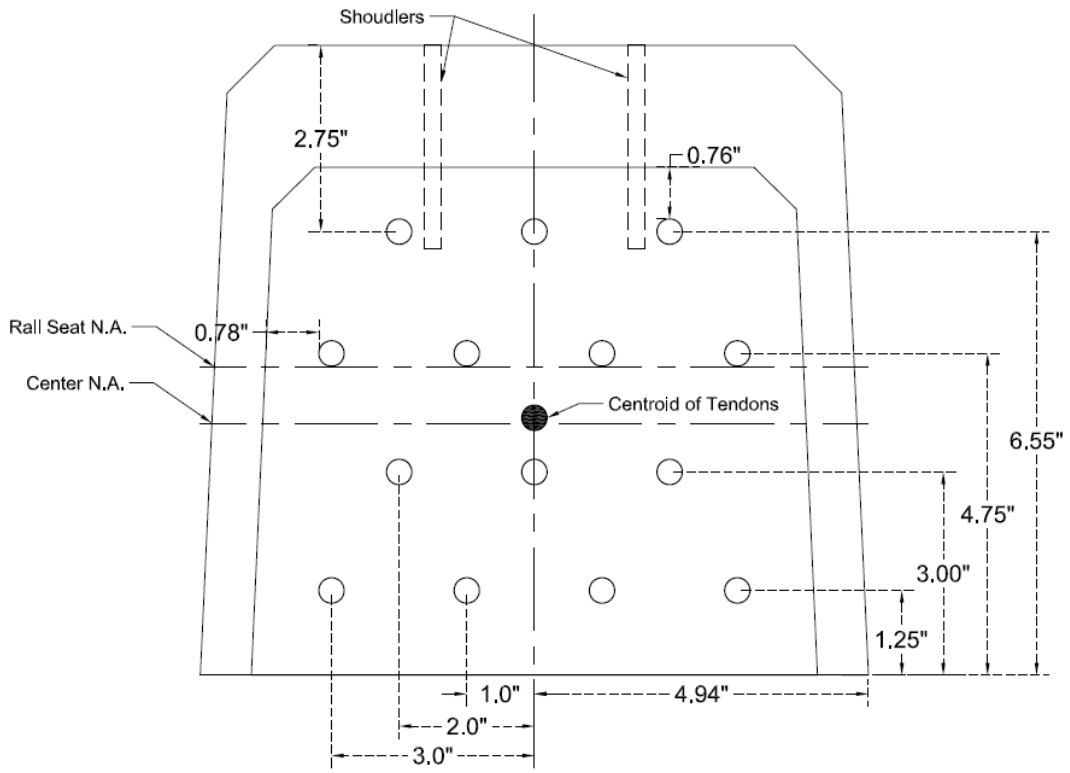

Figure 24: Final design layout to be used in construction and testing

This layout has 14 strands set in a staggered style, the centroid and eccentricities are calculated in Appendix B, Table 18. Using 14 strands maxes out the allowable spacing for the strands to maintain enough room for the anchor to be attached and still be over ¾ in. from the wall to maintain cover requirements. The centroid is calculated using Equation 3 with the diameter of the AFRP bars equaling 0.39 in. (10 mm). From that the eccentricity is simply the difference between the neutral axis of the respective cross section and the centroid of the AFRP. A negative eccentricity indicates the centroid is above the neutral axis while a positive eccentricity indicates the centroid is below the neutral axis. This becomes useful when calculating the stresses due to the AFRP.

Using Equations 1 and 2, the transfer and service stresses were calculated with details given in Appendix B. To fully complete the transfer calculations, self-weight moment was considered as an applied load. Table 4 shows that applied loads meet the stress requirements set forth in ACI 318.

Table 4: Transfer stress calculations

Stress @ Transfer			
	Initial PS Force, Fi =	154	kip
	Initial Tension Stress, σ_ti ≤	0.208	ksi
	Initial Compression Stress, σ_ci ≥	-2.88	ksi
Rail Seat	Self-Weight Moment =	6.278	kip-in
	Construction Stress @ Top =	-2.693	O.K.
	Construction Stress @ Bot =	-0.789	O.K.
	Storage Stress @ Top =	-0.884	O.K.
	Storage Stress @Bot =	-2.601	O.K.
Center	Self-Weight Moment =	9.371	kip-in
	Construction Stress @ Top =	-2.534	O.K.
	Construction Stress @ Bot =	-2.605	O.K.
	Storage Stress @ Top =	-2.823	O.K.
	Storage Stress @ Bot =	-2.319	O.K.

Because moment due to self-weight being so low relative to the service moments, it can be neglected when considering the service stresses and strength of the railroad tie. Also, since ties are continuously supported on compacted ballast, self-weight does not create an internal moment. Therefore the four cases considered under service load are based on the applied moments: positive moment at the rail seat and center, and negative moment at the rail seat and center. Under these conditions, the top and bottom of the tie are under the greatest compressive and tensile stresses so, like with transfer, each is checked relative to the applied moment. The fully detailed stress block for the service loads is shown in Figure 25 and depicts the positive and negative applied moment at each section. With a concrete strength of 8 ksi, and an assumed loss of 20%, Table 5 demonstrates that these stresses are within the limits for an un-cracked prestressed

section as stated in ACI 318 (2011). Like with transfer, tensile stresses are labeled as positive while compressive stresses are negative.

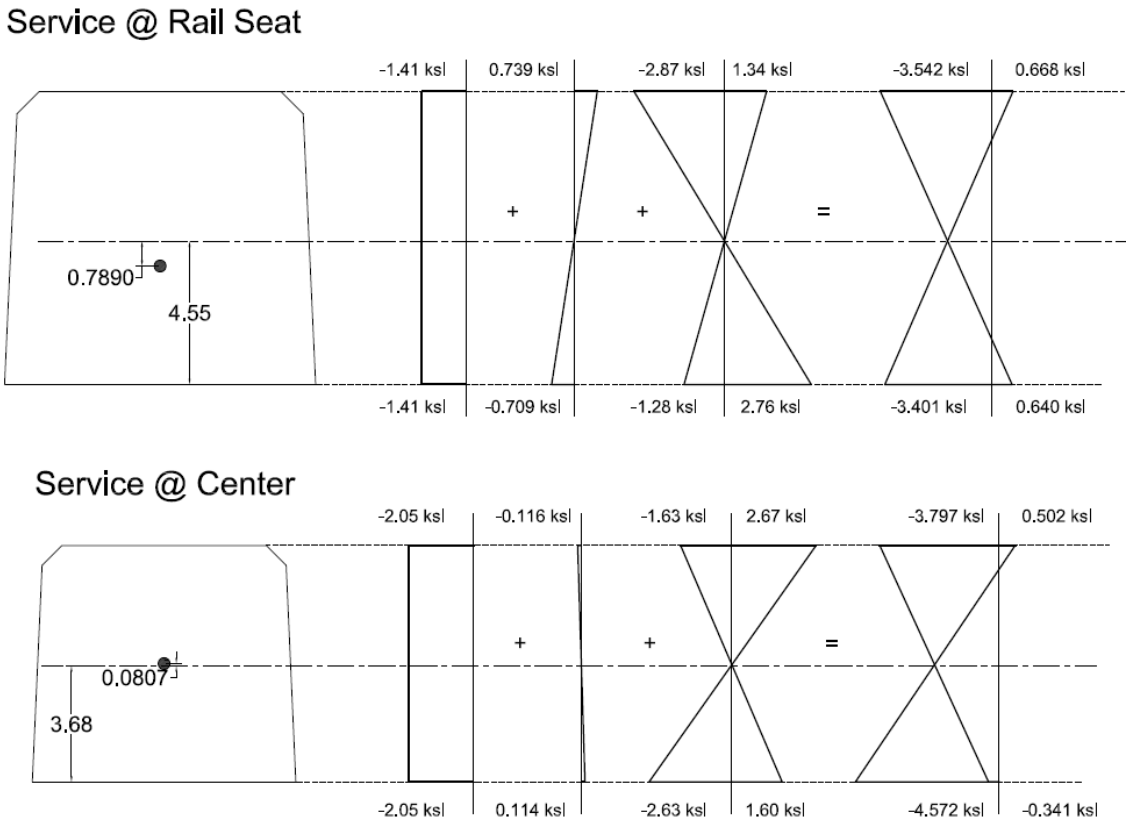

Figure 25: Stress blocks for service loads with positive and negative moments on each section

Table 5: Service stress calculations

Stresses @ Service			
	Final Service Stress, F =	123.2	kip
	Service Tension Stress, σ_ts ≤	0.671	ksi
	Service Compression Stress, σ_cs2 ≥	-4.8	ksi
Rail Seat	Positive Moment Stress @ Top =	-3.542	O.K.
	Positive Moment Stress @ Bot =	0.640	O.K.
	Negative Moment Stress @ Top =	0.668	O.K.
	Negative Moment Stress @ Bot =	-3.401	O.K.
Center	Positive Moment Stress @ Top =	-3.797	O.K.
	Positive Moment Stress @ Bot =	-0.341	O.K.
	Negative Moment Stress @ Top =	0.502	O.K.
	Negative Moment Stress @ Bot =	-4.572	O.K.

4. CONSTRUCTION

4.1 Introduction

This section discusses the construction of the railroad ties prestressed with AFRP. This process involved making a mold of a currently used original tie, designing and constructing a stressing bed at the Texas A&M Riverside Campus, stressing the AFRP, and pouring the concrete. Four molds were manufactured to produce four replica ties of the CXT 505S-50 tie used in the design calculations. Self-consolidating concrete was used to replicate the mix chosen for use in the CXT manufacturing plant.

4.2 Construction

4.2.1 Mold Development

In order to maintain cross sectional properties from the original to the new ties, negative polymer molds were cast which into the new concrete was eventually cast. The mold material chosen for this project was VytaFlex®-50; a urethane rubber manufactured by Smooth-On out of Macungie, PA. The material is formed by mixing two liquid parts, Part A and Part B shown in Figure 26, in a 1:1 ratio by weight or volume and poured it into a box, surrounding the object the mold is to represent. Although there are several different types of urethane rubbers that could have been chosen, VytaFlex® was selected due to its performance involving concrete. The properties for this material are shown in Table 6. There are also other levels of VytaFlex® based on the hardness; they range from 10A-60A. The 50A was selected by being the stiffest of the six with the lowest elongation at break percentage, has a 60min pot life, takes 16 hours to cure, and has tear strength of 102 pli (pounds per linear inch). Having a stiffer material means that it will hold its form better when concrete is poured into it. Since the 505S ties have a complicated shape, stiffness plays a significant role.

(a) (b)

Figure 26: VytaFlex-50 Parts A (a) and B (b)

Table 6: Properties of VytaFlex® series (Smooth-On)

Product Name	Mix Ratio	Demold Time	Elongation at Break	Mixed Viscosity	Shore A Hardness	Tear Strength	Weight (cu.in./lb.)
VytaFlex®-10	1:1	24 hr.	1000%	3100 cps	10	30 pli	27.9
VytaFlex®-20	1:1	16 hr.	1000%	1000 cps	20	58 pli	27.7
VytaFlex®-30	1:1	16 hr.	1000%	1800 cps	30	78 pli	27.3
VytaFlex®-40	1:1	16 hr.	660%	2000 cps	40	82 pli	26.9
VytaFlex®-50	1:1	16 hr.	400%	2000 cps	50	102 pli	26.7
VytaFlex®-60	1:1	16 hr.	480%	2000 cps	60	136 pli	26.6

The procedure that was followed in making the molds was to first to build the box the template tie would be placed in. A final design shown in Figure 27 depicts the layout of the box with the tie and mold included. The box was designed to allow a minimum mold thickness of ¼ in. Therefore, with the widest part of the tie being 11 in, the interior width of the coffin was set to 11.5 in. and utilized 2x12 lumber as the walls. Since the tallest part of the tie was 9.5 in., the 2x12 lumber was rip sawn to 10 in. width to allow a ½ in. thick bottom to the mold. This also allowed for a smoother, more level surface to attach to the bottom of the box; which was made of ¾ in. plywood. The end pieces were also ripped 2x12 lumber with an added 7 in. to the outside total length so

that 2x4 lumber could be placed at quarter points along the side walls to act as supports. To ensure all wood was as closely connected as possible the plywood was screwed every 12 in. along the wall and at each 2x4 support. Caulk was used to seal all the interior edges to prevent any liquid rubber material from leaking out during the pour.

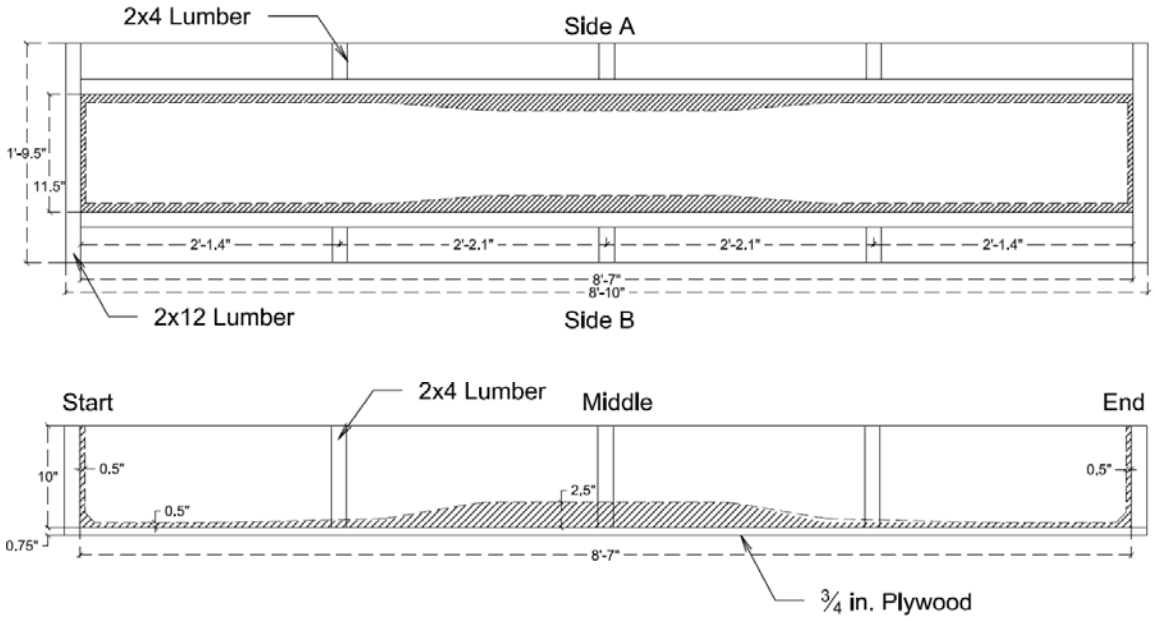

Figure 27: Plan and profile view of mold box

Four boxes were constructed to make four molds to allow for four new ties to be cast at the same time. These boxes were then moved indoors where the rubber mold could be mixed and cured in a climate controlled environment. Prior to pouring the mold, the template tie was coated in three layers of sealant and mold release. Smooth-On has a product, One-Step®, which is both a sealant and release agent in one. All sides of the tie were coated in this with 15-30min of dry-time left between coats. One hour after the final coat was applied, anchor bolts were attached to the underside of the tie following what is shown in Figure 28 and, using a crane, was lifted and carefully placed in its correct location within the box. The original tie had the imbedded shoulders installed in them which were not originally accounted for. Therefore, square holes of

approximately 2.5 in. x 1.0 in. were cut out of the bottom plywood and the shoulders were placed directly on the floor of the lab. The 1.25 in. height of the shoulders allowed for that to take place because once on the floor, the remaining space inside the box was the necessary 0.5 in. required to achieve proper thickness. Once the tie was placed in the box and properly spaced, Part A and Part B of the VtyaFlex® rubber mold were mixed and poured through a funnel into the box to fill the bottom and surround the walls. Each box was calculated to require 17 gallons of mixed rubber to fill approximately 3600 in^3 of space. Once the box was filled with the resin, it was cured for a minimum of 24 hours.

Figure 28: Original tie with anchor bolts and straps used for lifting in and out of box

Figure 29: Tie in wet mold

After the cure time passed, a straight blade was carefully slid around the edge of the tie to separate the mold from the tie to allow a simpler demolding process. Straps were then reattached to the anchor bolts and the tie was lifted to allow gravity to help pull the mold off the tie. After the mold came off a negative of the original tie seen by Figure 30 was left. With the tie out, another layer of One-Step® was applied to the tie and left to dry. Meanwhile, using a sharp blade, excess rubber was carefully removed from the edges of the mold and the next box was prepped. The tie was replaced in the new, empty box and the process was repeated.

Figure 30: Negative mold of CXT 505S-50 tie

4.2.2 Prestressing Bed Design and Construction

To enable the construction of the four ties, a prestressing bed needed to be constructed. A steel reaction frame was developed using existing steel members at the Riverside Campus of Texas A&M University, its design is described in Appendix C.

4.2.3 Stressing the AFRP

The four molds were set up and placed back-to-back to create a long line stressing bed. End plates were installed in the setup to be used to stress against. Figure 32 shows the dead end of the beams. The procedure to stress AFRP was adopted from Gar (2012), Medina (2011), and Cummings (2014). Each strand required the use of a 1.5 in. diameter schedule 80 (0.2 in wall thickness) steel pipe filled with an expansive grout. Gar and Medina used 18 in. pipes while Cummings used a 36 in. long pipe in conjunction with a threaded rod. For this research, tests were performed using both 18 in. long pipes and 36 in. long pipes to determine which worked best. It was found that tendon slip was experienced just prior to the desired load in the 18 in. pipes while tendon slip occurred at near double the load with the use of 36 in. pipes. This test was setup with two pipes straddling a center hole jack, Figure 31, and were each filled with the grout. After curing, the jack was loaded until failure occurred. This test was also used to determine the best ratio for the grout to water mix. The ratio was based on viscosity of the grout and its strength.

Figure 31: Grout ratio and pipe length test

After in lab testing of the grout and jacking procedure, the decided mix and method were taken to the site. The final mix design chosen was 4 lb. of grout to 16 fl. oz. of water and mixed in a Hobart counter mixer. By using the pipe straddling system for the live end, 3 pipes were required for each strand: 1 at the dead end, 2 at the live end as depicted in Figure 32. This required the use of 42 – 36 in. long x 1.5 in. inner diameter x 0.2 in. wall thickness pipes and therefore 189 lb. of grout and 756 fl. oz. (5.9 gal) of water. To speed up the stressing process, all 14 strands were placed at once and their dead ends grouted in one day and they were left to cure for 2 days before grouting and stressing the live ends. Through past experience, experimentation, and manufacturer's recommendation, a minimum cure time of 3 hours was required to meet strength to begin applying the stress. This requires that grout must be mixed and poured every 3 hours around the clock as to prevent as much differential loss as possible; thus requiring 6 hours of work per strand. Due to the quick setting aspect, the grout would set in 5-10 min after mixing, ice was used constantly to cool the pipes and water to delay the initial set of the grout.

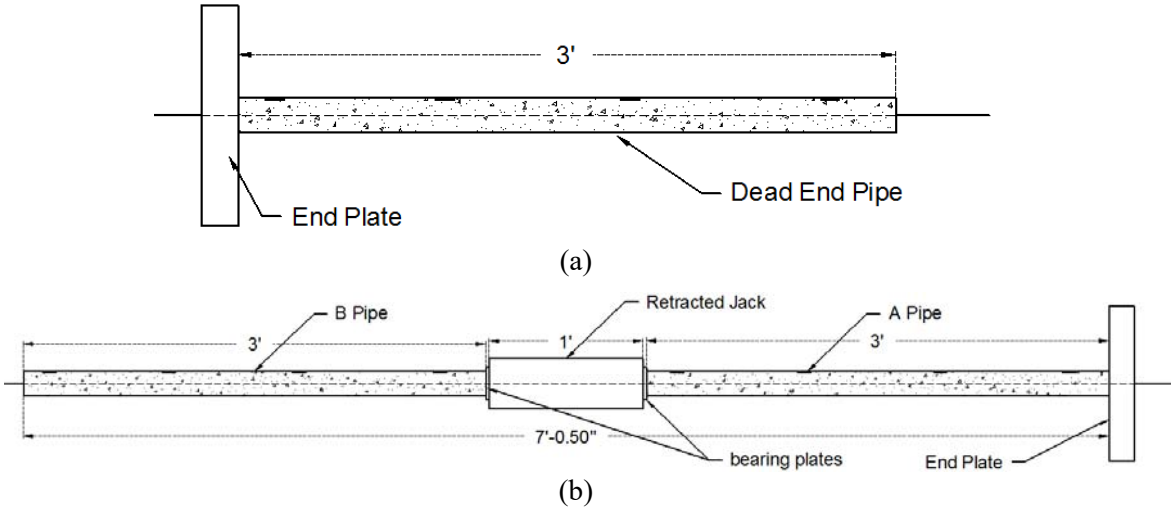

Figure 32: Pipe and grout set up for (a) dead end, and (b) live end

Another way the stressing process was sped up was to use two jacks simultaneously; an Enerpac RCH206 and a PowerTeam RH306D. Respective specifications for the jacks are shown in Table 7 and were used to determine the specific stress each jack needed to obtain to achieve proper prestressing force in the AFRP strand, and how to properly space them in the layout. Since the strands were spaced 2 in. on-center; the PowerTeam jack had geometric constraints because its radius is 2.375 in. which is greater than the 2 in. strand spacing. This meant that a new procedure had to be developed to best utilize the two jacks while not interfering with one another. A second check was done to determine if the jacks had enough extension to reach the desired elongation of the AFRP strands. The total free length of each strand was found to be 42 ft. (504 in.) from the dead end to the grouted live end, pipe B. This span along with the 11 kips of load and an approximate Modulus of Elasticity of 10000 ksi (Medina 2011), the elongation was calculated to be 4.6 in. which is well within the allowable stroke of each jack. This elongation was used as an on-site check to determine if the desired stress had been reached without relying solely on the gauges on the jacks themselves.

Table 7: Specifications of both jacks (Enerpac, SPX)

Property	Enerpac	PowerTeam
Capacity	20 Ton	30 Ton
Diameter	3.88 in.	4.75 in.
Length	12.05 in.	11 7/16 in.
Effective Area	4.73 in^2	5.89 in^2
Stroke	6.10 in.	6.0 in.

Stressing the strands started at 12:00 PM Sunday, August 2, 2015 and went every three hours after until all strands were stressed and grouted. The Enerpac jack was set to apply 2350 psi of pressure to achieve the desired 11 kips and the PowerTeam was set to 1900 psi.

Although the strands were eventually stressed and grouted as desired, 3 strands fractured early on during the stressing process. These were removed and replaced with getting the dead end grouted first and set to cure so the stressing could restart as soon as possible. To prevent the replacement strands from breaking, the applied load was reduced to 8 kips, and all remaining strands were also reduced the same prevent breakage. In the end, only three strands were able to retain the original 11 kip of initial force, the remaining had 8 kips of load on them. That reduction resulted in a new overall initial prestressing force of 97 kips. The final appearance of the four boxes with the stressed AFRP bars is shown in Figure 33 from the live end perspective showing everything set and prepared for the concrete pour to follow.

Figure 33: Fully stressed AFRP bars just prior to concrete pour

4.2.4 Concrete Casting

CXT provided a mix designed used in their Tucson, AZ manufacturing plant, Table 2. For construction, the same mix design was used which required a concrete specified strength of 8 ksi, and to be a self-consolidating concrete (SCC) mix. Therefore the mix had a water-cement ratio of 0.286, with the addition of a High-Range Water Reducer (HRWR) agent to ensure adequate workability. The actual batched mix is presented in Table 8. To test the mix, a slump test, air test, and spread test were performed to judge if the concrete met the fresh property requirements. Test cylinders were also cast using 24 standard 4 in. diameter x 8 in. tall cylinders. Results of the cylinder compression tests are listed in Table 9 with a strength gain graph plotted in Figure 34.

Table 8: Batched concrete mix used for construction

Material	Size/Type	Weight / yd^3
Cementitious Material	Type I Portland Cement	647 lb.
	Fly Ash	193 lb.
Aggregate	Fine Aggregate	867 lb.
	Coarse Aggregate	1027 lb.
	Pea Gravel	787 lb.
Water	-	155 lb.
Admixtures	Sika Air 360	8.3 oz.
	Sika 2110 HRWR	68 oz.

Table 9: Compression results for concrete cylinders (ksi)

Specimen	24-hour	5-day	7-day	14-day	28-day
1	6.29	8.51	9.45	9.65	10.8
2	6.44	8.21	9.30	9.95	11.4
3	6.55	9.15	8.83	9.80	10.7
Average	6.43	8.62	9.19	9.80	10.97

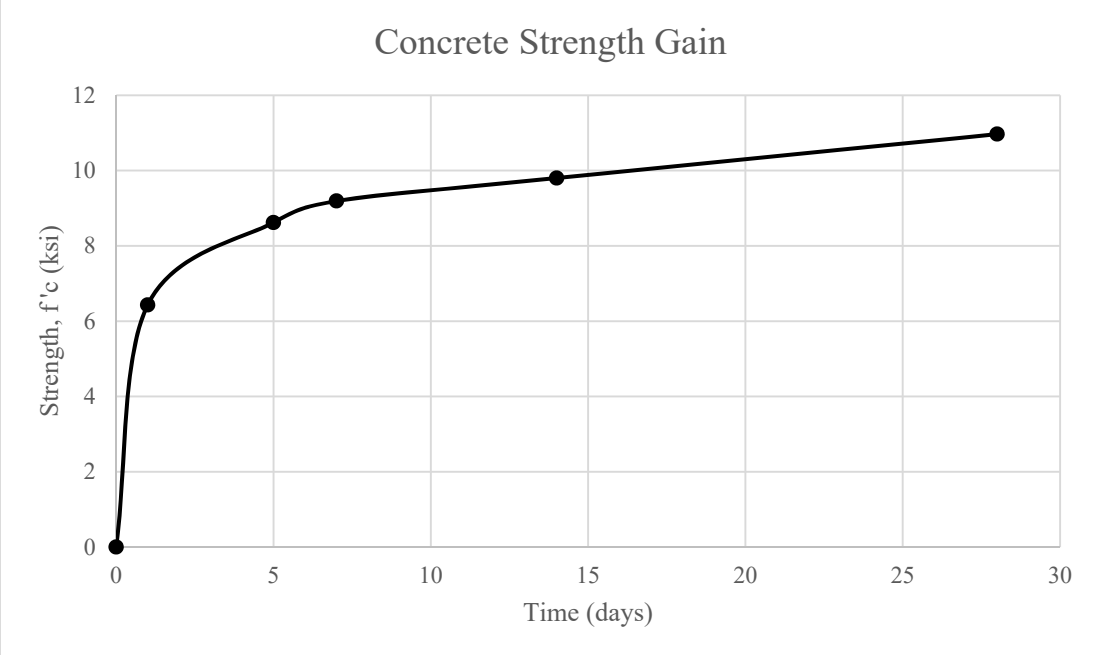

Figure 34: Compressive strength gain over time

Fresh property tests conformed to the requirements set by the American Society for Testing and Materials (ASTM). Slump tests were performed in accordance with ASTM C143. Because the concrete ordered was a SCC mix, the slump was not useful. Therefore a slump flow test was conducted in accordance with ASTM C1611 (2009). The design spread was set to be 16.5 in. ± 2.5 in.

To calculate the quantity of concrete needed, the volume of the tie was calculated using the dimensions of the tie shown in in Appendix B. When the concrete arrived on the day of the pour, it came with a very low slump of 5 in. and when using self-consolidating concrete the mix is expected to be far more fluid. Therefore 3 gallons of water were added and workability was achieved. However, due to the high heat of the day (above 90°F) the concrete began to set more quickly than expected. Therefore light vibration was used along the inside and outside the molds in order to ensure the concrete flowed into all voids. Figure 35 depicts this action and the method in which the concrete was poured into the molds.

Figure 35: Pouring the concrete into the molds and using light vibration to help flow of concrete

Following pouring, the top surface was lightly troweled. Figure 37 shows the finished ties that were then covered with burlap mats and kept continuously wet with cool water over the next 48 hours to minimize the heat gain from the hydration reaction and to also minimize the effect of high ambient (100°F) temperature. After at least 48 hours passed and the concrete met transfer strength, 4.8 ksi, the AFRP bars were cut and the ties were brought to the lab to be removed from their molds. Figure 37 shows a finished AFRP railroad tie on complete of the manufacturing process.

Figure 36: Finished ties

(a) (b)

Figure 37: (a) Plan view of AFRP tie; (b) cross sectional view of tie showing AFRP

5. EXPERIMENTAL PROGRAM

5.1 Vertical Load Test

This series of tests are used to determine if the concrete ties meet cracking strength. AREMA states that once a crack has occurred in a concrete railroad tie, it is deemed failed for service and thus require repair or replacement (AREMA 2014). This is because of the potential for water infiltration leading to possible corrosion of the prestressing steel within, and loss in strength of the concrete post cracking. To test this, AREMA has developed four test procedures for critical sections of the ties. For this research, a 100 kip actuator was selected to apply the load onto the tie. The actuator has a built in load cell to control the applied force as prescribed by the associated computer program. The program also measures time, and deflection by recording the change in stroke of the actuator piston. These data will be used in interpreting the results of the test.

Set up for these tests follows AREMA Chapter 30.4.1 and are described in Chapter 2 of this thesis. During testing, some adjustments were made to enable the completion of the experiment. First, the 1" x ½" rubber strips supporting the actuator, applied load, were replaced with ½" x ½" strips to increase the stability of the load. Next, the hardness of both actuator support strips and tie support pads were increase from 50A as prescribed by AREMA to a stiffer 70A to be more efficient with the materials. 50A rubber would splinter and tear after only a few tests and would need near constant replacement. Using Equations 1, 2, and 3 along with the design moments from Table 3 required loads were calculated and shown in Table 10.

Table 10: Applied loads for the vertical load test.

Applied Loads		
Positive Moment @ RS =	61.8	kip
Negative Moment @ RS =	28.8	kip
Negative Moment @ C =	17.0	kip
Positive Moment @ C =	10.4	kip

5.2 Instrumentation

Along with information provided directly from the actuator. Two other sensors were used on the tie to obtain data that were used in analysis. Two Linear Variable Differential Transducers (LVDTs) were placed along the side of the tie, one at the top and one at the bottom. These were used to measure differential displacement along the lateral face of the tie to assist in producing an accurate strain profile based on the applied load. String Potentiometers (string pots) were placed underneath the tie to measure the vertical deflection of the tie under load. Three string pots were used to create the deflection profile: two adjacent to the supports and the third at midspan under the load and within the constant moment region. Data collected from these sensors were used to compare to theoretical values and display the performance under the load and to detect whether cracking had occurred during testing. Figure 38 shows the design set up for the LVTDs for the rail seat section and center section respectively. LVDT 1 was always designated as the top and LVDT 2 the bottom no matter which way the tie was oriented. String pots 1-3 were labeled as such from right to left for both rail seat and center sections.

From the experimental test setup shown in Figure 38, the experimentally observed curvatures were derived as follows. First a strain profile was created by calculating the change in length of the LVDT and dividing by the length of that LVDT.

$$\varepsilon_i = \frac{LV_i - LV_0}{x} \tag{6}$$

Each strain then forms a profile and using geometry, curvature is found with

$$\phi_i = \frac{\varepsilon_t - \varepsilon_b}{h} \tag{7}$$

where LV_i refers to the data collected at time i from that specific LVDT, whether it be a top, t, or a bottom, b, sensor. LV_0 then refers to the initial length of the LVDT which is typically seen as zero. A typical strain profile of the tie is shown in Figure 39.

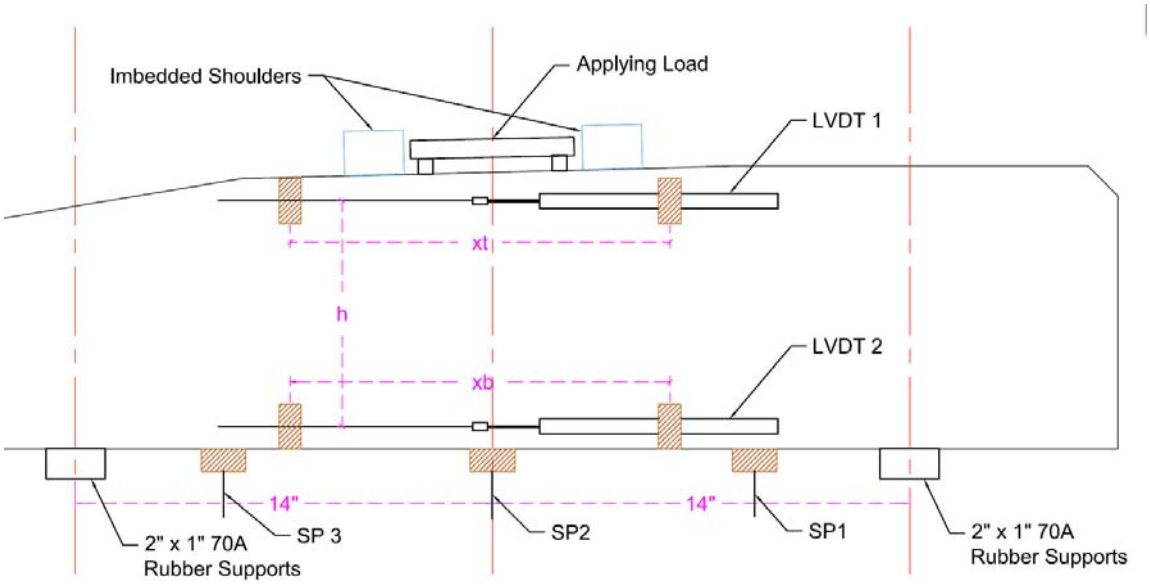

(a) rail seat

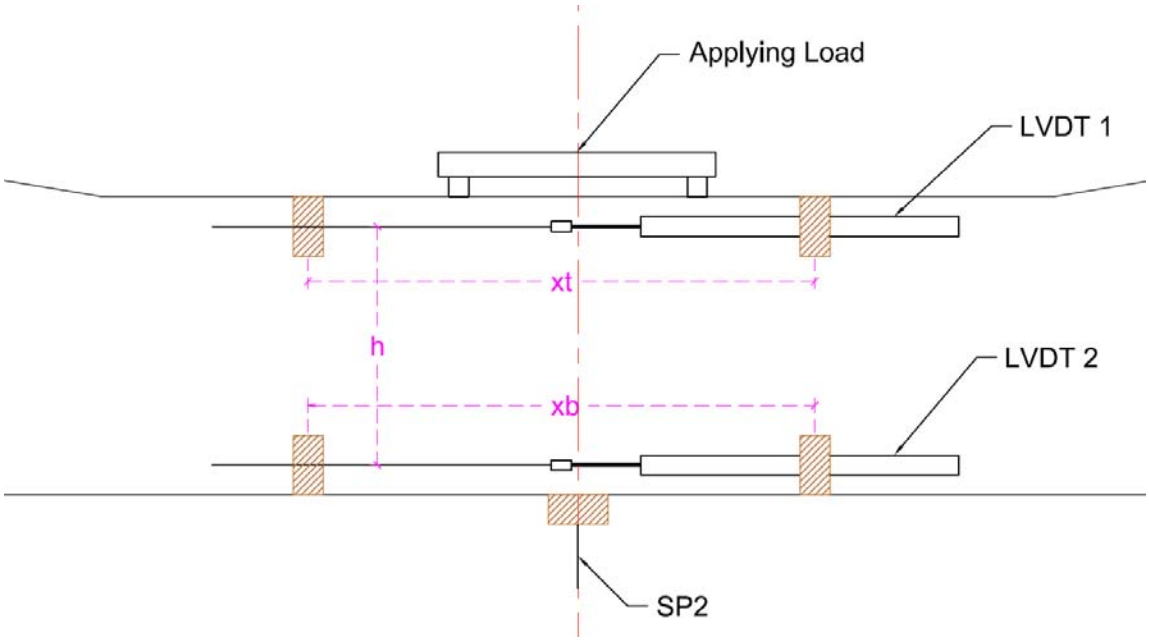

(b) center section

Figure 38: Instrumentation layout

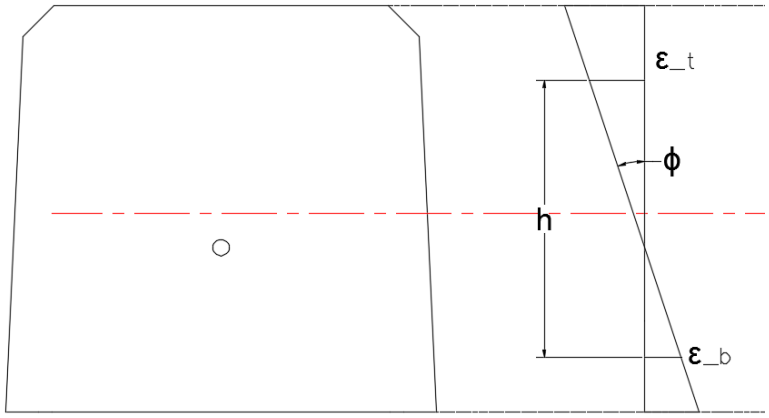

Figure 39: Typical strain profile for positive moment @ rail seat.

Using the fundamentals of material mechanics equation, $\phi = \frac{M}{EI}$, and integrating it over the length of the specimen, angle of deflection and the deflection profile were calculated. Because of the varying cross section of the rail tie across its length, a series of slices where made to plot the change in moment of inertia across the span. This was then used in combination with the bending moment diagram to determine the overall curvature diagram at each designated point, followed the deflection angle, and finally the displacement of each section. This theoretical deflection profile was then plotted against the measured deflection found from the string pots' data. With this information it was concluded that a theoretical deflection was unnecessary in determining adequacy of the newly constructed ties reinforced with AFRP. Because of a lack in information regarding expected/required deflection from AREMA and the knowledge that in-service ties are continuously supported on compacted ballast, only a comparison of deflection was done between ties using steel reinforcement and AFRP.

5.3 Repeated Load Test

The repeated load test is intended to simulate fatigue loading on the tie. Setup for this experiment follows AREMA Chapter 30.4.9.1.5 *Rail Seat Repeated-Load Test* and is previously described in Chapter 2 of this thesis. The design cracking moment to be used in this experiment was 398 kip-in which follows the manufacturer's guidelines for the rail seat positive test. Following Equation 1 from the previous section, the cracking load, P_c is equal to 67.7 kips.

The lab set up followed similarly to the setup for the positive rail seat vertical load test but with the 2"x1" rubber support strips replaced with 8" x ¼" thick sheets of 70A rubber. The sheets are far superior to the strips, being able to withstand the repetitive load due to the lack of compression seen by the thicker rubber strips. Another change that was made was to replace the load supporting rubber with ¼ in. thick birch hardwood plywood. Also, to prevent the tie from 'walking' while the cycles commenced, the two rocker supports were tack welded to the floor a piece of sheet metal securely fastened to the strong floor of the lab. The completion of this test was not covered in the scope of this research.

5.4 Ultimate Load Test

The ultimate load test is intended to determine the failure point and mode of the ties and follows AREMA Chapter 30.4.9.1.8 *Bond Development, Tendon Anchorage, and Ultimate Load Test* for the setup and running of the experiment. This procedure was described previously in Chapter 2 of this thesis, but the completion of this test was not covered in the scope of this research

5.5 Electrical Resistivity

An electrical resistivity test was a non-destructive test performed on the ties. Electrical resistivity describes a concrete structure's ability to resist electrical current across the length of the structure. Knowing the resistivity of the concrete can help determine if corrosion has occurred or has the potential to occur, and how fast it will

corrode. Because railroads use a low voltage electrical current through the rails to form the train circuits, having a high resistant tie across the two rail seats should prevent any false shorts from occurring. These false shorts may cause loss of track occupation. If a sufficiently large resistance can be demonstrated with the non-conducting AFRP tendons then it may be possible to modify and relax the Pandrol fastening insulation requirements between the rails and the Pandrol shoulders.

Two methods were used to determine the resistance of the ties: a resistivity meter and a MultiMeter. The resistivity meter was a Resipod Proceq© meter which incorporates a 4-point Wenner probe to measure the electrical resistance of concrete over a known distance. This is done by sending an electrical current into the concrete through the outer two probes and the potential difference is read by the inner two, as seen in Figure 40. The resistivity is then calculated by the probe using Equation 6

$$\rho = 2\pi a \frac{V}{I} \tag{8}$$

where ρ = the resistivity (kΩcm); a = the cross sectional area; V = the potential difference (or voltage); and I = the current. It was determined that the larger the resistivity the less likely corrosion will occur and the lower the rate corrosion will take place if prevalent.

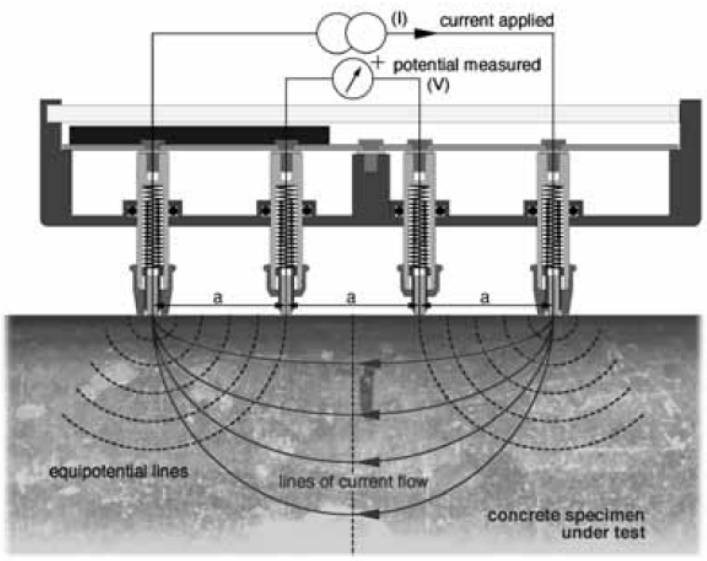

Figure 40: Proceq resistivity measurement principle (Proceq SA)

Using this information, 30 different locations were tested for each tie following the pattern laid out in Figure 41. This pattern includes longitudinal measurements (1-17) and transverse measurements (18-30) to compare how the reinforcement affects the reading of the meter. There were also specific tests within the rail seat area to determine if there were significant differences there compared to sections with less steel involved, i.e. the center of the tie. These same measurement points were used on both ties with AFRP and Steel reinforcement and are labeled as such in documenting the results.

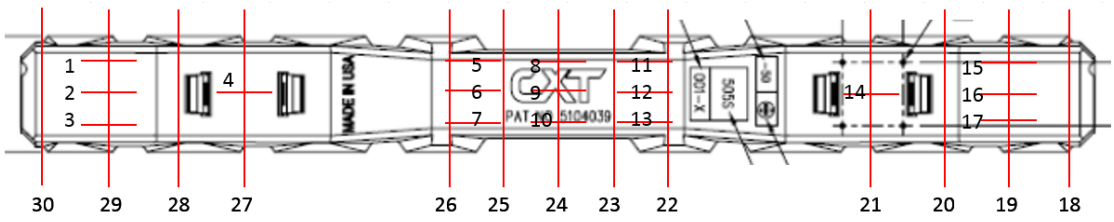

Figure 41: Plan view of tie with Proceq© measurement points labeled 1-30

The second method involves using a standard MultiMeter. The positive and negative leads of the MultiMeter are attached to the embedded shoulders, seen in Figure 42 and the resistance is measured and read by the meter. MultiMeters create an electrical potential that is sent through the positive lead into the subject from which resistance is measured, then picked up by the negative lead which returns the change in electrical potential (voltage) to the meter which then calculates, using Ohm's Law, the resistance of the specimen. This method was used primarily as a comparison test to see the difference in resistance between the AFRP and steel reinforced ties.

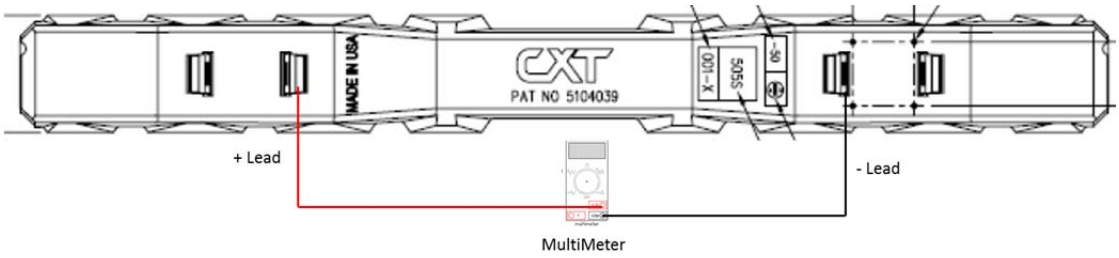

Figure 42: MultiMeter setup with positive and negative leads attaching to the inner shoulders

6. EXPERIMENTAL RESULTS OF AFRP REINFORCED TIES

6.1 Introduction

This chapter focuses on the results of the vertical load test on the newly constructed concrete ties utilizing the AFRP reinforcement. Four ties were constructed out of the molds made from one of the steel reinforced ties. All four ties were tested in accordance with AREMA testing procedure for mono-block ties under static vertical load. The primary purpose of the vertical load test was to determine if the tie met service load requirements by not cracking under a specified load. Therefore, a theoretical cracking load is needed so that a comparison can be made between the physical test results and the theory. Using the theoretical cracking load, moment-curvature plots were created and used to compare to curvature data recorded during testing. Curvature is defined from the relationship

$$\phi = \frac{M}{EI} \tag{9}$$

in which EI = the flexural stiffness derived from the modulus of elasticity of the concrete and the gross section moment of inertia; and M = the applied moment where the cracking moment is defined by Equation 10 with $S_{x,bot}$ = the section modulus of the cross section at the tension face of the concrete tie.

$$M_{cr} = f_t S_{x,bot} + \frac{FS_{x,bot}}{A} \pm Fe \tag{10}$$

$$f_t = 6\sqrt{f'_c} \tag{11}$$

Using Equation 10 and substituting into Equation 9, the cracking curvature can now be defined as

$$\phi_{cr} = \frac{M_{cr}}{E_c I_g} \tag{12}$$

The experimental curvature may be found from the sectional strain considerations as follows:

$$\phi = \frac{\varepsilon_{LV1}}{x_t h} - \frac{\varepsilon_{LV2}}{x_2 h} \tag{13}$$

in which ε_{LV} refers to the strain recorded by the LVDT sensor as previously described in Chapter 5. This curvature was used to create a moment-curvature plot where a comparison was made between the experimentally determined curvatures and the theoretical cracking curvatures for each test case.

A second comparison was made through the deflection profile of the specimen measured via the strings pots described previously. To obtain this deflection profile, three string pots were placed under the tested section; two adjacent to each support and one at midspan under the applied load, Figure 38. To complete the calculations, general section properties were calculated based on information provided by the manufacturer found in Appendix A. This information is then shown in Figure 43and in Appendix B for further detail. With this information and the previously described equations, the cracking moment and curvatures were found for each test case and are listed in Table 11.

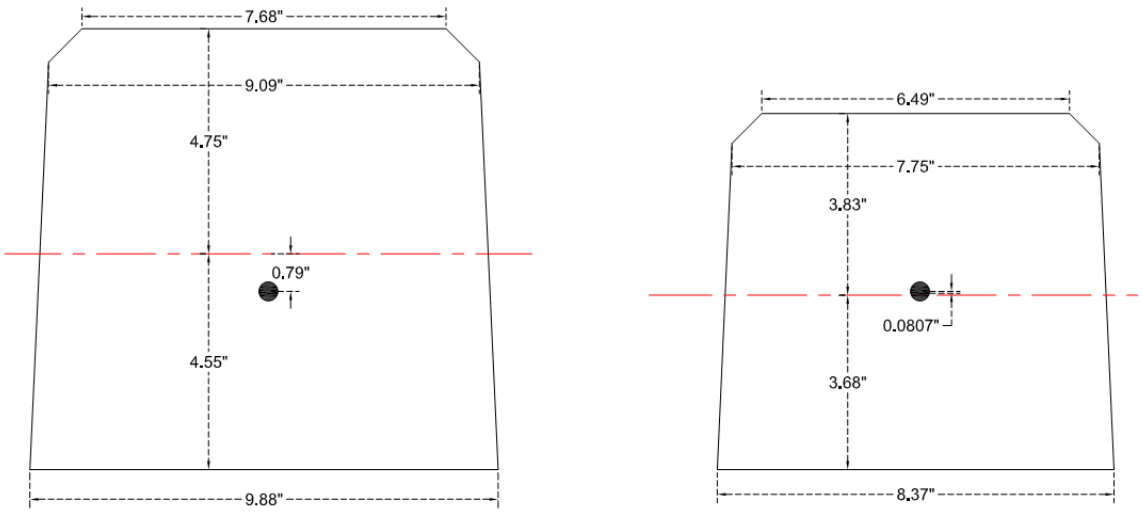

Figure 43: Cross section of rail tie with netural axis and AFRP centroid location

Table 11: Theoretical cracking moment and curvature for AFRP reinforced ties

Section Property	Rail Seat		Center	
	+	-	+	-
A (in^2)	87.57		59.94	
I_g (in^4)	623.8		324.5	
S_x (in^3)	136.8	131.3	75.68	72.91
E_c (ksi)	5973		5973	
f_t (ksi)	0.628		0.628	
M_{cr} (kip-in)	268.3	137.5	139.0	146.7
ϕ_{cr} (rad/in x 10^{-6})	72	36.9	83.6	88.2

6.2 Rail Seat Positive

This section focuses on the results from the rail seat positive moment, RSP, test. This test follows the set up described by Section 5.1.1 and AREMA 30.4.9.1.4. Cracking moment and curvature were first determined by means of the equations presented previously and because the applied load for this test was expected not to cause any cracking, the cracking moment and curvature were plotted linearly for comparison to the physical results. To accommodate the service moment of 378 kip-in a vertical load of 61.8kip was applied to the rail seat section as shown previously in Figure 6. The load was applied at a rate of 4 kip/min and checked for cracking along the bottom edge. The four newly constructed ties reinforced with AFRP were tested and compared to the theoretical values. The raw data was collected from a data acquisition system (DAQ). The DAQ saved data at one second intervals and collected data provided by the 100 kip actuator, and the sensors attached to the specimen.

It was found that cracking occurred in all four ties under the applied load. This can be attributed to the problems during construction. A majority of the AFRP bars were not able to be stressed to the design load because of breakages during the stressing procedure. Nonetheless, the ties did see noticeable strength that can be comparable to a tie with steel assuming similar prestressing levels. Recommendations for improving the stressing procedure are outlined in the recommendations section of Chapter 8. Although cracking occurred, crack size did not exceed 0.004 in. in width. This indicates that the

depth of the crack may not have reached the AFRP bars within and only cracked the cover concrete. Figure 44 shows the profile of the tie section under full load with the cracks outlined in blue. The location of the cracks falls within the expected region of the tie, the constant moment region.

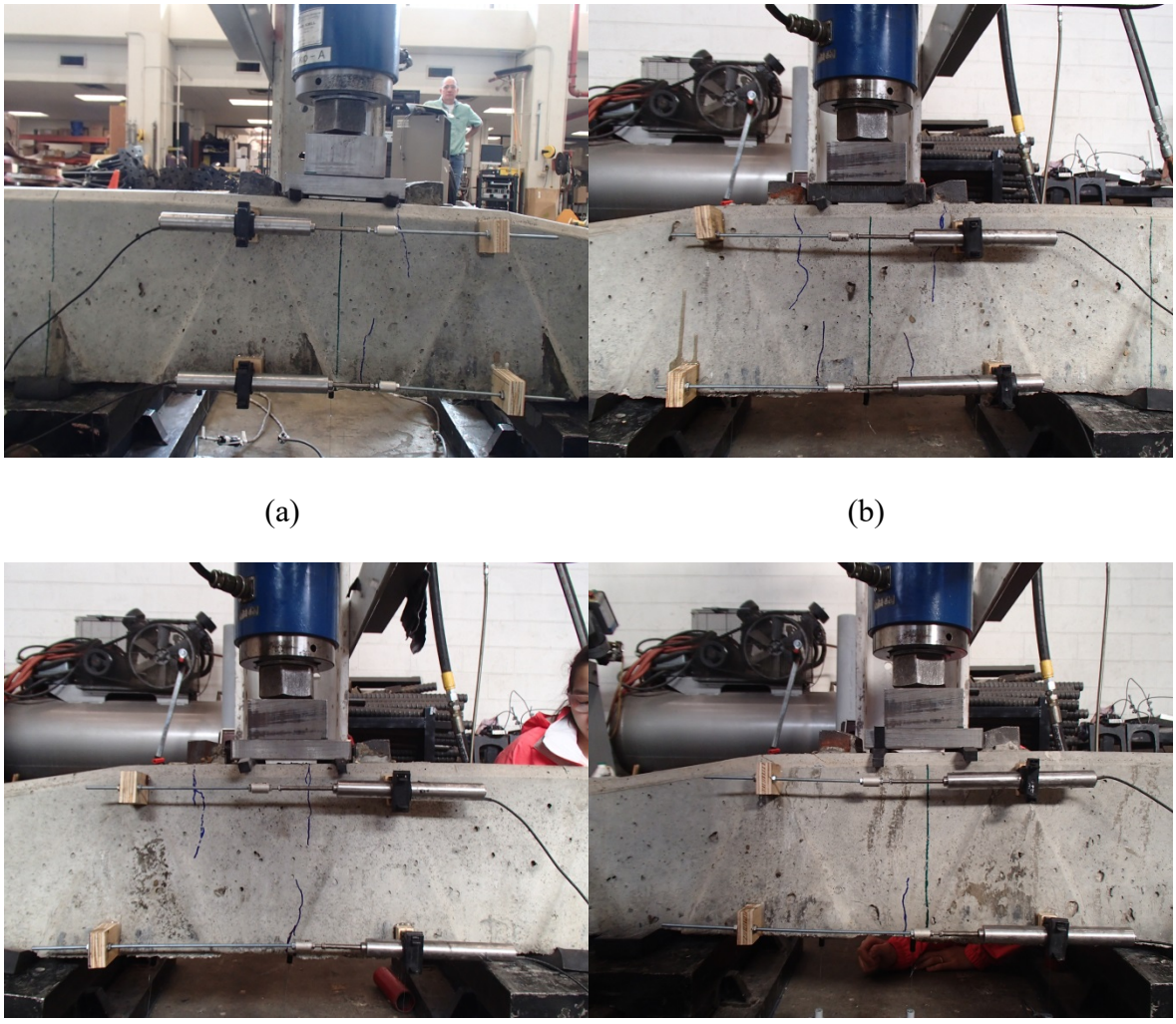

(a) (b)

(c) (d)

Figure 44: Fully loaded ties under rail seat positive testing for (a) AFRP 1, (b) AFRP2, (c) AFRP 3, and (d) AFRP 4

6.2.1 Moment-Curvature

Using the cracking moment of Table 11, experimentally observed moment-curvature relationships were used to check the accuracy of the theoretical equations discussed previously. Following the procedure of Chapter 5, moments and curvatures were calculated based on the data provided from the installed instrumentation. The curvature values were then plotted against the applied moment at the time, i and are shown in Figure 45. It can be seen that the theoretical values accurately portray the behavior of the specimen under this loading with the cracking moment = 268.3 kip-in. with a curvature = $72x10^{-6}$ $^{rad}/_{in.}$. Even the post cracking moment and curvature has been accurately portrayed.

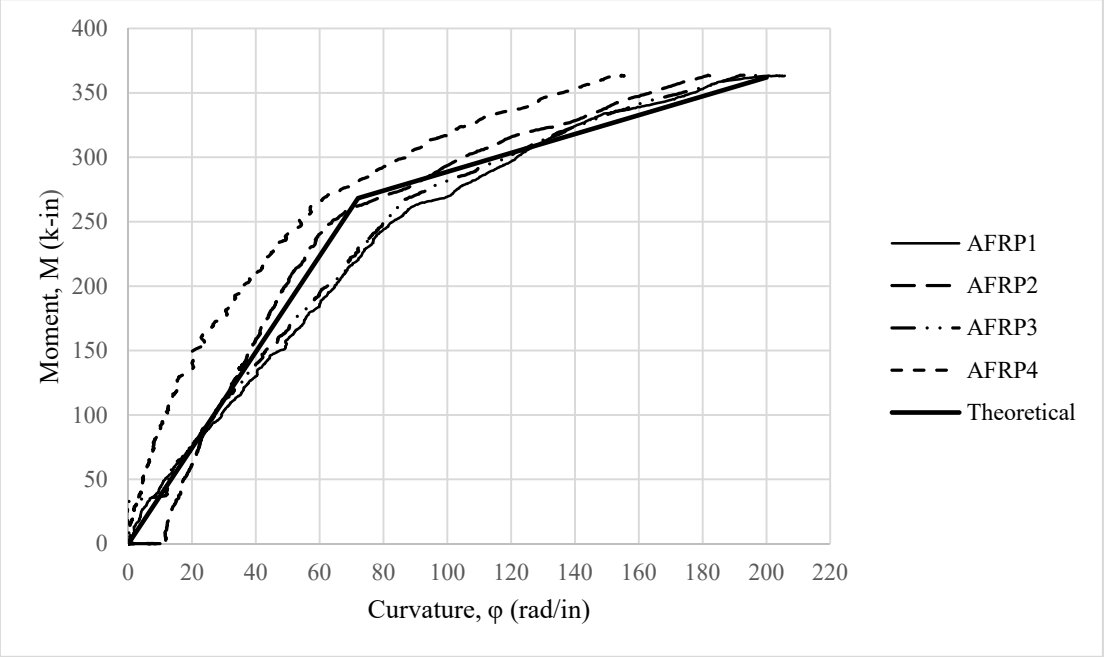

Figure 45: Moment-curvature plot for AFRP reinforced ties for rail seat positive testing

6.2.2 Deflection Profile

The deflection of the ties was determined from the string pots placed beneath the loaded side of the tie. The string pots were secured by small pieces of plywood glued onto the tie with epoxy. A small metal hook was then attached to the wood where the line of the string pot was hooked onto. After being zeroed out with no load applied, the measured change in length represented the deflection of the tie at that specific point. With the full load applied, the deflection was averaged for each string pot and was plotted at the location where the hook was placed along the tie. This created the deflected profile shape seen in Figure 46. It was noticed that the deflection was more linear than the expected symmetric curve. This occurred because of the non-symmetric cross section through which testing took place, and therefore non-symmetric stiffness. Also, by having one of the supports directly in line with the transition section of the tie, applied loads created a small sloping affect which altered the deflection data. Due to compression of the rubber strips at the supports, initial deflection is a non-zero value making the actual deflection observed less than what was recorded by the string pots. Because of this and the lack of requirements involved with deflection, theoretical values were not calculated but direct data was compared to deflection data of ties reinforced with steel strands which will be discussed later.

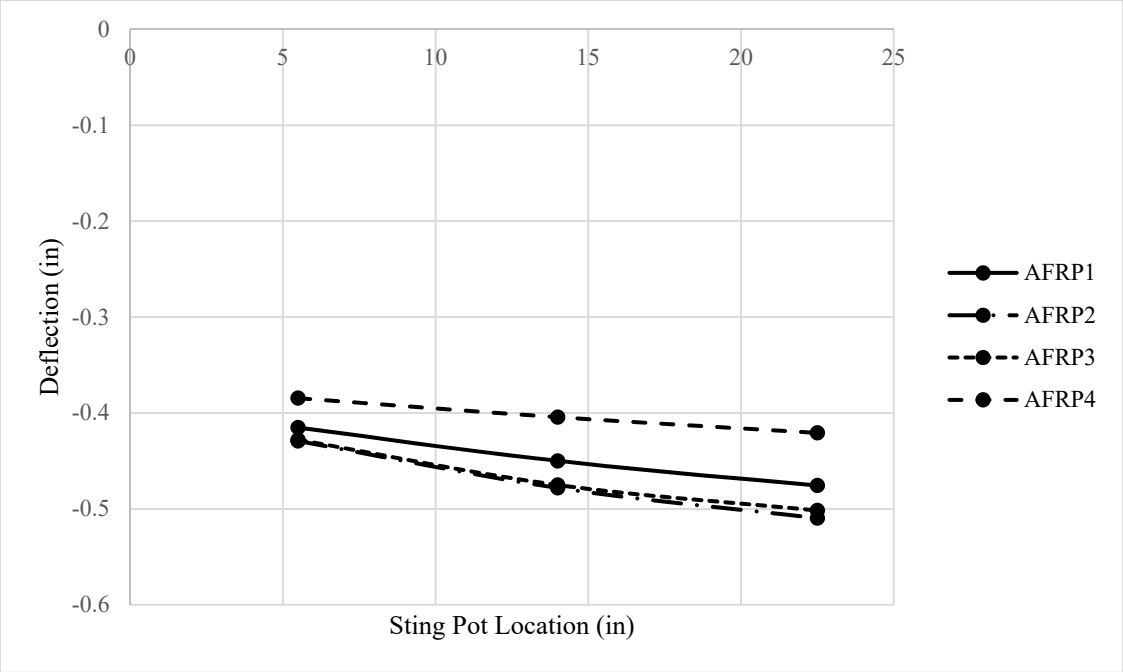

Figure 46: Deflection profile for the rail seat positive test

6.3 Rail Seat Negative

This section focuses on the results from the rail seat negative moment, RSN, test. This test follows the set up described by Section 5.1.2 and AREMA 30.4.9.1.4. Cracking moment and curvature were first determined by means of the equations presented previously and because the applied load for this test was expected not to cause any cracking, the cracking moment and curvature were plotted linearly for comparison to the physical results. To accommodate the service moment of 157 kip-in a vertical load of 28.8kip was applied to the rail seat section as shown previously in Figure 7. The load was applied at a rate of 4 kip/min and checked for cracking along the bottom edge.

After completion of the static load testing, data points were plotted similarly to the RSP test previously completed. Like the RSP test, all four of the AFRP ties saw cracking under the full load. This crack is most likely due to the embedded rail seat; cracks initiated and propagated along the inside face of one or both steel shoulders. This indicated a stress concentration at the steel shoulder that was larger than the tensile stress

at the maximum moment region. Another cause for the cracking is due to the previous test; because cracking occurred in the RSP test the specimen became damaged and therefore lost strength allowing for a premature cracking. Figure 47 shows these cracks and their height; however, none saw a width of more than 0.004 in. which, like the RSP test, shows that only cover concrete cracked and there was no loss in development of the AFRP bars.

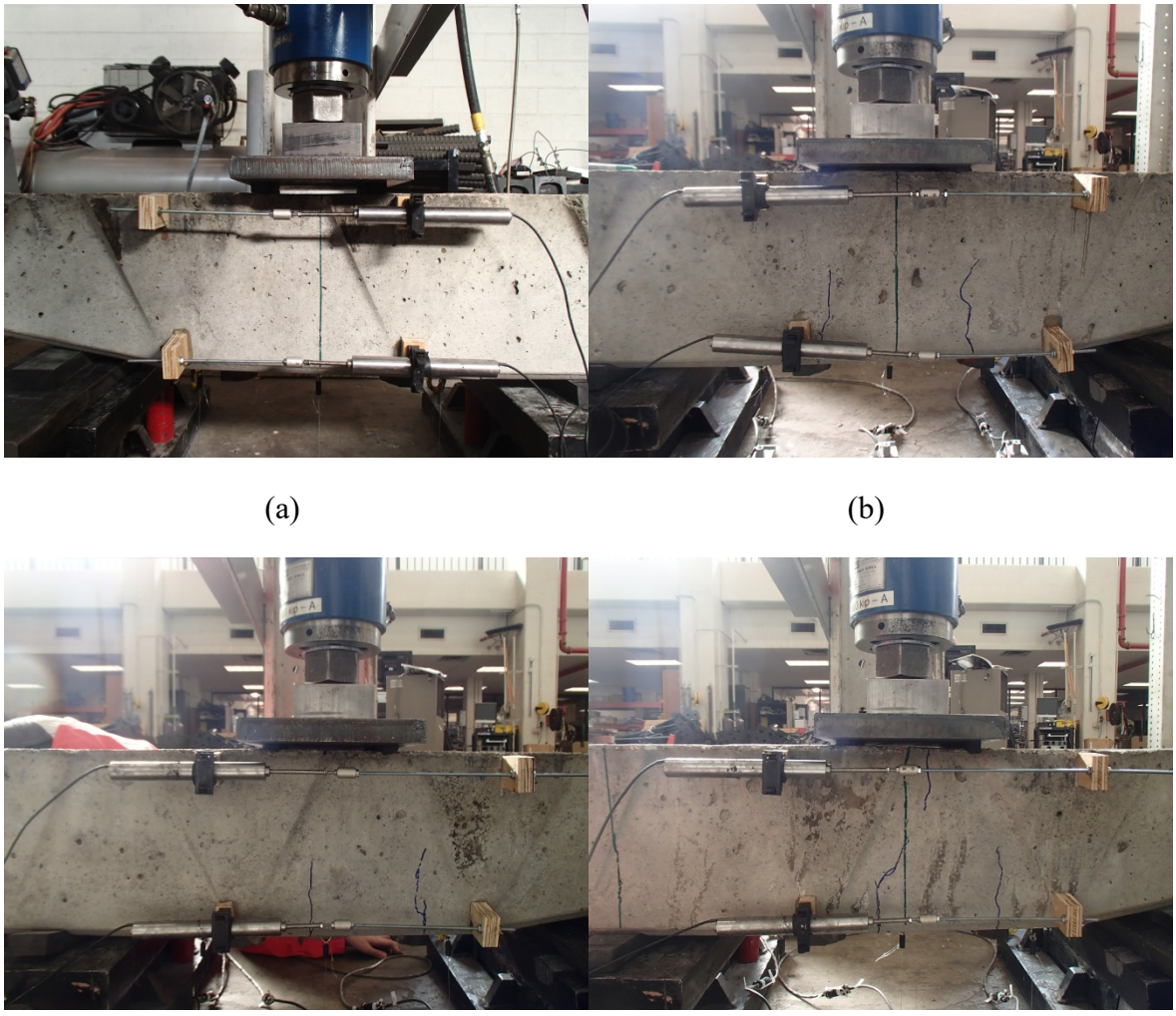

(a) (b)

(c) (d)

Figure 47: Fully loaded rail seat negative testing for (a) AFRP 1, (b) AFRP 2, (c) AFRP3, (d) AFRP 4

6.3.1 Moment-Curvature

With the completion of the RSN testing, data were gathered and interpreted by means of the equations discussed previously and a moment curvature plot was developed. This plot, Figure 48, was made using the data collected from the LVDTs installed on the side of the tie specimen outlined in Figure 38; the increase or decrease in length, based on a zero value prior to testing, was used to determine the strain profile of the specimen which was then used to calculate the curvature. Positive strain represented tension while negative represented compression so by having a positive curvature means the underside of the tie is in tension as expected.

For this chart, it is clearly seen that the ties accurately follow the theoretical line of curvature. However, it can be seen that all four ties cracked around 90 kip-in of applied moment which is far below the calculated moment of 139 kip-in. This can be attributed to a stress concentration at the embedded shoulders or damage caused by the previous test compromising the strength of the tie.

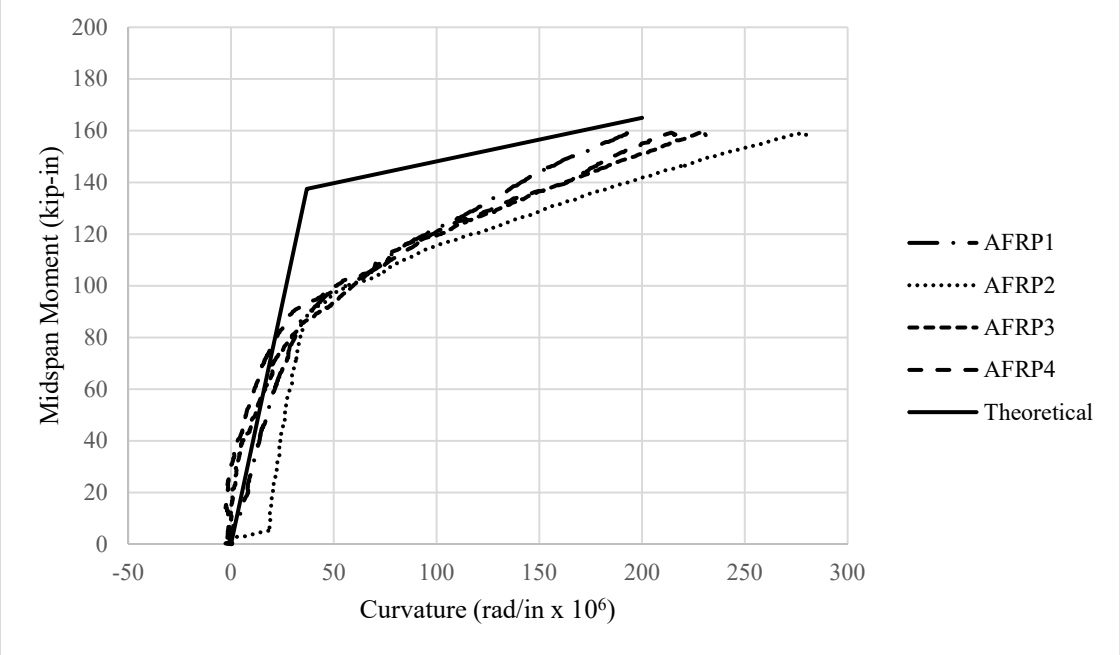

Figure 48: Moment-curvature plot for rail seat negative testing of AFRP reinforced ties

6.3.2 Deflection Profile

As with the RSP test, three string pots were placed underneath the tie specimen and were used to measure total deflection of the tie as the load is applied. The string pot data under full load was then averaged together and plotted with respect to its specific location under the tie to create a profile of the deflected shape. Figure 49 reveals the profile of the tie. This profile is slightly more curved than the RSP test because of the lower loading applied. The tie's differential stiffness did not play as large of a role in altering the deflection profile. However, like with the RSP test, initial deflection is non-zero because of the compression of the rubber supports. AFRP 2 had sensor 1 become detached during testing resulting in a skewed profile for that tie.

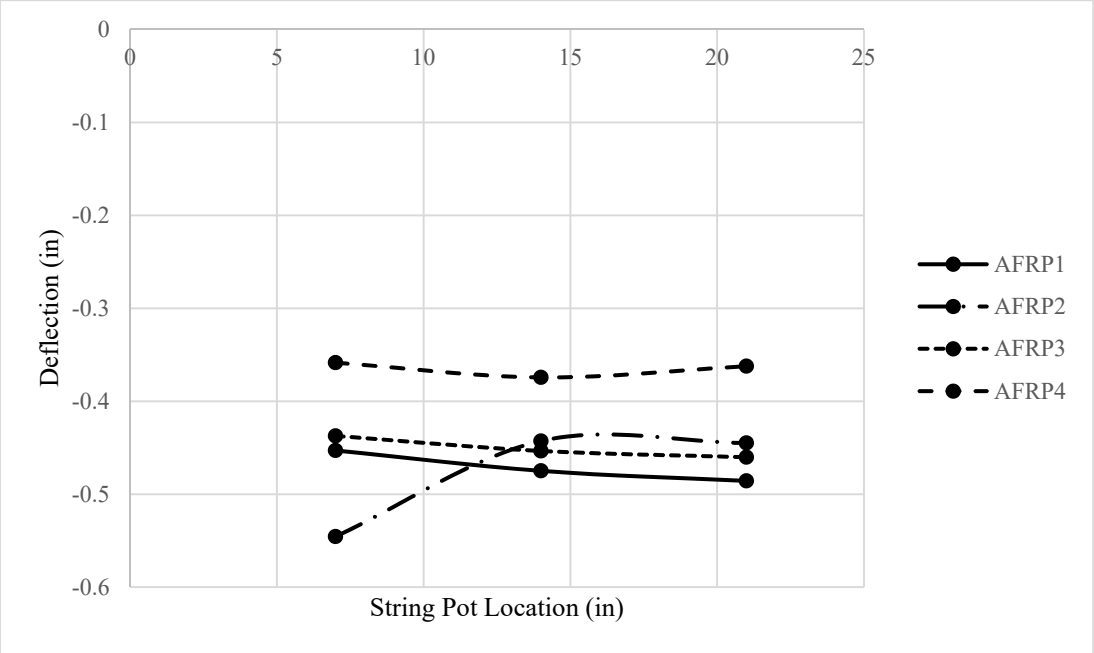

Figure 49: Deflection profile for rail seat negative testing with AFRP

6.4 Center Positive

The center positive, CP, test followed the procedure outlined in Section 5.1.2 with having supports located 30 in. from the center and an applied load of 10.34 kips. Like the prior tests, the load was increased at a rate of 4 kip/min and was subsequently checked for cracking. It should also be noted that this was the only load condition that did not alter based on information provided by the manufacturers. Figure 50 shows the four tested ties under the full load displaying the lack of cracking. Like the rail seat tests, LVDTs and string pots were used to measure relative deflections and used to determine moment-curvature plots and deflection profiles for each specimen.

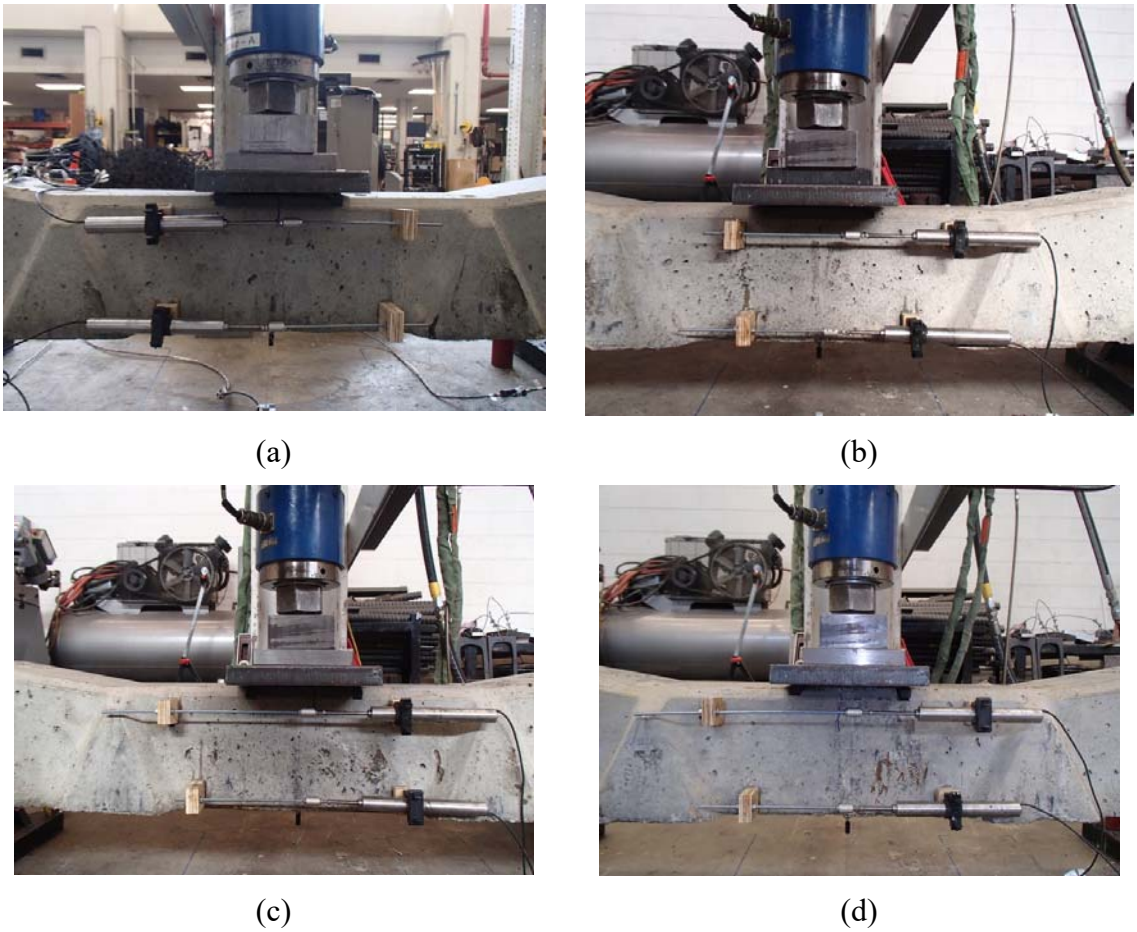

(a) (b)

(c) (d)

Figure 50: Fully loaded center positive testing for (a) AFRP 1, (b) AFRP 2, (c) AFRP3, (d) AFRP 4

6.4.1 Moment-Curvature

With the completion of the CP testing, data were gathered and interpreted by means of the equations discussed previously and a moment curvature plot was developed. Figure 51 was made using the data collected from the LVDTs installed on the side of the tie specimen outlined in Figure 38; the increase or decrease in length, based on a zero value prior to testing was used to determine the strain profile of the specimen which was then converted into a curvature. All four ties had curvature slopes parallel to the theoretical line and it is seen that testing concluded before any could reach cracking which met the expected value. The initial spike in moment with no increase in curvature is simply due to the compression of the rubber supports prior to bending of the tie.

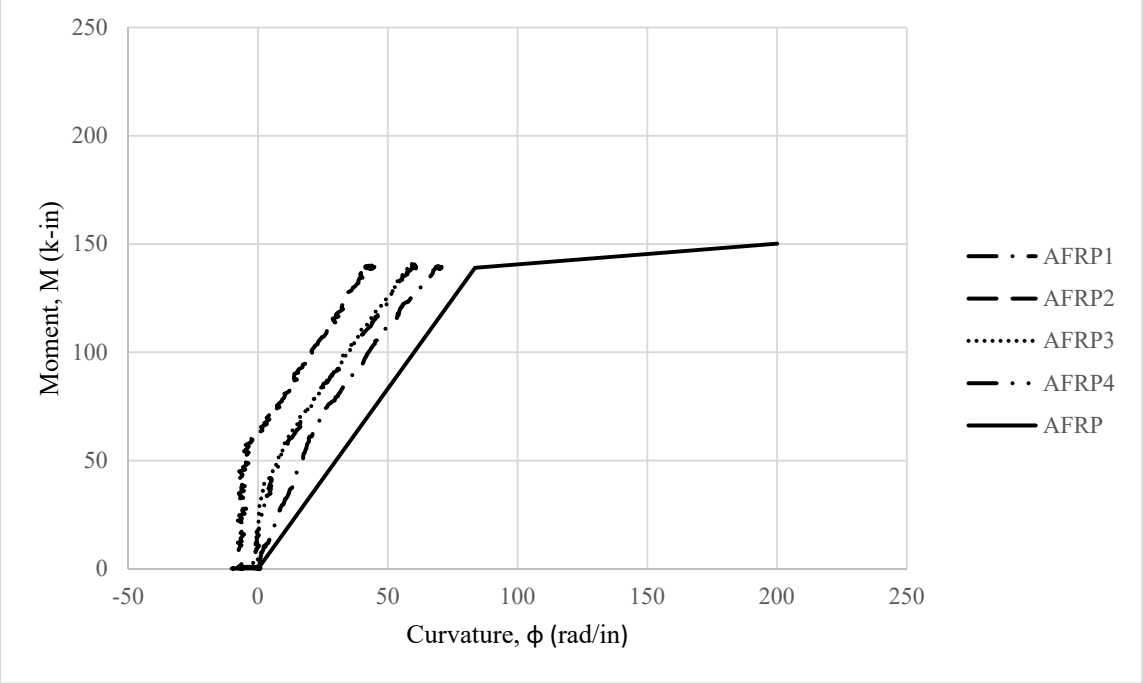

Figure 51: Moment-curvature plot for center positive testing of AFRP reinforced ties

6.4.2 Deflection Profile

As with the other previous tests, three string pots were placed underneath the tie specimen and were used to measure total deflection of the tie as the load was applied. The string pot data under full load was then averaged together and plotted with respect to its specific location under the tie to create a profile of the deflected shape. AFRP 3 and 4 have smaller deflections because during testing, the rubber support strips were switched from 50A rubber to 70A rubber. The increased hardness did not allow as much initial compression allowing the tie to show a smaller deflection. However, the profiles for all four are similar enough to draw accurate conclusions about the test as a whole.

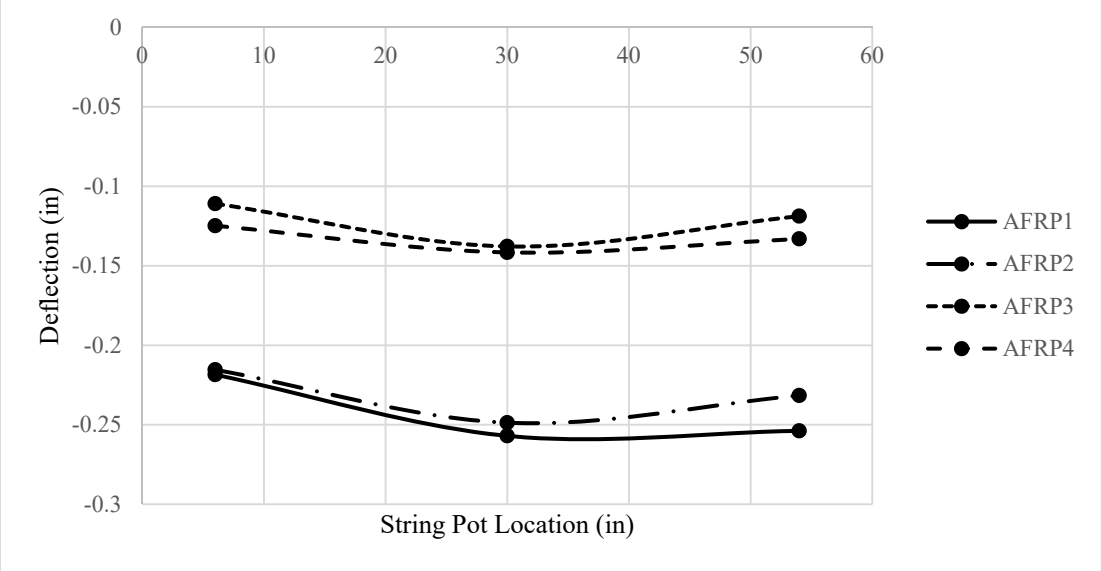

Figure 52: Deflection profile for center positive testing with AFRP

6.5 Center Negative

The final test performed on the newly constructed concrete ties was the center negative, CN, test. Similarly to the center positive test, supports were placed 30 in. on center and the load applied to a plate that was supported on ½ in. x ½ in. rubber strips spaced 6 in. on center. A load of 17 kips was then applied to the tie at a rate of 4

kips/min and the tie was then checked for cracks. Figure 53 shows each fully loaded specimen and any cracking seen in that tie. Three out of the four tested specimens saw cracking under the full load, however, cracking occurred at approximately 15 kips and their respective widths were no more than 0.004 in.

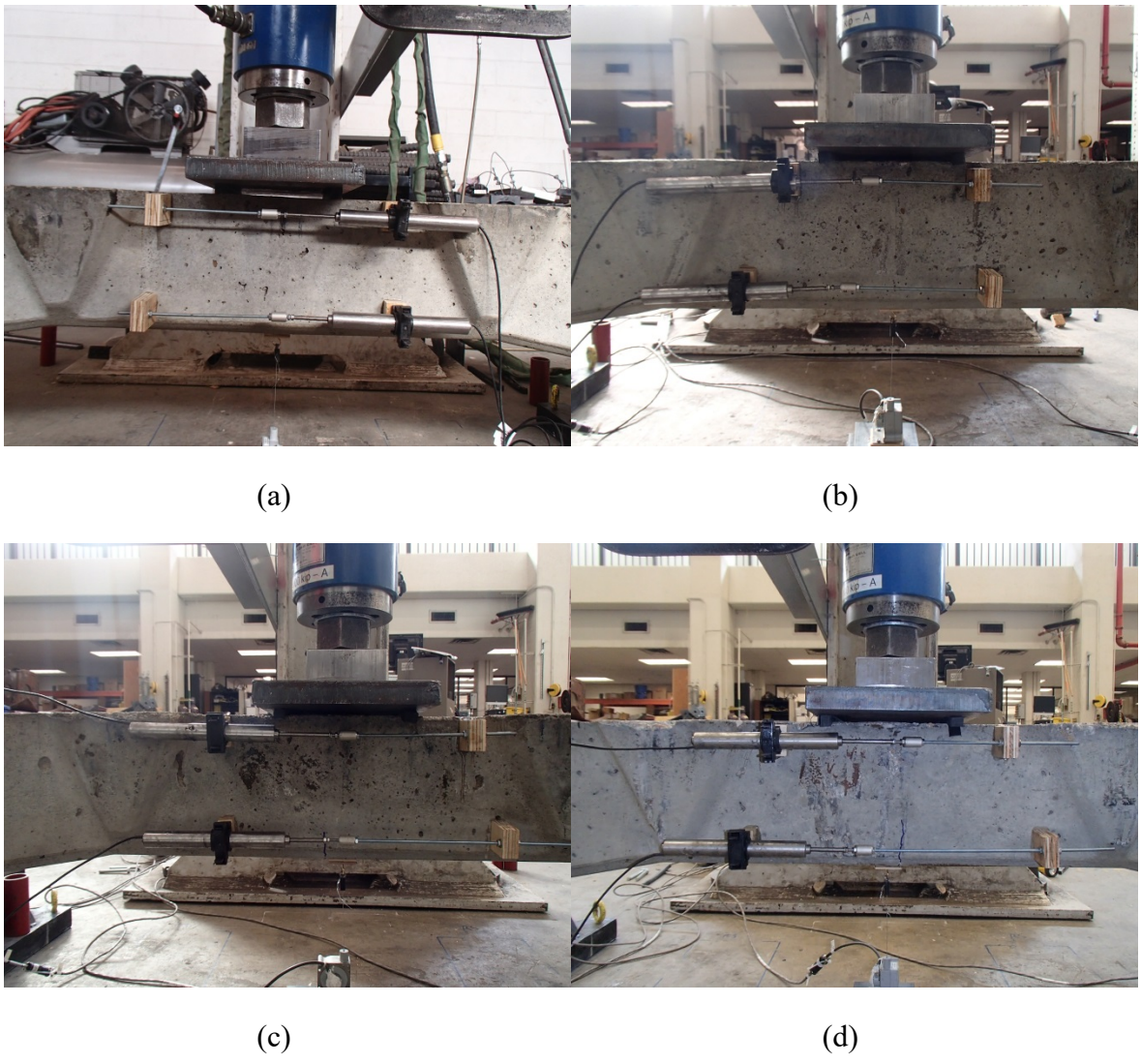

(a) (b)

(c) (d)

Figure 53: Fully loaded center negative testing for (a) AFRP 1, (b) AFRP 2, (c) AFRP3, (d) AFRP 4

6.5.1 Moment-Curvature

As with the CP test, LVDTs were placed along the side of the specimen to track the strain changes at the top and bottom as the load increased. Strain was calculated via the ratio of measure length change over the original length. Negative strain indicates compression while positive strain indicates tension. These strain values were then used to calculate the curvature of the specimen at the point of loading. Data points converted to curvature points were then plotted against the increasing moment applied at this location laid out in Figure 54. Collected data follows closely with the slope of the theoretical line until approximately 160 kip-in moment where a slight change in slope occurs. This depicts the cracking in the ties that experienced cracks during testing. The line for AFRP 2 was cut short due to a programming error in the actuator causing the test to stop before the full load was applied, but based on the projection of the curvature, similar results should have been attained.

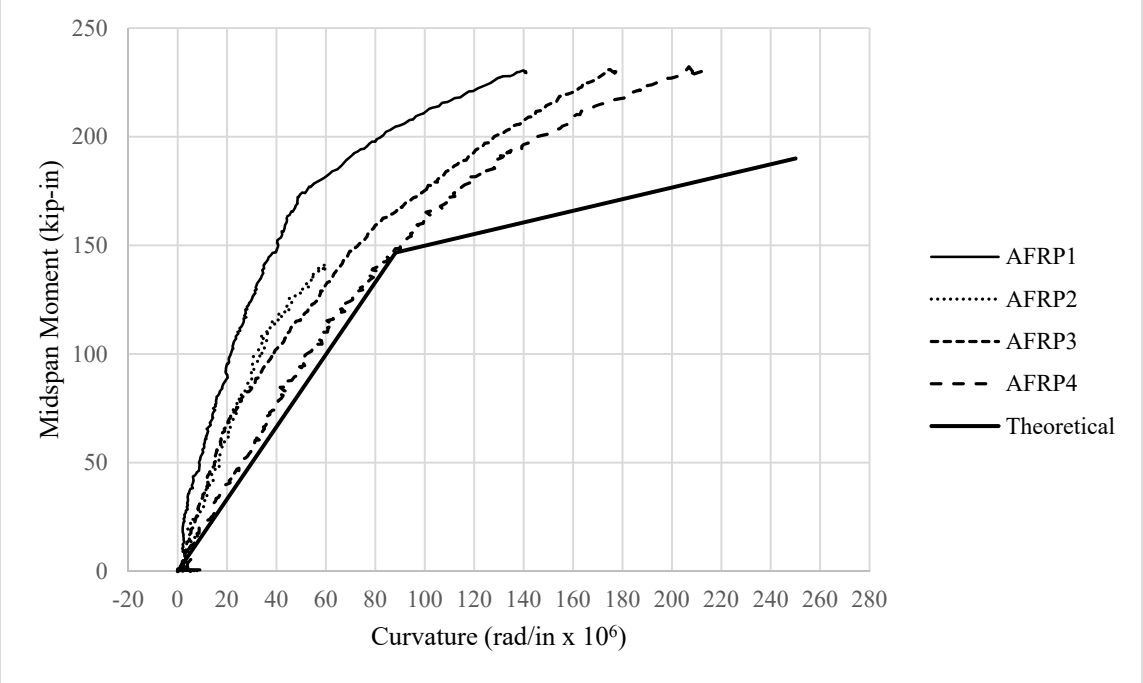

Figure 54: Moment-curvature plot for center negative testing with AFRP

6.5.2 Deflection Profile

String pots were placed under the tie specimen at three different locations: two adjacent to the supports, and one directly under the load. These sensors measure deflection of the tie and can be used to plot a deflection profile of the tie. To obtain the deflection profile, data from the string pots at the point of full load were compiled together to create an average deflection at the location of the string pot. These data points were then plotted in Figure 55 against their location relative to the end of the tie creating the deflection profile. Clean symmetric curves were seen in nearly all tested ties. AFRP 2 had a shallower curve due to an error in testing, and AFRP 4 had stiffer support rubber preventing the large initial deflection seen by the others.

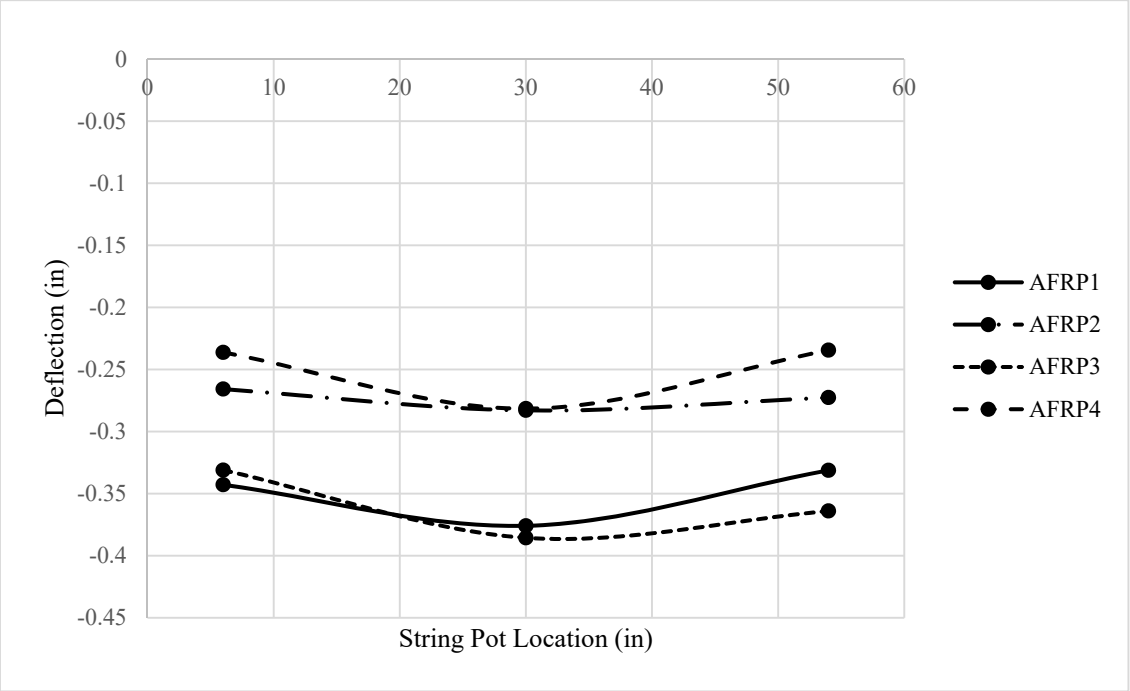

Figure 55: Deflection profile for center negative testing of AFRP ties

7. COMPARISON OF AFRP AND STEEL REINFORCED TIES

7.1 Introduction

This chapter looks at the results of the tested concrete ties with AFRP reinforcement laid out in Chapter 6 and compares them to an assumed steel result based on geometry and data provided by the tie manufacturer. Using the geometry and design moment, theoretical material property equations were used to estimate the moment-curvature and deflection profile of a tie reinforced with steel strands to compare to the AFRP bars that were used in construction and experimentation.

The other comparison that was made was for the electrical conductivity of the ties. Since no major theoretical values were provided or calculated, this was a direct comparison between the resistance found in the ties reinforced with steel and the ties reinforced with AFRP. As described in Chapter 5, a MultiMeter was used to measure the resistance across the ties. The positive lead and negative leads were attached to the inner steel shoulders and the resistance provided by the tie was read. Ties with higher resistance values have a lower chance of corroding or experiencing accidental shorting during its service life.

7.2 Electrical Conductivity Results

When conducting the electrical conductivity tests using the Proceq resistivity meter, a plan of measurement was made utilizing both longitudinal and transverse data. The longitudinal data were taken in parallel with the reinforcement along the edge of the tie and at the centerline, Figure 41. This was done to compare how concrete cover affected the results and the location of the reinforcement. On average, resistivity was greatest at the edges of the tie in the longitudinal direction. These data points are laid out in greater detail in Appendix D. Because the concrete in the AFRP reinforced ties was still curing, resistivity increased over time. Therefore measurements were taken each week in the same pattern to compare how concrete curing affected the results and are listed in Table 12. The fact that the concrete was young relative to the ties with steel reinforcement meant that there was still a good amount of moisture remaining within the

concrete. This moisture makes the concrete tie much more conductive than its steel reinforced counterpart which is proved by the results. It can be assumed that over a much longer period of time and with proper drying of the cured concrete, resistivity results are expected to be more comparable to the manufactured ties.

Table 12: Proceq measured resistivity averages and standard deviations (kΩcm)

Testing Date	AFRP_1		AFRP_2		AFRP_3		AFRP_4	
	Mean	Std. Dev	Mean	Std. Dev	Mean	Std. Dev	Mean	Std. Dev
8/23/2015	15.3	2.9	15.8	2.7	16.5	3.6	26.6	42.8
9/1/2015	20.8	4.5	20.1	4.5	19.6	4.1	36.8	58.5
9/8/2015	23.6	5.1	23	5.2	22.3	4.7	44.6	74.3
9/14/2015	26.1	6.8	25.8	5.3	25.9	6.9	52	88
	STEEL_1		**STEEL_2**		**STEEL_3**		**STEEL_4**	
	Mean	Std. Dev	Mean	Std. Dev	Mean	Std. Dev	Mean	Std. Dev
	497.4	143.1	476.8	146.6	471.3	171.2	440.6	125.5

This inconsistency created the need for a more sound and repeatable testing procedure. Therefore the use of the MultiMeter was adopted. Resistance measurement was used for this experiment. The two leads were attached to the two inside steel shoulders to measure the resistance through the concrete. The MultiMeter was able to output far more consistent values that required no further conversion to become proper data points. Since there was no available method to calculate the theoretical resistance in a concrete tie with either steel or AFRP reinforcement, a straight comparison was made between the two. This comparison is mapped out in Table 13. Data points were taken over the course of one week to map any changes that may have occurred due to curing. The table shows that the AFRP reinforced ties had an average resistance of 2.42 MΩ while the steel reinforced ties had an average of 1.11 MΩ. Although, on average, AFRP reinforced ties show to have better resistance compared to steel, some overlap does exist where AFRP 3 has a lower resistance than STEEL 2 and therefore makes an inconclusive result which requires further testing.

Table 13: MultiMeter measured resistance (MΩ)

	TEST #	1	2	3	4	5	6	Average
AFRP Tie	1	2.00	1.80	1.80	1.80	1.80	1.80	1.833
	2	2.00	2.20	2.20	2.20	2.00	2.20	2.133
	3	1.00	0.80	0.80	1.80	0.80	0.60	0.967
	4	4.60	4.60	4.80	4.80	4.80	4.80	4.733
STEEL Tie	1	0.80	0.40	0.60	0.60	1.00	0.80	0.700
	2	3.00	2.40	2.60	2.40	3.00	2.20	2.600
	3	0.60	0.60	0.40	0.20	0.20	0.20	0.367
	4	1.40	0.40	0.60	0.40	0.40	1.40	0.767

7.3 Moment – Curvature

Like the Chapter 6 which compared the moment-curvature of the experimentally tested ties with AFRP reinforcement to the calculated values for the AFRP reinforced ties, this section will compare that calculated result to what a tie reinforced with steel strands would be. Those calculations follow the same procedure as before but use the information provided by the manufactures to provide accurate information about strand location, size, and prestressing force which can be found in Appendix A. This data was used to determine a theoretical curvature for the design cracking moment based on the service strength required. Like with the AFRP theoretical tie the steel ties' curvature was assumed to linearly increase until cracking due to the elasticity of the specimen. Plotting the results comes down to the four primary testing locations: RSP, RSN, CP, and CN. Those plots are represented by Figure 56-59 respectfully. It can be seen that all four test results follow a similar line to their steel counter-part, but the steel ties had larger moment capacities over the AFRP. This is because of the construction woes mentioned previously and how that caused the as-built specimens to not have the strength as what was originally designed for. Therefore, by having all four plots remain in close company to the steel values, a more properly constructed tie may match the strength of the steel reinforced ties.

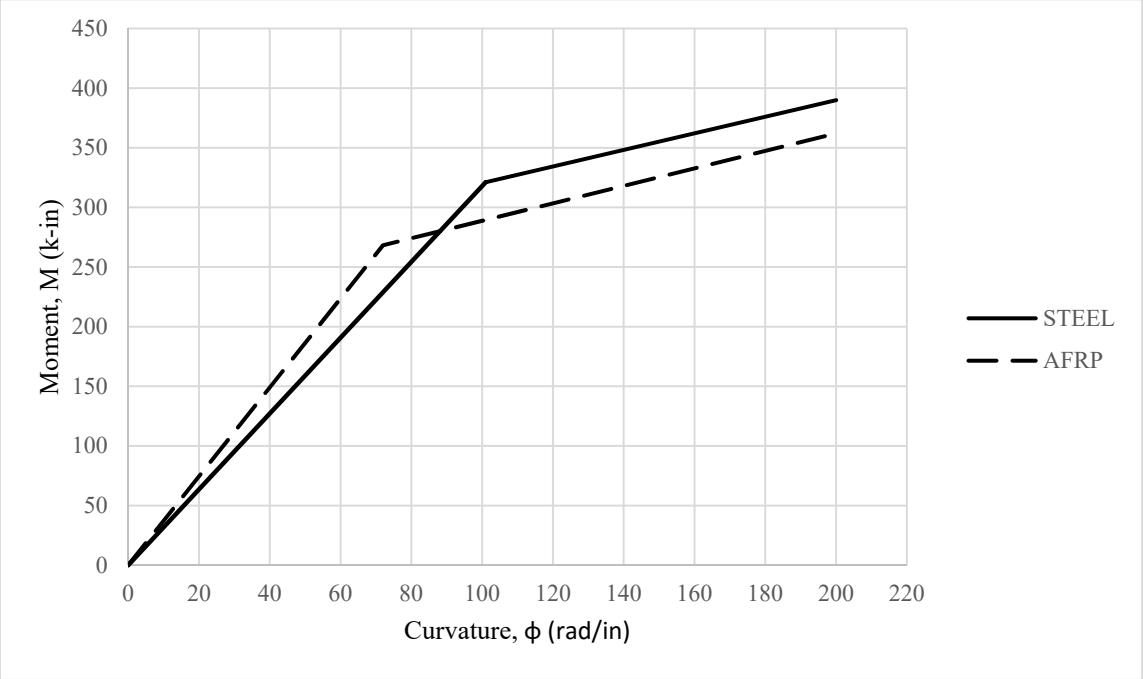

Figure 56: Theoretical moment curvature plots steel and AFRP reinforced ties (rail seat positive)

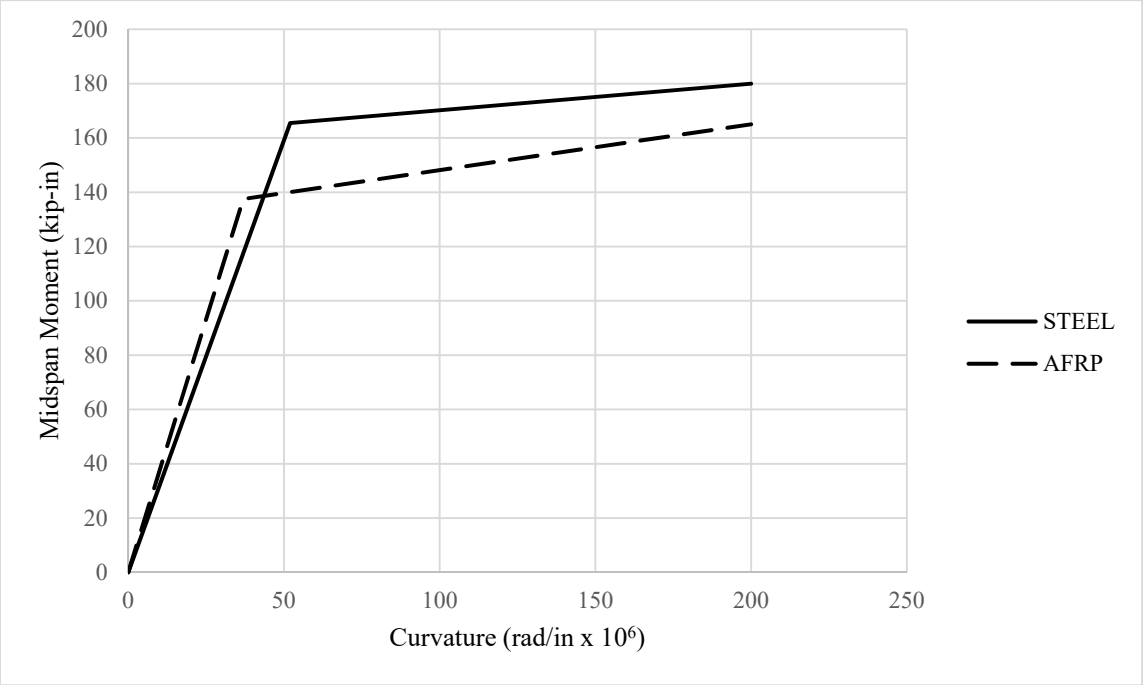

Figure 57: Theoretical moment curvature plots steel and AFRP reinforced ties (rail seat negative)

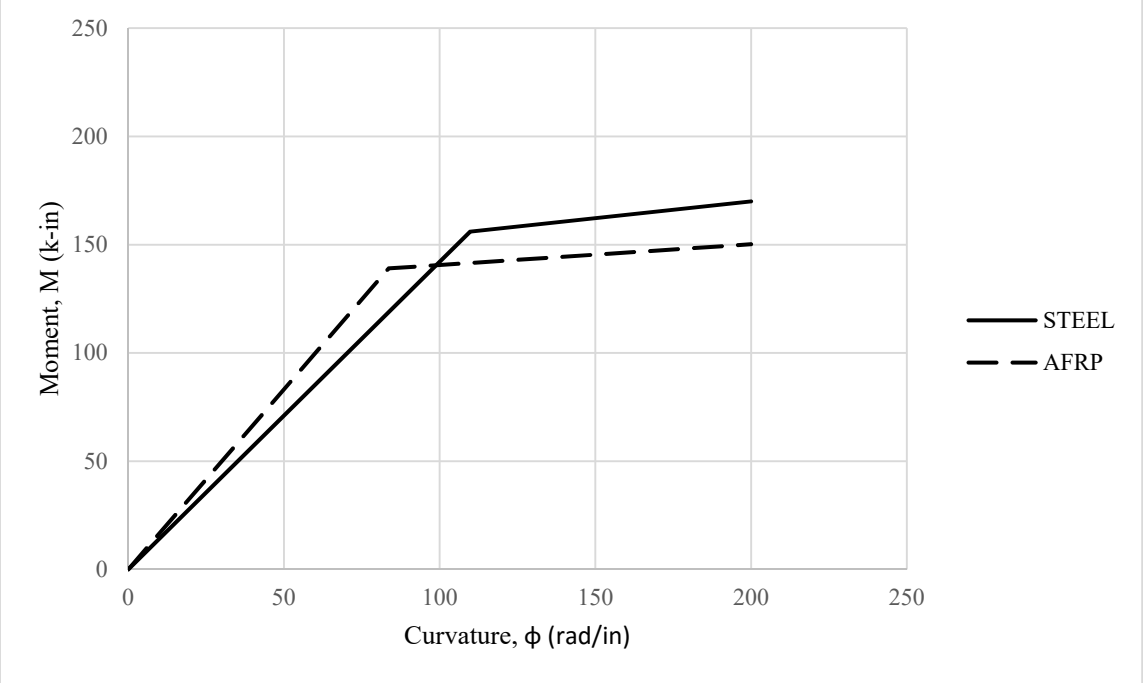

Figure 58: Theoretical moment curvature plots steel and AFRP reinforced ties (center positive)

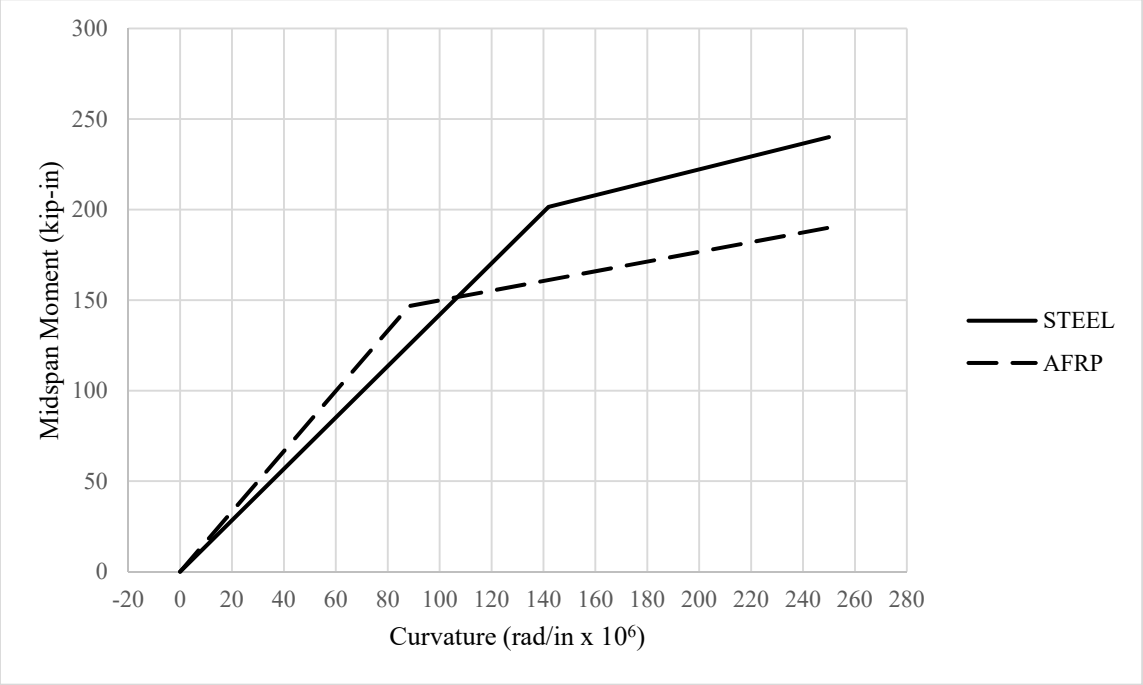

Figure 59: Theoretical moment curvature plots steel and AFRP reinforced ties (center negative)

8. SUMMARY, RECOMMENDATIONS, AND FUTURE WORK

8.1 Summary

Concrete railroad ties have been becoming increasingly popular amongst railroad industrialists compared to their timber counterpart. Because of this, newer, more durable, cheaper, and safer ties have to be researched and developed in order to keep industry moving in the right direction. One of these developments has been the use of a new prestressing material than can replace the corrosive and electrically conducting steel whilst maintain design strength. Aramid Fiber-Reinforced Polymer bars (AFRP) was the subject of this research. Its ability to resist corrosion by being electrically insulating was paramount to the decision on its use over other fibrous materials, glass and carbon. The AFRP bars were pre-tensioned and cast into a concrete tie. The railroad tie the research was based around was the CXT 505S-50 which is typically used by Union Pacific on their main heavy haul lines. The design parameters followed the American Railroad Engineering and Maintenance-of-Way Association (AREMA) guidelines for load calculation and testing procedures, and the American Concrete Institute (ACI) for stress design and analysis for both the concrete and AFRP bars.

Four tests were conducted on the built up concrete tie specimens each involving a 3-point bending analysis at separate locations. These locations were deemed critical in determining the strength of the tie and include the rail seat section and the center of the tie. These are critical because as the train rolls over the cross ties, the load travels directly from the wheel into the rail seat which causes a bending moment at that point and due to the same load applied at the opposite side, an inverse moment is caused at the center of the tie. This creates two critical load cases: the wheel directly over the tie and the wheel between ties. Those two load cases create four moments which are needed to be designed for and tested: rail seat positive, center negative, rail seat negative and center positive. A static load of 61.8 kip, 17.0 kip, 28.8 kip, and 10.3 kip was applied to those locations respectively and the deflection and strain was measured using string pots and LVDTs. Based on the data resulting from the experiments and the calculated

theoretical values expected, it can be concluded that AFRP show promise as a material to replace steel in prestressed concrete railroad ties. Further research is needed to be conducted before a final recommendation can be made.

8.2 Recommendations

Throughout this research several recommendations can be made to better further experimentation and in-practice testing. The primary testing recommendation is to replace the rubber strips used to support the tie and the load plate for the static testing. It was seen that the rubber would become nearly useless after only 4 or 5 tests. A replacement idea is to use birch plywood to completely replace the load supporting rubber. Birch, has a strong splitting resistance and can be used several times without losing any strength. A second idea is to use small metal stubs resting on a much thinner strip of rubber. The presence of the rubber still allows for the load to be distributed evenly across an uneven surface but without the extra compression that causes deflection differentials and splitting of the rubber.

Another area where recommendations for improvements were found was through the stressing procedure for the AFRP. During the construction of the new ties, AFRP bars had to be stressed using a 3-pipe system. These pipes were 36 in. long and filled with a quick setting, expansive grout. The primary problem was not with the grout but with the application of stress. Stressing one strand at a time leads to a very long and uneconomical use of time to construct a tie using AFRP. By developing a system to stress all the strands simultaneously, not only will construction time and costs be reduced, accuracy and consistency of stress will be achieved across every strand.

It was found during construction that contact with the embedded shoulders caused some of the strands to rupture due to the friction that occurred during stressing. It is hence recommended that both more precision be placed in locating the strands as to avoid contact all together, and that temporary plastic covers be placed on the shoulders during stressing to reduce any possible friction that may occur. Beyond construction woes, causes for insufficient strength can be due to bond length. This can be mitigated

by decreasing the bar diameter, or installing a head onto the ends of the bars to act as an anchoring point.

A final recommendation is to use a different material other than the urethane rubber as a mold making material. It was found that after sitting in the hot sun for several days, the rubber began to soften and lose grip to the wood box holding it. This resulted in warping which effected the AFRP hole locations between adjacent molds causing possible bending of the AFRP during stressing which results in a loss in stress and possible rupture.

8.3 Future Work

With the completion of this work on design and testing of concrete railroad ties pretensioned with AFRP bars, more research opportunities have arose. These are derived from objectives that this thesis could not cover nor had the resources to complete. Some further investigations into this research include:

1. Complete fatigue and ultimate strength testing
2. Use the design in a full-scale field test
3. Observe the long term effects on the crosstie including corrosion effects

8.3.1 Creating a Finite Element Model

As a research objective, one could develop the FEM that incorporates AFRP as a material option for prestressed concrete analysis. That would include a creep model and take long term losses into consideration. Without the improved FEM, one could still develop the model of the crosstie using traditional steel in place of the AFRP to create a comparison between experimental results using AFRP and FEM results using steel.

8.3.2 Field Test

Due to constraints on funding and materials for this research project, only four ties were able to be constructed. This means that only laboratory experiments were performed on the ties to determine their strengths. However, when placed into in-track

service, the results may vary. This would require constructing many more ties, designing an appropriate ballast and sub ballast, and using a fully loaded rail car and locomotive to travel across the ties repeatedly over a number of years. During that time, checks for fatigue cracking will need to be done along with stress checks within the concrete using strain gauges. This experiment may also require the use of non-destructive testing techniques, currently in development, to locate cracks within the concrete. By being exposed to the elements, this experimentation can also show the durability of the ties in the presence of moisture.

8.3.3 Long Term Effects

Along with experimenting on the physical strength of the crosstie under real-life load conditions, performance should be investigated under natural weathering conditions. Therefore, testing should be done on the effect corrosion has on the AFRP reinforced crosstie and compared to that of a traditional steel tie. Along with corrosion testing, long term losses come into effect and should be analyzed and the electrical resistivity should be measured over that time as well. That information can be used not only for more accurate crosstie design, but general AFRP material properties.

Two different environmental conditions should be used to assess the performance of the ties: a well-drained ballast and mud surrounding the ties. By having mud consistently interacting with the concrete, chemical reactions may take place affecting either the concrete or the reinforcement within. Also, having the ties in the presence of large daily temperature swings similar to that of an arid climate may show the long term durability of the reinforcement to resist the constantly changing temperature induced stresses on the tie and how it affects in-service performance.

REFERENCES

AAR “Class I Railroad Statistics”. Association of American Railroads (2013). 1-3

ACI Committee 440.4R, 2004, “Prestressing Concrete Structures with FRP Tendons”, ACI 440.4R-04 ed.

ACI Committee 318, 2011, “Building Code Requirements for Structural Concrete (ACI 318-11) and Commentary (ACI 318R-11). ACI 318-11, ed.

AREMA "Chapter 30 - Part 4: Concrete Ties." *2014 Manual for Railway Engineering*. Lanham, MD: American Railway Engineering and Maintenance-of-Way Association, 2014. N. page. Print.

ASTM C143 (2012) “Standard test method for slump of hydraulic-cement concrete” In *Annual Book of ASTM Standards*. West Conshohoken, Pennsylvania: The American Society for Testing and Materials.

Donovan, B. M. "Development of a Durable Concrete Railroad Tie." MS Thesis, University of Nevada, Reno, 1997. Ann Arbor: *ProQuest.* Web. 19 Jan. 2015.

Enerpac. "RCH-Series Dimensions and Specifications." *Hollow Plunger Cylinders: RCH Series*. N.p., n.d. Web. July 2015. <http://www.enerpac.com/en-us/industrial-tools-imperial/hydraulic-cylinders-jacks-lifting-products-and-systems/general-purpose-hydraulic-cylinders/rch-series-hollow-plunger-cylinders>.

Ehsani, M. R., H. Saadatmanesh, and C. T. Nelson. "Transfer and Flexural Bond Performance of Aramid and Carbon FRP Tendons." *PCI Journal Pcij* 42.1 (1997): 76-86. Web.

Gar, S. P., M. H. Head, and S. Hurlebaus. "Computation Modeling of Aramid Fiber-Reinforced Polymer Prestressed Girder in Composite Action with Bridge Deck." *ACI Structural Journal* (2013): 965-75. Web

Gar, S. P., M. H. Head, S. Hurlebaus, and J. B. Mander. "Experimental Performance of AFRP Concrete Bridge Deck Slab with Full-Depth Precast Prestressed Panels." *Journal of Bridge Engineering* (2013): 1-10. Web.

Gar, S. P. "Structural Performance of a Full-depth Precast Bridge Deck System Prestressed and Reinforced with AFRP Bars." Diss. Texas A&M U, 2012. Print.

Hanna, A. N. "Prestressed Concrete Ties for North American Railroads." *PCI Journal* (1979): 32-61.

Hollaway, L.C. "A Review of the Present and Future Utilization of FRP Composites in the Civil Infrastructure with Reference to Their Important In-service Properties." *Construction and Building Materials* 24.12 (2010): 2419-445. Print.

Johnson, M. "How Track Circuits Detect and Protect Trains." Weblog post. *Greater Greater Washington*. Greater Greater Washington, 5 Mar. 2010. Web. 9 Feb. 2015.

Kaewunruen, S., A. M. Remennikov, and M. H. Murray. "Greener and Leaner—Unleashing Capacity of Railroad Concrete Ties via Limit States Concept." *J. Transp. Eng. Journal of Transportation Engineering* 137.4 (2011): 241-47. Web.

Layssi, H., P. Ghods, A. Alizadeh, and M. Salehi. "Electrical Resistivity of Concrete." *Concrete International* 37.5 (2015): 41-46. Web.

Li, D. and D. Davis “Transition of Railroad Bridge Approaches.” *Journal of Geotechnical and Geoenvironmental Engineering* 131.11 (2005) 1392-98.

Lutch, R. H., (2009). “Capacity Optimization of a Prestressed Concrete Railroad Tie.” MS Thesis, Michigan Tech Univ., Houghton, MI

Medina, J. C., (2011). “Characteristics of AFRP Bars for Prestressing Applications.” MS thesis, Texas A&M Univ., College Station, TX

Mielenz, R. C., S. L. Marusin, W. G. Hime, and Z. T. Jugovic. "Investigation of Prestressed Concrete Railway Tie Distress." Concrete International (1995): 62-68. Print.

Mindness, S., C. Yan, and W.J. Venuti. “Impact Resistance of Fiber Reinforced Prestresseed Concrete Railroad Ties” *ACI Special Publication* 128.12 (1991): 183-200

Monfore, G. E. "The Electrical Resistivity of Concrete." *Journal of the PCA Research and Development Laboratories* 10.2 (1968): 35-48. Print.

Naaman, Antoine E. *Prestressed Concrete Analysis and Design: Fundamentals*. 3rd ed. Ann Arbor, MI: Techno 3000, 2012. Print.

National Transportation Safety Board. “Organizational Factors in Metro-North Railroad Accidents.” *Special Investigation Report.* SIR-14/04. Notation 8605. (2014): 105-15

Proceq SA© (2013) “Operating Instructions: Concrete Durability Testing”. Schwerzenback. Part Number: 820-381-04-E. <www.proceq.com>

Prouty, J. M. (2014) “Sustainable and Durable Infrastructure with Advanced Construction Materials”. MS Thesis, Texas A&M University, College Station, TX

Sengul, O., and O. E. Gjørv. "Effect of Embedded Steel on Electrical Resistivity Measurements on Concrete Structures." *ACI Materials Journal MJ* 106.1 (2009): 11-18. Web.

SPX. "High Force Hydraulic Tools & Equipment." *PowerTeam Catalogue* (2013): 21. Web. July 2015. <http://www.spx.com/en/multimedia-library/pdf/spx-brand-pdf/industrial/power-team/product-catalogues/SPX_PowerTeam_Fullline_Catalog_PT1403_EN_rev1.pdf>.

Venuti, W. J. "Concrete Railroad Ties in North America." *Concrete International* (1980): 25-32.

White, J. G. "Concrete Tie Track System." *Rail Papers* (1984): 5-11. Print.

Zeman, J. C., J. R. Edwards, C. P. L. Barkan, D. A. Lange. "Failure Mode and Effect Analysis of Concrete Ties in North America". *Proceedings - 9th International Heavy Haul Conference: "Heavy Haul and Innovation Development"* (2009): pp. 270-77. Print.

APPENDIX A: PLANS OF ORIGINAL TIE

This appendix includes the manufacture's drawings of the original CXT 505S-50 heavy haul concrete railroad tie with steel strand reinforcement. This was used to calculate the properties of the ties and redesign using AFRP as a replacement for steel.

Figure 60: Detail of concrete railroad tie used as model

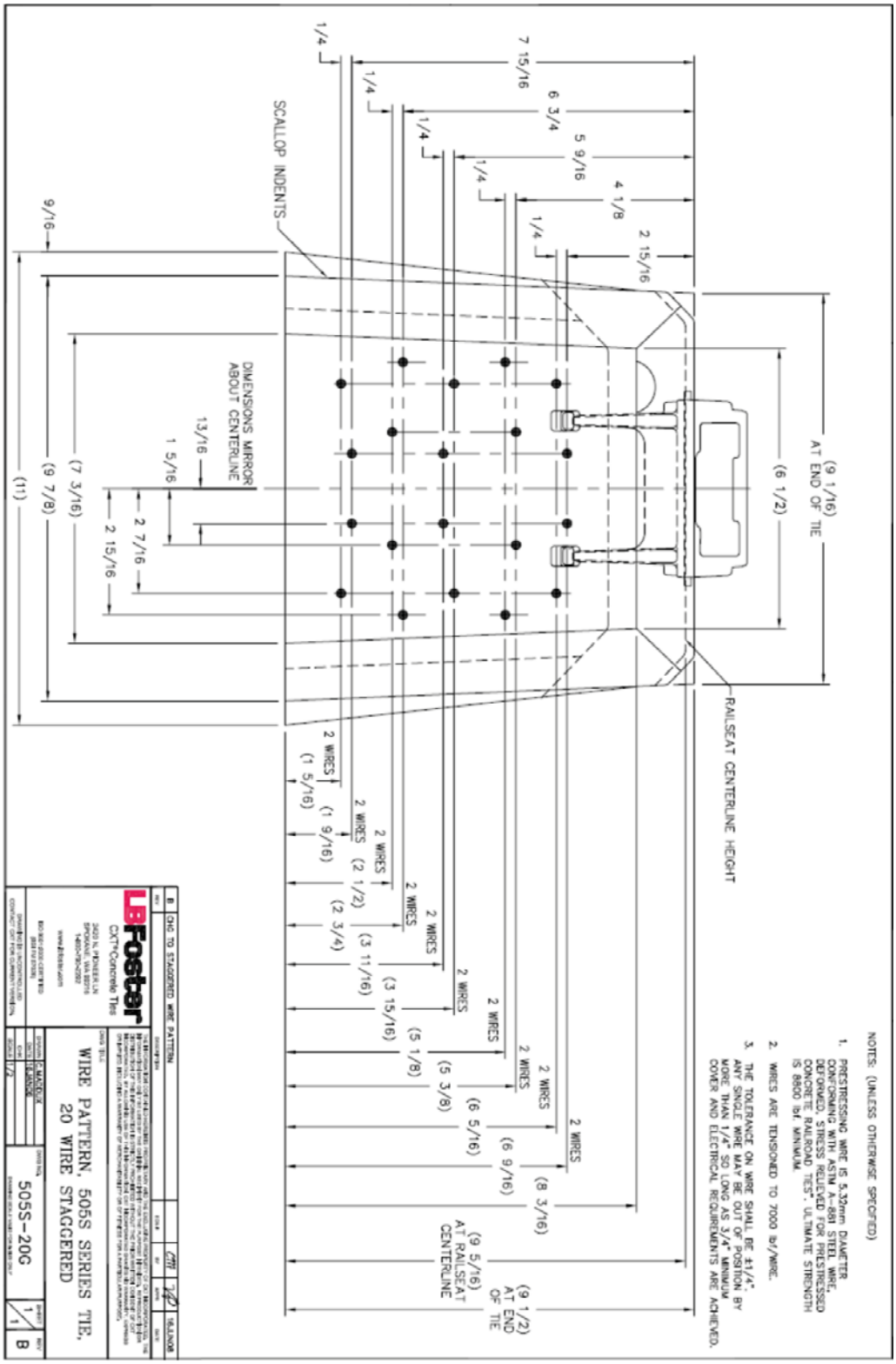

Figure 61: Cross section of tie used as comparison and model

APPENDIX B: TIE PROPERTIES AND DESIGN

This appendix details geometry of the tie, the process taken when using AREMA to calculate the design moments at the critical sections, the spreadsheet used in designing the tie with prestressed AFRP as the reinforcement, and three options that meet the criteria but were not used because they did not satisfy the more stringent manufacturers requirements. By using ACI 318-11 code for uncracked, prestressed concrete, this spreadsheet has the capability to assess the adequacy of the design based on the concrete strength, location of reinforcement, and the initial prestressing force.

B.1 Tie Geometry and Section Properties

Table 14: Cross section properties of the rail seat and center sections

Rail Seat

Section	Height, h (in.)	Width, b (in.)	Area, A (in^2)	Centroid, y (in.)	Moment of Inertia, I (in^4)	Centroid Difference, d (in.)	Parallel Axis Theorem I+Ad^2 (in^4)
A	8.59	9.1	78.17	4.295	480.66	0.26	485.99
B	8.59	0.39	1.68	2.863	6.87	1.69	11.67
C	8.59	0.39	1.68	2.863	6.87	1.69	11.67
D	0.71	7.68	5.45	8.945	0.23	-4.39	105.26
E	0.71	0.71	0.25	8.827	0.01	-4.27	4.60
F	0.71	0.71	0.25	8.827	0.01	-4.27	4.60
Sum			87.48				623.79
ybar	4.56						

Center

Section	Height, h (in.)	Width, b (in.)	Area, A (in^2)	Centroid, y (in.)	Moment of Inertia, I (in^4)	Centroid Difference, d (in.)	Parallel Axis Theorem I+Ad^2 (in^4)
A	6.88	7.75	53.32	3.44	210.32	1.12	276.75
B	6.88	0.31	1.07	2.293	2.80	2.26	8.26
C	6.88	0.31	1.07	2.293	2.80	2.26	8.26
D	0.63	6.5	4.10	7.195	0.14	-2.64	28.65
E	0.63	0.63	0.20	7.090	0.00	-2.53	1.28
F	0.63	0.63	0.20	7.090	0.00	-2.53	1.28
Sum			59.94				324.48
ybar	3.68						

The total volume of one tie was found to be about 8200 in^3 or 4.75 ft^3; this requires 19 ft^3 or 0.703 yd^3 of concrete to fill all four ties. Because the mix plant involved with providing the concrete could not batch such a small mix and maintain accuracy with the design, 3 yd^3 were ordered and excess would be dumped in a single spot to be removed at a later date. This also provided plenty of extra to perform all necessary tests on the wet mix and make all the required cylinders.

Table 15: Concrete volume calculations

Location	Cross Section (in^2)	Length (in)	Volume (in^3)
Rail Seat (x2)	87.5	29.4	5145
Center	60	24	1440
Transition (x2)	1/2*(9.5+7.5)*9.6 = 81.6	10	1632
		Total	8217

B.2 AREMA Service Moment Calculations

To determine the typical loading the ties will undergo during their design life, the AREMA manual for concrete railroad tie design was consulted. The manual states that the positive rail seat moment is a function of the length of the tie and the center to center spacing of the ties which is plotted in a chart shown in Figure 62. In this research, a spacing of 24 in. is used with a tie length of 8'-6" which reveals a positive rail seat moment of 300 kip-in. This moment is then factored using speed and tonnage coefficients. These coefficients are found using a chart, Figure 63, where the annual tonnage and average speed are selected, and then the intersection is found on the relative plotted line to indicate the appropriate coefficient to use. An average speed of 60 mph was selected to best represent typical speeds on main line heavy haul track; this speed corresponds to a factor of 0.9. An annual tonnage of 75 MGT was also selected to best represent the loading a freight line would experience each year; this then corresponds to a factor of 1.1. Following the AREMA equation for positive rail seat moment, $M = BVT$ where B is the moment from Figure 62 and V & T are the speed and tonnage

coefficients, the tie is expected to sustain a moment of 297 kip-in. From there, the moments in the negative rail seat, positive center, and negative center are found using the pre-determined factors shown in Table 16.

Table 16: Moment factors (AREMA 2014)

Tie Length	Rail Seat Negative	Center Negative	Center Positive
7’-9”	0.72 *M*	1.13 *M*	0.61 *M*
8’-0”	0.64 *M*	0.92 *M*	0.56 *M*
8’-3”	0.58 *M*	0.77 *M*	0.51 *M*
8’-6”	0.53 *M*	0.67 *M*	0.47 *M*
9’-0”	0.46 *M*	0.57 *M*	0.40 *M*

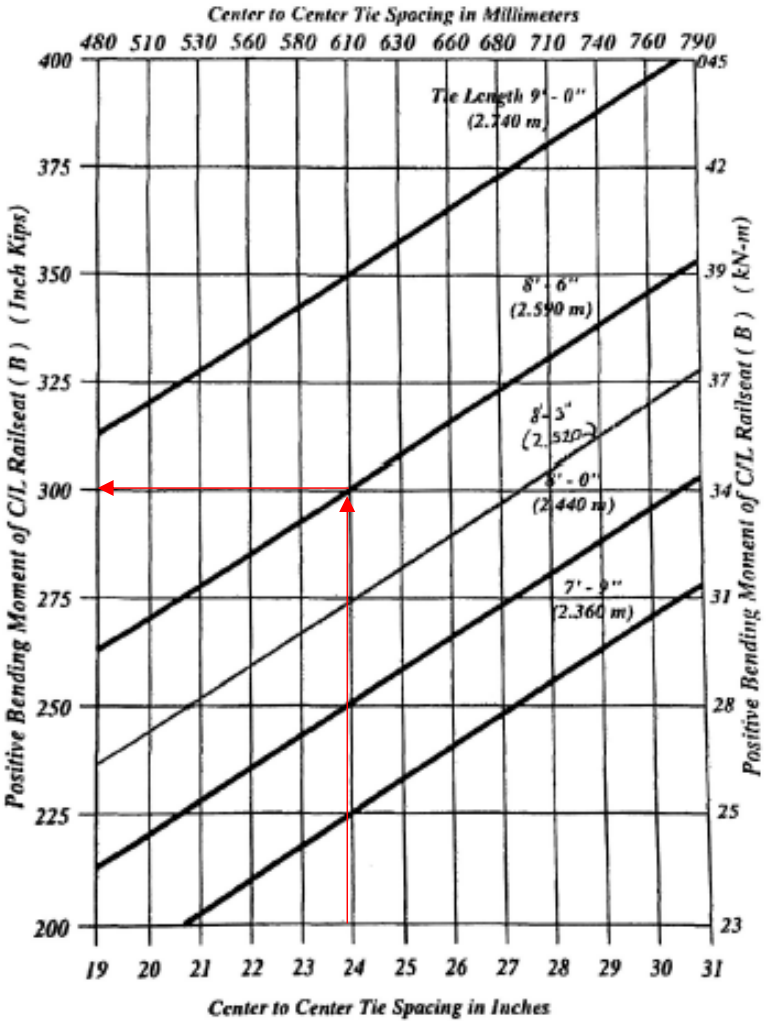

Figure 62: Positive rail seat bending moment based on tie spacing

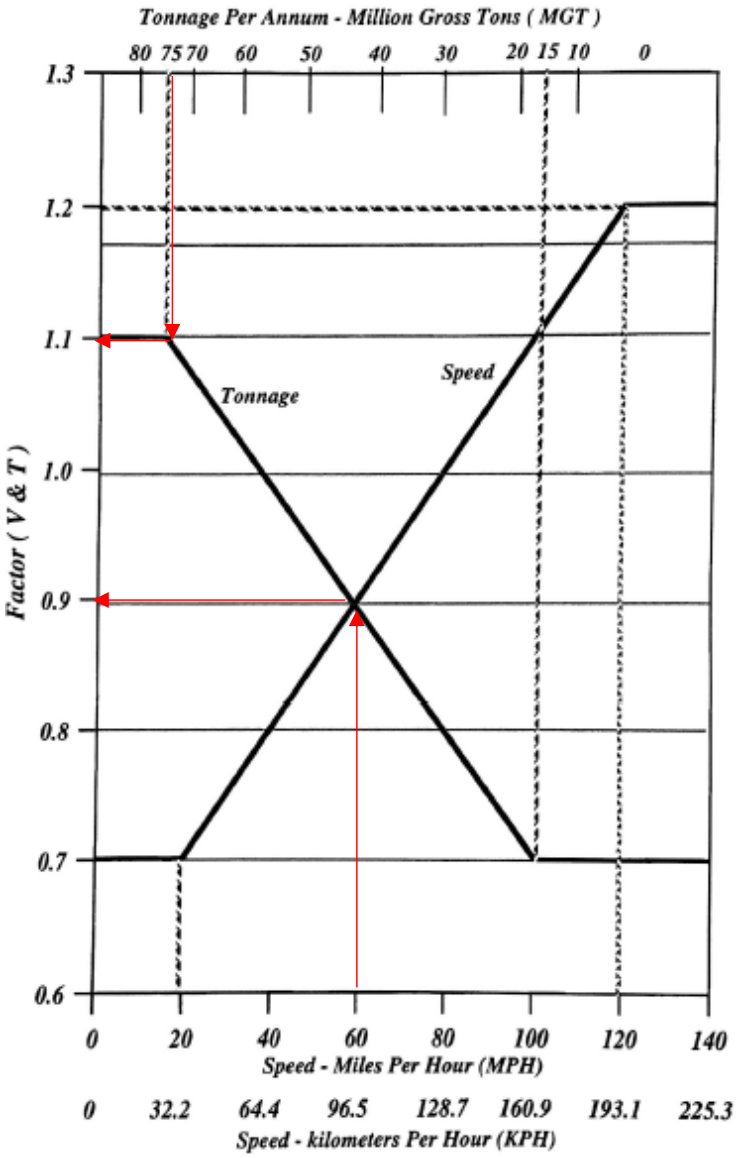

Figure 63: Speed and tonnage factors

With an 8'-6" tie length, the rail seat negative moment is 0.53M or 157 kip-in, the center negative moment is 0.67M or 199 kip-in, and the center positive moment is 0.47 M or 140 kip-in. These moments are used to determine the point load that is applied to the tie during testing and as a comparison for adequacy. Although these loads meet AREMA requirements, Union Pacific requires the 505S tie to withstand larger loads. These new loads will serve as the basis for the design and testing requirements.

B.3 AFRP Centroid Tables

Table 17: General centroid calculation table

Layer	No. Tendons	Area (in^2)	y	Ay
1	2	0.24	y1	0.24y1
2	3	0.36	y2	0.36y2
3	4	0.48	y3	0.48y3
4	3	0.36	y4	0.36y4
Totals:	12	1.44	-	1.44(y1+y2+y3+y4)
			Centroid	1.44(y1+y2+y3+y4)/1.44

Table 18: AFRP centroid and eccentricity calculations relative to the bottom face of tie

Prestressing Centroid Calculations

Layer	No. Strands	Area (in^2)	$\bar{y}$ (in)	A $\bar{y}$
1	4	0.478	1.25	0.597
2	3	0.358	3	1.075
3	4	0.478	4.75	2.270
4	3	0.358	6.55	2.347
5	0	0.000	0	0.000
6	0	0.000	0	0.000
Totals:	14	1.672	-	6.290
			Centroid	**3.761**

Eccentricity Calculations

Section	$\bar{y}$ (in)	e (in)
RS	4.55	0.789
C	3.68	-0.081

AFRP Properties			Moments			Stresses @ Transfer			Stresses @ Service		
Numer of Tendons	14		M_P,RS =	378	kip-in	Fi =	146.3 kip		F =	123.2 kip	
Diameter of Tendon	2/5 in		M_N,RS =	-176	kip-in	σ_ti =	0.208 ksi		σ_ts =	0.787 ksi	
Area of Tendon	0.119 in^2		M_N,C =	-230	kip-in	σ_ci =	-2.88 ksi		σ_cs2 =	-6.6 ksi	
Strength	203 ksi		M_P,C =	140	kip-in						
Strain	0.0209						Mo =	6.129 kip-in	Pos,Top =	-3.542	O.K.
Mod of Elasticity	10231 ksi		Eccentricity Calcs				Man,Top =	-2.559 O.K.	Pos,Bot =	0.640	O.K.
			Tie Loc	yBar_con	ecc	Rail Seat	Man,Bot =	-0.748 O.K.	Neg,Top =	0.668	O.K.
	11		RS	4.55	0.7893		Stor,Top =	-0.842 O.K.	Neg,Bot =	-3.401	O.K.
Prestressing Load	8.8 kips	92.1	C	3.68	-0.0807		Stor,Bot =	-2.470 O.K.			
Concrete Strength	11 ksi	45%					Mo =	9.371 kip-in	Pos,Top =	-3.797	O.K.
Min Conc St at Trans	4.8 ksi						Man,Top =	-2.413 O.K.	Pos,Bot =	-0.341	O.K.
			Prestressing Centroid Calculations			Center	Man,Bot =	-2.469 O.K.	Neg,Top =	0.502	O.K.
Tie Dimensions			Layer	No. Tend	Area	yBar	A*yBar		Stor,Top =	-2.687 O.K.	Neg,Bot =	-4.572	O.K.
- Length	102 in		1	4	0.478	1.25	0.597		Stor,Bot =	-2.198 O.K.			
- Width, T	9 in		2	3	0.358	3	1.075						
- Width, B	11 in		3	4	0.478	4.75	2.270						
- Height, RS	9.5 in		4	3	0.358	6.55	2.347						
- Height, C	7.5 in		5	0	0.000	0	0.000						
Concrete Area			6	0	0.000	0	0.000						
- At Rail Seat	87.48 in^2		7	0	0.000	0	0.000						
- At Center	59.94 in^2		Totals:	**14**	1.672		6.290						
- Of bottom	1122 in^2					centroid	3.76						
Moment of Inertia													
- At Rail Seat	623.79 in^4												
- At Center	324.5 in^4												
Neutral Axis													
- Bottom Dist, RS	4.55 in												
- Bottom Dist, C	3.72 in												
- Top Distance, RS	4.74 in												
- Top Distance, C	3.78 in												
Weight	735 lb												
Self weight	7.206 lb/in												
dist from RS to edge	21 in												
Section Modulus													
- RS_Top	131.6013 in^3												
- RS_Bottom	137.0967 in^3												
- C_Top	85.847 in^3												
- C_Bottom	87.231 in^3												

$$\sigma = \frac{F}{A} \pm \frac{Fe}{S_x} \pm \frac{M_L}{S_x}$$

$$e = \left(\sigma_{c,t} + \frac{F}{A_t} \pm \frac{M_L}{S_x} \right) * \frac{\pm S_x}{F}$$

Ranges of possible eccentricities					
		Center		Rail Seat	
		comp	ten	comp	ten
+M	top	-2.034	3.113	-2.478	5.413
	bottom	4.351	-0.879	8.845	0.626
- M	top	-5.030	0.117	-6.974	0.916
	bottom	1.355	-3.875	4.349	-3.871
Range of ecc.		-0.879	0.117	0.626	0.916
Range of centroid		4.559	3.563	3.924	3.634
			2.325	5.714	

Trying to find an eccentricity that fits within all ranges found here, then make AFRP layout match. Changing F via P &#tendons

Stress Diagram Calculations @ Service						
			F/A	Fe/Sx	M/Sx	Total
RS+	Top		-1.408	0.739	-2.872	-3.542
	Bottom		-1.408	-0.709	2.757	0.640
RS-	Top		-1.408	0.739	1.337	0.668
	Bottom		-1.408	-0.709	-1.284	-3.401
C-	Top		-2.055	-0.116	2.673	0.502
	Bottom		-2.055	0.114	-2.631	-4.572
C+	Top		-2.055	-0.116	-1.626	-3.797
	Bottom		-2.055	0.114	1.600	-0.341

Stress Diagram Calculations @ Transfer								
				Fi/A	Fie/Sx	Total	Moment	M/Sx	Total
Man_RS	Top			-1.672	-0.842	-2.515	6.129	-0.0447	-2.559
	Bottom			-1.672	0.877	-0.795		0.0466	-0.748
Man_C	Top			-2.441	0.135	-2.305	9.371	-0.1074	-2.413
	Bottom			-2.441	-0.138	-2.578		0.1092	-2.469
Stor_RS	Top			-1.672	0.877	-0.795	6.129	-0.0466	-0.842
	Bottom			-1.672	-0.842	-2.515		0.0447	-2.470
Stor_C	Top			-2.441	-0.138	-2.578	9.371	-0.1092	-2.687
	Bottom			-2.441	0.135	-2.305		0.1074	-2.198

Figure 64: Spead sheet of stress calculations at transfer and service

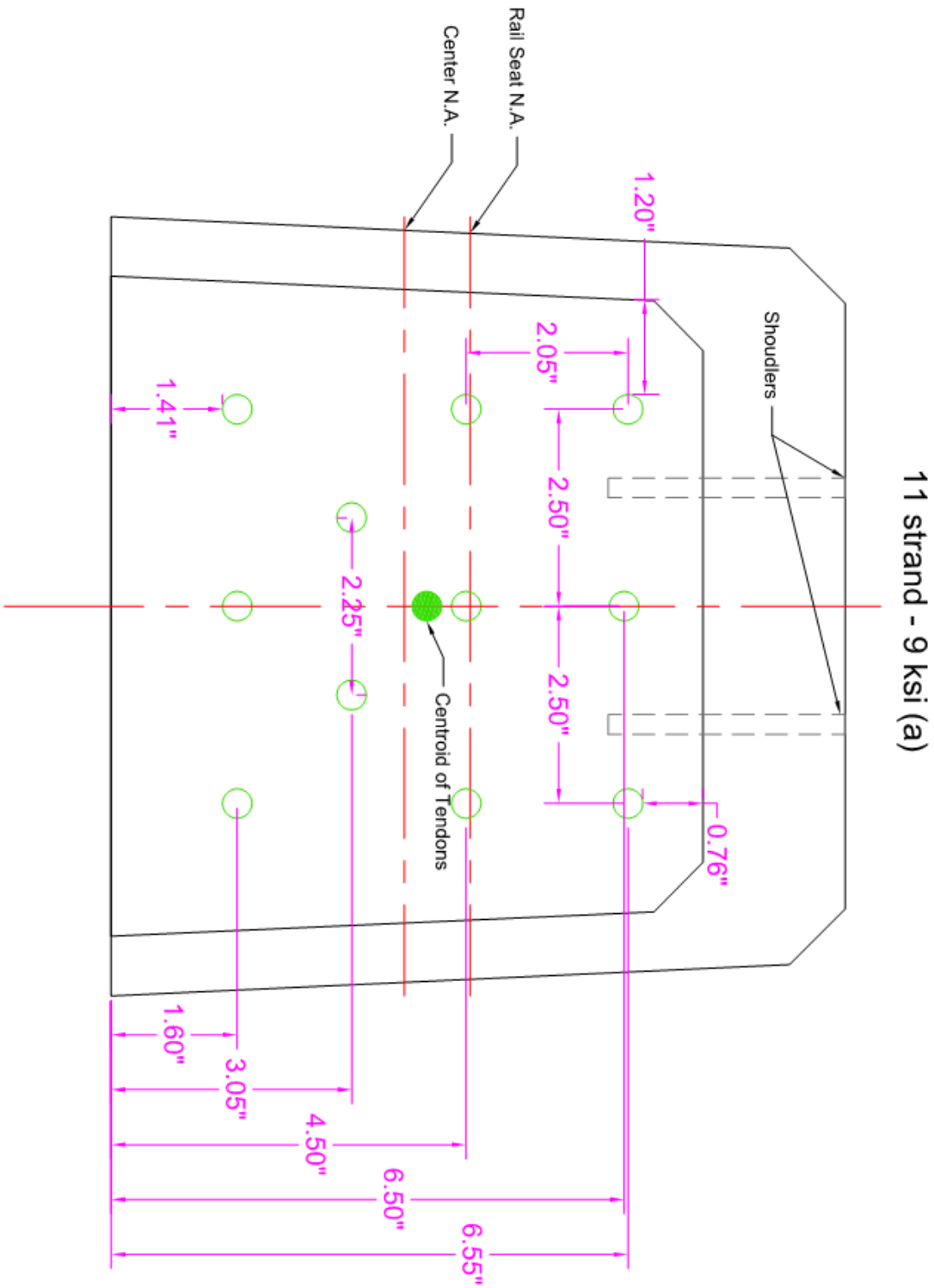

Figure 65: Option A; 11 strands and 9ksi concrete

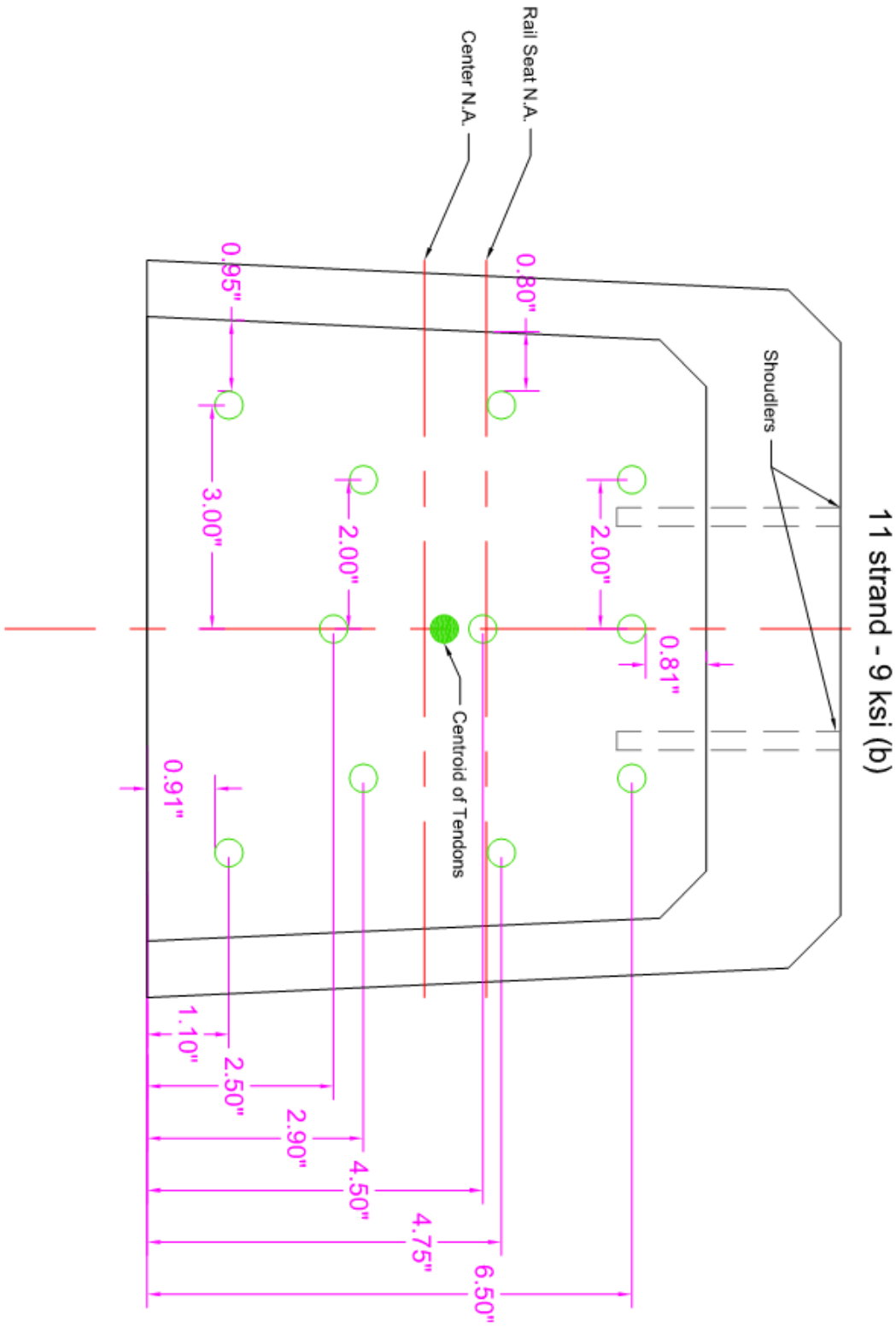

Figure 66: Option B; 11 strands with 9 ksi concrete

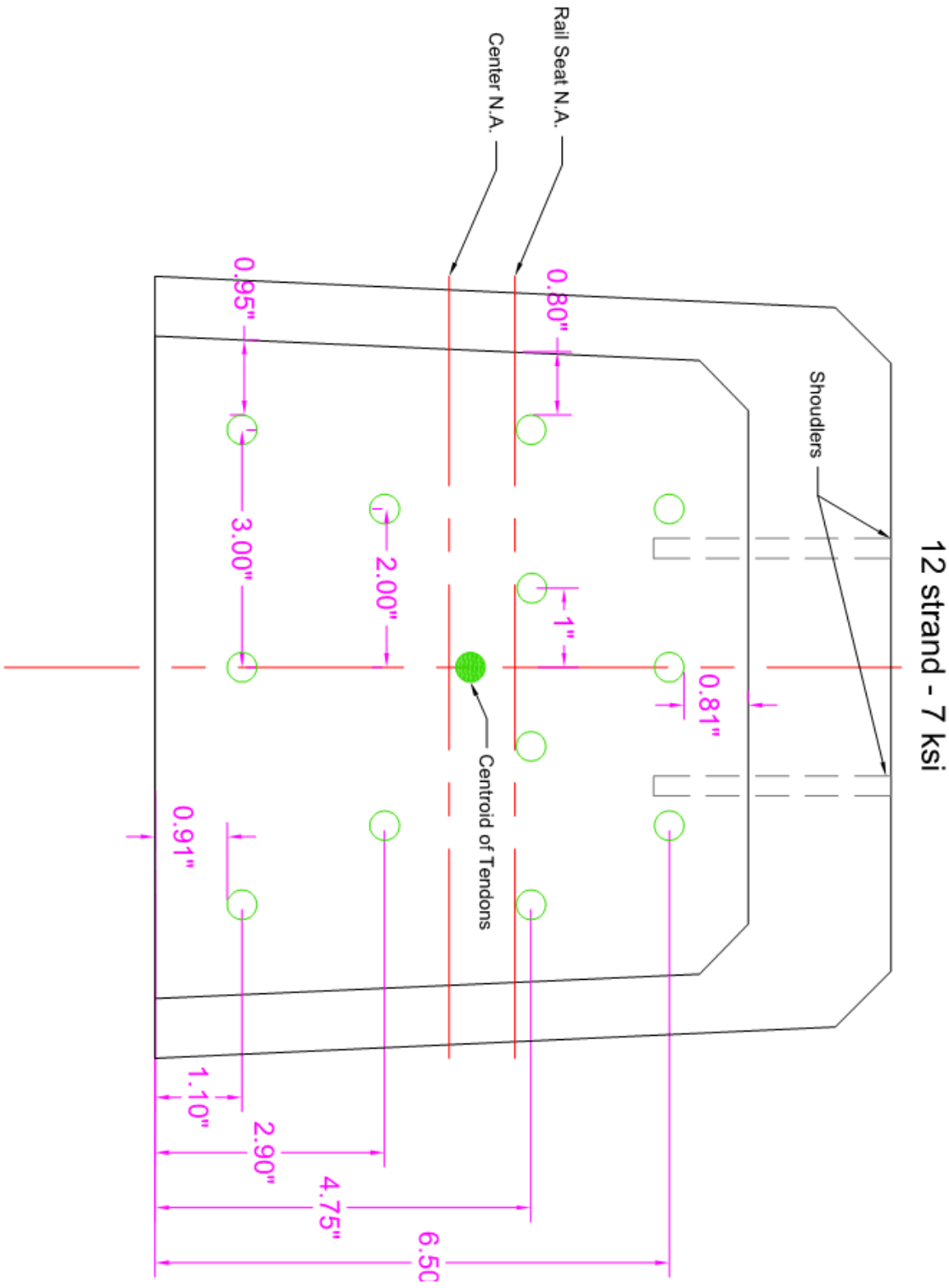

Figure 67: Option C; 12 strands with 7 ksi concrete

APPENDIX C: PRESTRESSING BED

This appendix provides construction details for the prestressing bed used in construction of the ties: a full plan & profile of the bed, and cross section details of the connection and location of the boxes on top of the flange. The connection followed the guidelines of AISC 14th edition using factored loadings. To counter the flexural moment caused by the prestressing load, a dywidag bar was placed under the beam and made snug tight.

With the molds complete, a location was needed to place the molds, stress the AFRP and pour the concrete. Texas A&M Riverside Campus has an area where used structural materials are located after being replaced in labs. At this site, two 26 ft. long, steel I-beams were discovered and selected as the base for making a prestressing bed. These I-beams, Figure 68, are known to have adequate strength to resist the loads required for the needed prestressing. However, the length of just one was not enough to hold all four molds plus room the stressing mechanism. This meant that a connection design had to be made to join the two beams together. Alongside the beam were four built up C-shapes with bolt holes matching the beams to a point to where it was discovered that they were made purposefully to be attached to said beams. It was then decided to use these as connectors to combine the two beams together.

Figure 68: I-Beams to be used for prestressing frame

Each shape was 36 in. long, 12 in. tall, with 6 in. long flanges, and 1 in. thick steel. The hole diameter was found to be $^{13}/_{16}$ in. which would allow for a ¾ in. bolt to be used in the connection. AISC guidelines were used to design the connection and check if these plates would work to withstand the 154 kip load applied through stressing the AFRP strands. A spreadsheet was developed to assess the adequacy of the design by allowing the size of each plate to be altered and the bolt hole size to alter as well. The beams were subjected to a series of checks complying with the guidelines set by AISC: buckling, flexure (both yielding and lateral torsional buckling), and combined loading. It was determined that compression was the controlling failure mode, yet the beams have a strength of approximately 645 kips meeting the requirements for stressing. From there the connection was checked using the design chapter of AISC. Using a spacing of 3 in. and assuming that threads were included in a double shear loading; the shear strength was found to be 35.8 kip/bolt (AISC Table 7-1).

The connection was broken up into 4 plate groups: Plates A, B, C, and D with A being the top plate. Figure 69 shows the plate groups and how they were designed to attach to the beam. Plates B and C were single C-shapes that were flame cut through its centerline to make 2 independent angles. This was done because the web height (13 in.) was larger than the depth of the C-shape (12 in.). For Plate A, a different I-beam was

found to have the same bolt hole size and pattern on its flange, therefore that part of the flange was cut off and used in the frame connection.

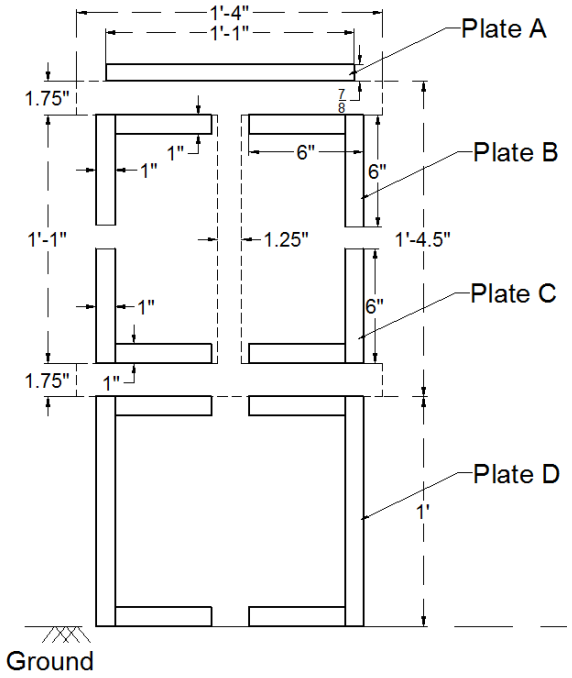

Figure 69: Connection setup

The controlling design parameter for the connection came from compression in the top plates (Plates A and B) where approximately 400 kips of load are applied from both direct prestressing compression and the flexure caused by the eccentricity of the AFRP strands on the frame. To help mitigate this compression load, a 1.75 in. diameter Dwyidag bar was installed under the frame at the same height as the AFRP centroid above. The bar was made snug tight with the expectation that the eccentric load of the AFRP would tension it more. The use of the Dwyidag bar was also found to help reduce losses in the AFRP from deflection of the end plates and frame as a whole. Figure 70 shows the completed connection as both design and as built.

Due to the thickness of the top plate and bolt head, the molds cannot sit flush on the frame. If they did, over 3 ft. of AFRP would be wasted by spanning the connection. To avoid this, the molds were placed on 1.5 in. shims made simply out of 2x4 lumber, and that allowed a mold to be place on top of the connection, therefore wasting as little AFRP as possible. The next pages show an entire plan and profile view of the prestressing frame with the molds included and an approximation of the pipe locations for stressing.

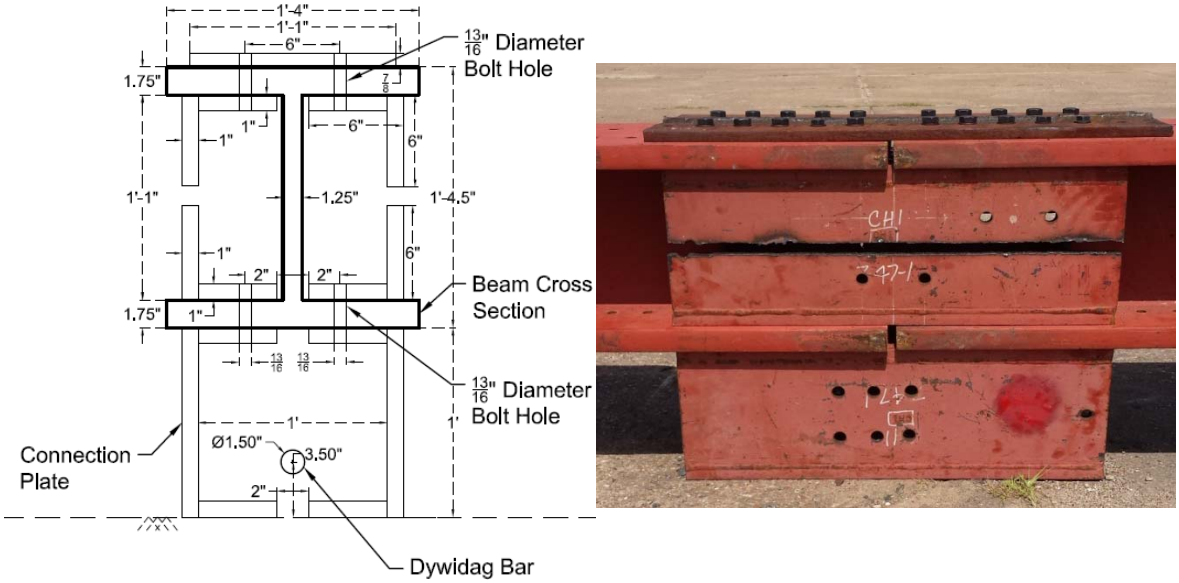

(a) (b)

Figure 70: (a) Complete cross section of the connection; (b) profile view of constructed connection

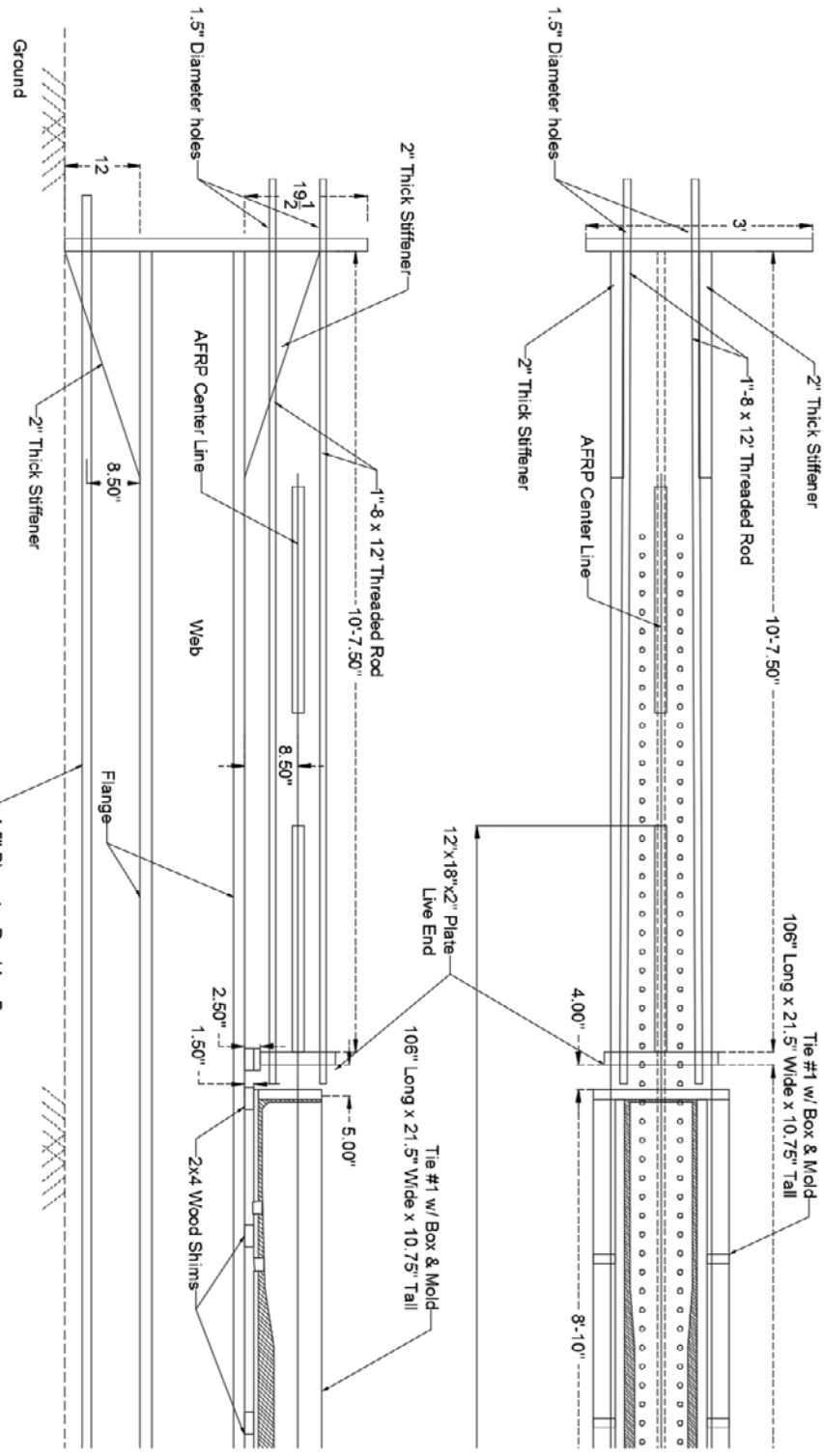

Figure 71: Detail of the prestressing bed at section A

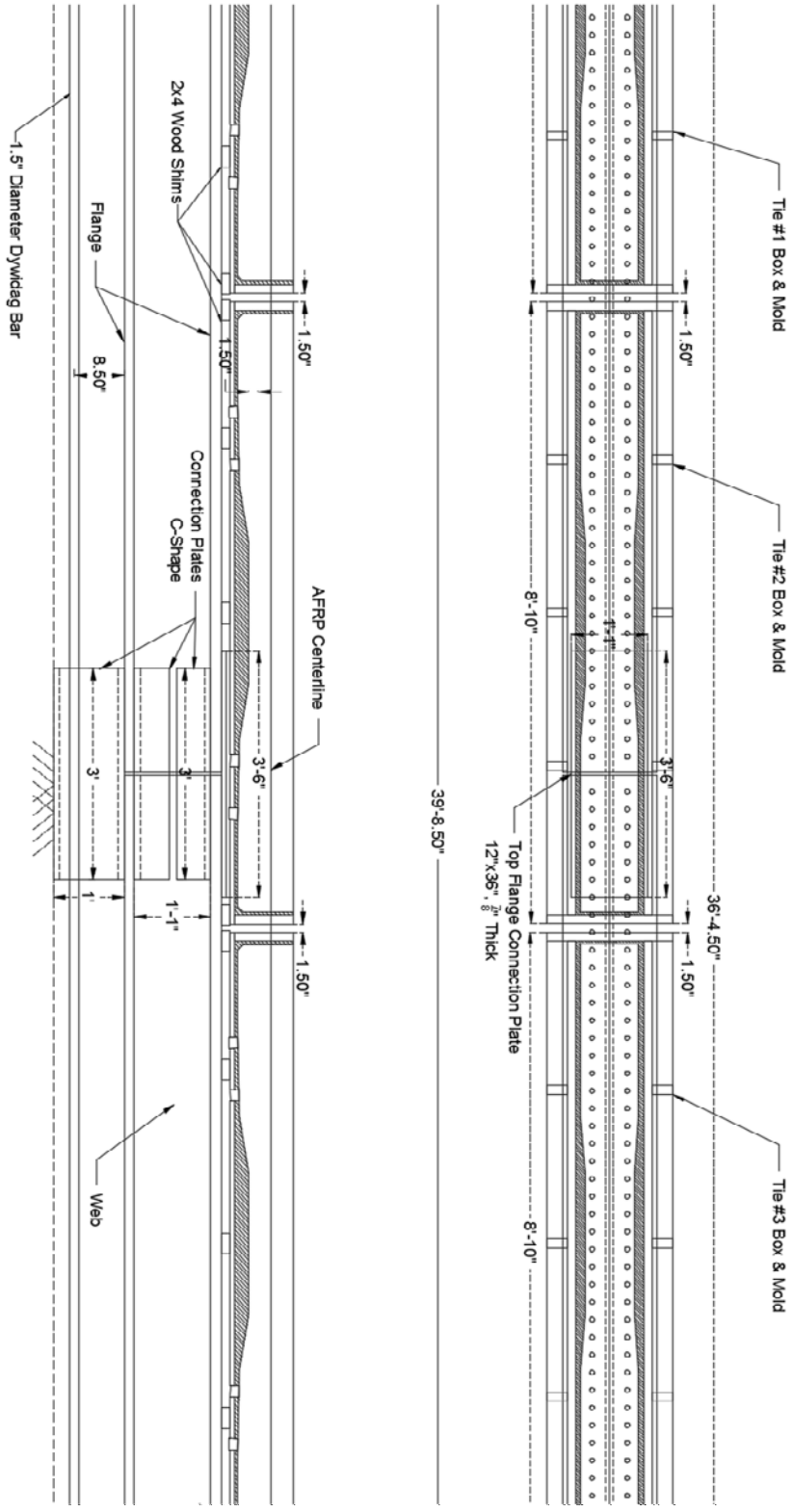

Figure 72: Section B

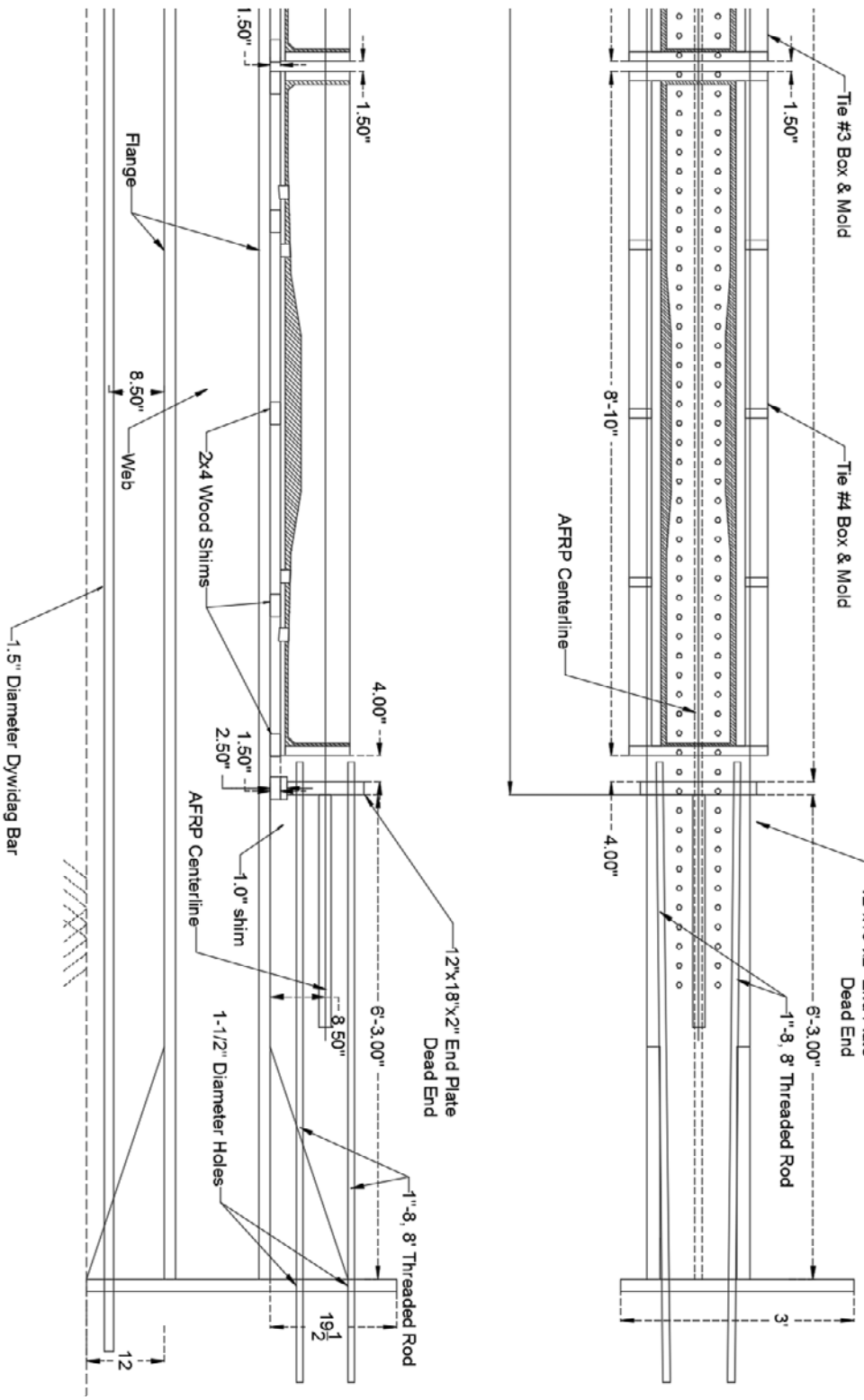

Figure 73: Section C

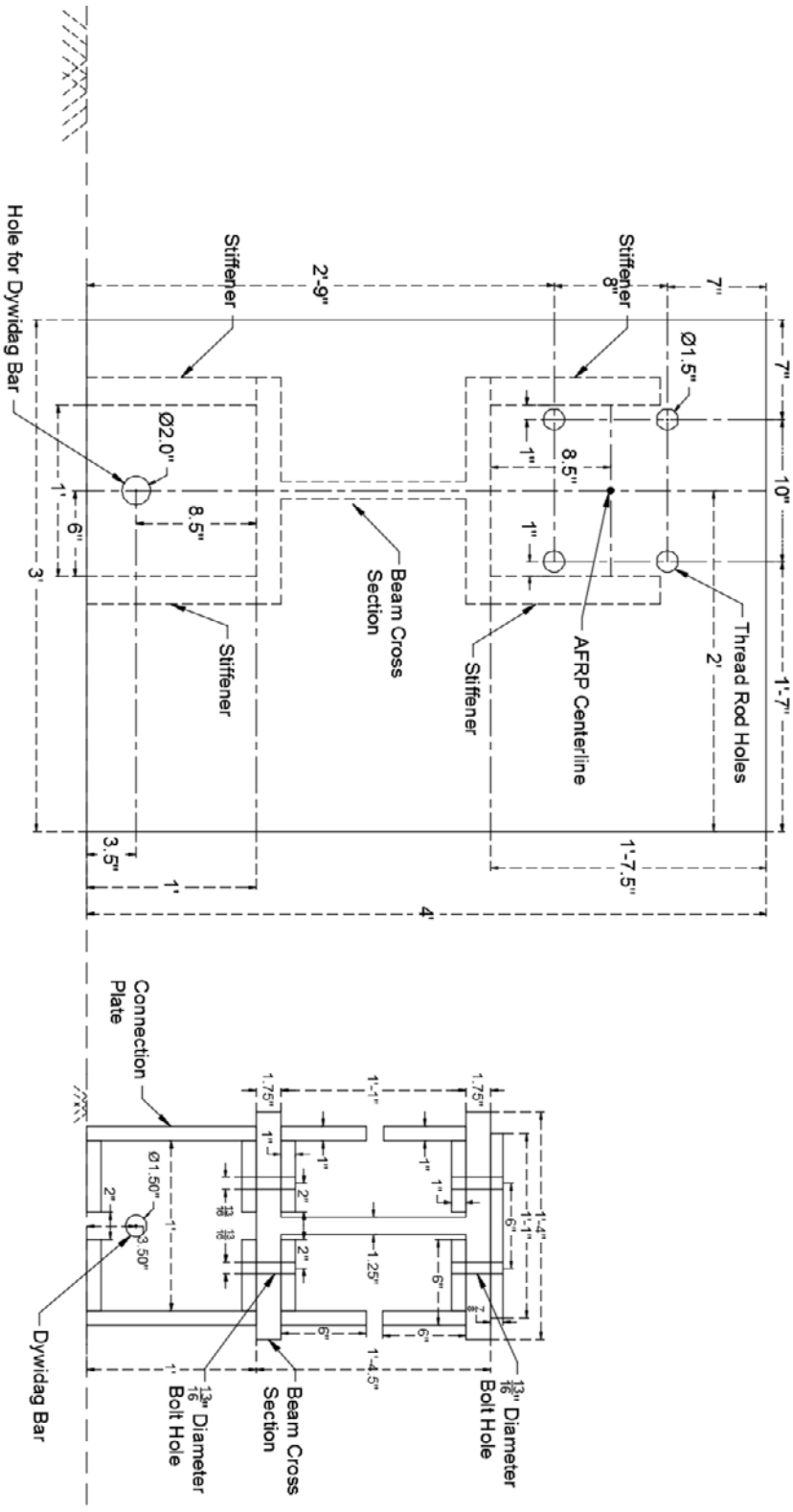

Figure 74: Cross section of frame at end and connection

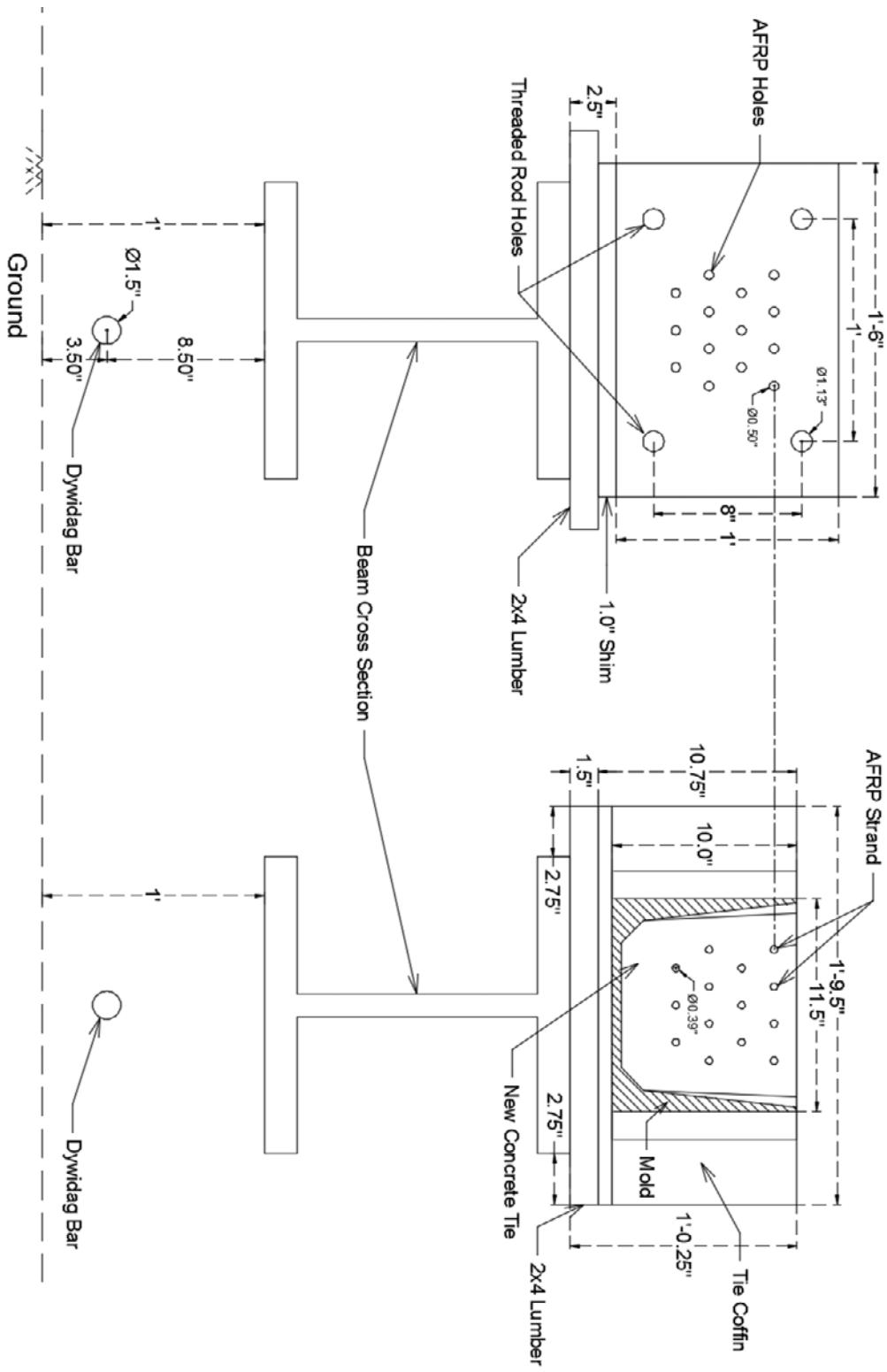

Figure 75: Cross section of frame and end plate and mold sections

APPENDIX D: PROCEQ RESISTIVITY METER READINGS

This appendix provides a comprehensive set of tables and charts documenting the data collected by the Proceq Resipod Resistivity Meter for both AFRP and STEEL concrete railroad ties. Longitudinal and transverse measurements switch between points 17 and 18 respectively. The location points are based on Figure 48 where longitudinal refers to measurements taken in parallel to the reinforcement while transverse refers to perpendicular to reinforcement. Due to the width of the tie, three longitudinal measurements were taken at each major section of the tie: 2 at the edges and 1 at the center. The transverse measurements were taken such that the center of the meter was along the centerline of the tie. Charts presented in this appendix map the data points in total then separate longitudinal and transverse charts are presented to provide a closer look at the effect of that specific orientation for the AFRP reinforced ties.

D.1 AFRP1

Table 19: Resistivity of AFRP1

Location	Resistivity (kΩcm)			
	8/23/2015	9/1/2015	9/9/2015	9/14/2015
1	14.3	22.8	23.5	29.8
2	14.9	18.8	19.4	19.7
3	13.6	26.3	27.4	33
4	12.6	16.7	20.2	19.4
5	19.0	27.9	30.4	32.2
6	15.9	18.6	20.9	24
7	19.8	27.5	24.1	33.5
8	17.6	27.5	32.1	38.3
9	13.6	20.9	21.6	23.9
10	20.5	26.4	32.7	37.2
11	20.0	29.2	33.1	34
12	13.2	19.3	22.2	23.3
13	19.8	27.1	31.1	36.4
14	12.7	13.5	16.2	20
15	18.9	19.0	27.1	30.4
16	14.2	16.0	22.8	23.7
17	20.2	27.8	30.4	33.1

Table 20 Continued: Resistivity of AFRP1

Location	Resistivity (kΩcm)			
	8/23/2015	9/1/2015	9/9/2015	9/14/2015
18	14.3	21.3	24.5	32.1
19	13.8	18.6	16.4	22.5
20	13.0	15.7	13.7	12.7
21	12.7	16.3	21.3	21.3
22	14.5	19.4	22.4	23.3
23	13.6	19.4	22.5	24.7
24	17.7	21.1	23.1	26.3
25	13.6	19.3	21.8	26.1
26	15.4	17.3	21.9	20.5
27	13.0	15.8	16.8	19.2
28	11.7	17.7	21.9	13.9
29	11.8	17.4	19.6	21.2
30	12.3	20.9	27.8	28
Average	15.3	20.9	23.6	26.1
Std Dev	2.826	4.429	5.055	6.643

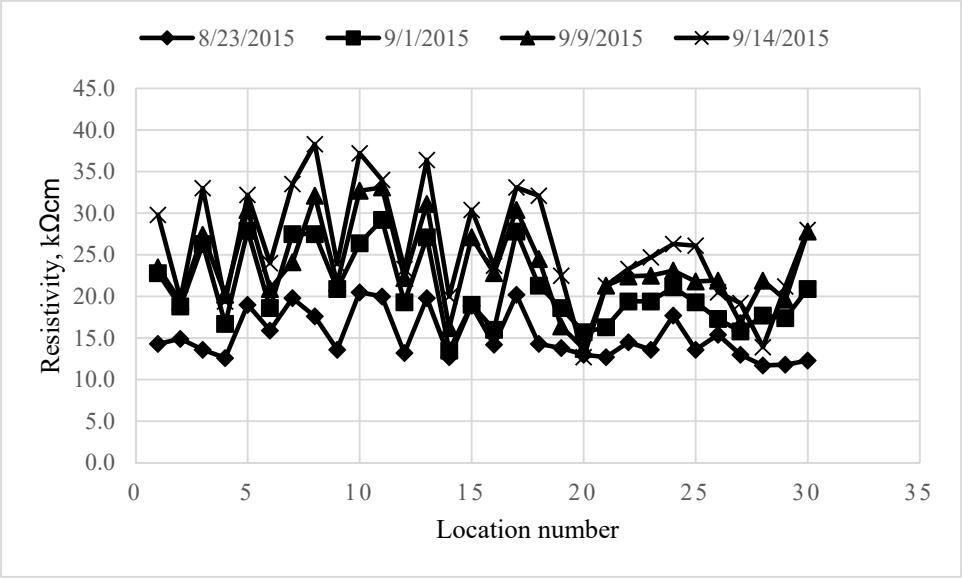

Figure 76: Overall plot of resistivity points of AFRP1

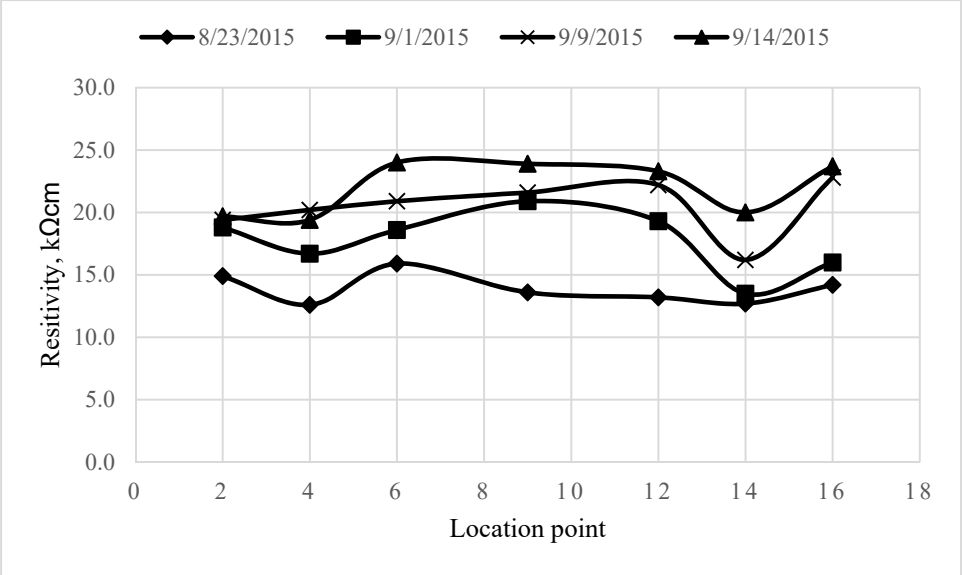

Figure 77: Center points in the longitudinal direction, AFRP1

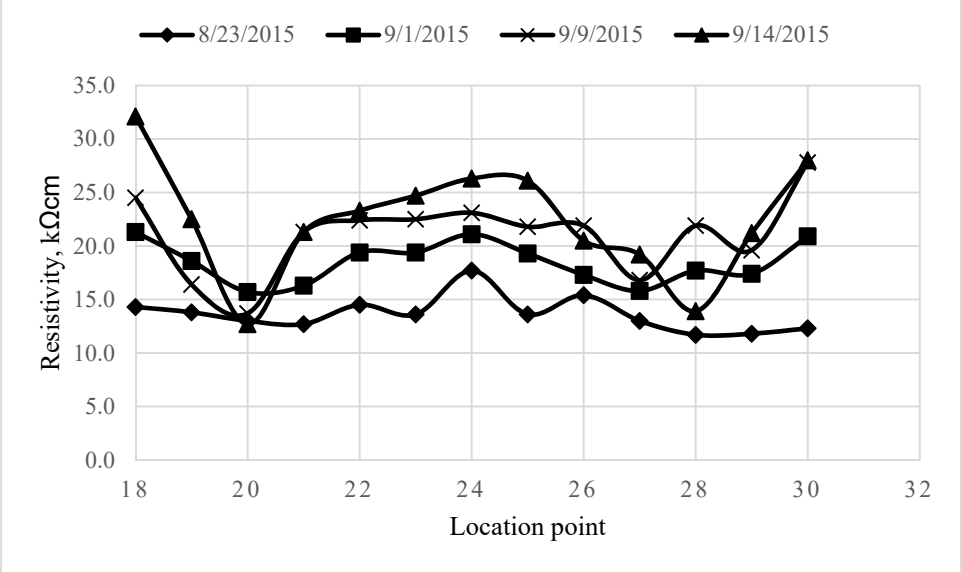

Figure 78: Transverse resistivity points, AFRP1

D.2 AFRP2

Table 21: Resistivity points for AFRP2

Location	Resistivity (kΩcm)			
	8/23/2015	9/1/2015	9/8/2015	9/14/2015
1	15	18.9	25.8	30.5
2	13.6	16.2	19.2	21.2
3	16.1	15.9	25	28.7
4	12.3	15.3	17.6	21
5	22.5	25	28.8	20.6
6	14.7	19	18.5	25.1
7	17.8	24.9	25.8	33.1
8	17.1	29.6	29.5	30.4
9	15.6	16.8	19.9	24.4
10	19.2	25.8	28.5	36.1
11	20.5	24.1	32.7	33
12	14.8	17.7	20.2	22.9
13	19.7	25.8	31.5	34.6
14	11.8	15.7	19.7	19.8
15	16	25.4	31.2	33.6
16	13.4	18	23.2	24.4
17	20.9	28.5	32.9	30.4
18	17.3	23.2	22.2	28.2
19	14	16.5	19.4	22.5
20	13.6	14.5	14.7	16.6
21	14.7	15.9	17.8	19.6
22	16.1	20.9	24.6	23.6
23	16.3	18.6	20.4	22.5
24	14.3	19.2	21.2	25.1
25	15.2	18.9	19.6	21.7
26	15.4	19.1	21.3	24.2
27	14.3	15.6	18.6	20.9
28	11.4	16.3	17.8	21.7
29	14.5	14.4	16.7	18.2
30	15.7	26.2	25.2	28.6
Average	15.79	20.06	22.98	25.44
Std Dev	2.616	4.464	5.090	5.229

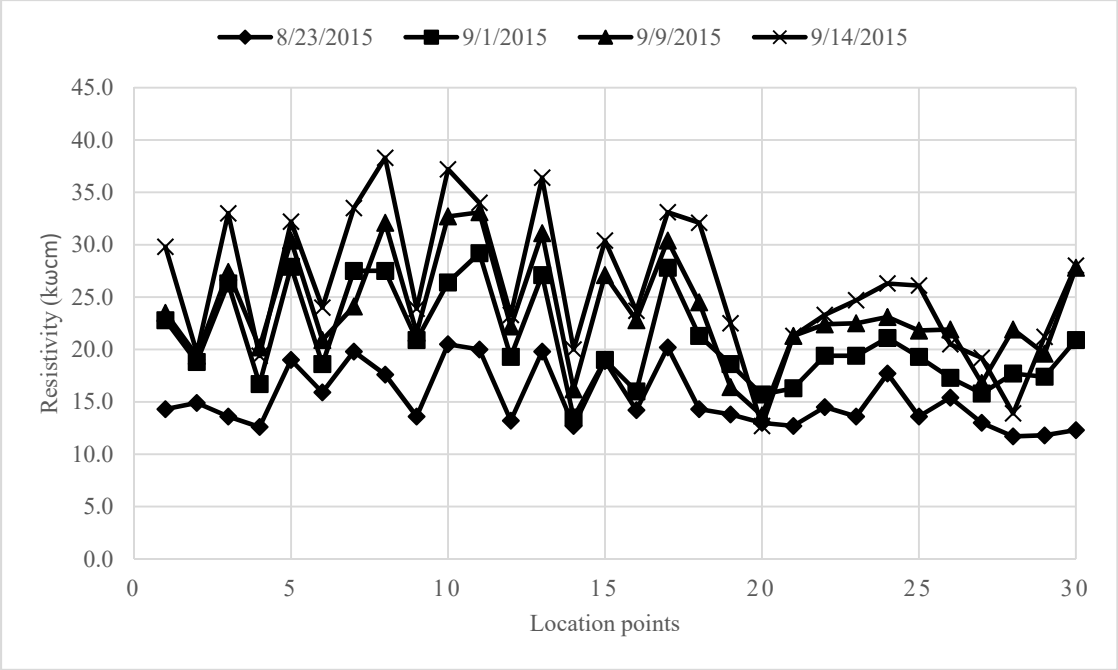

Figure 79: Resistivity plot points for AFRP2

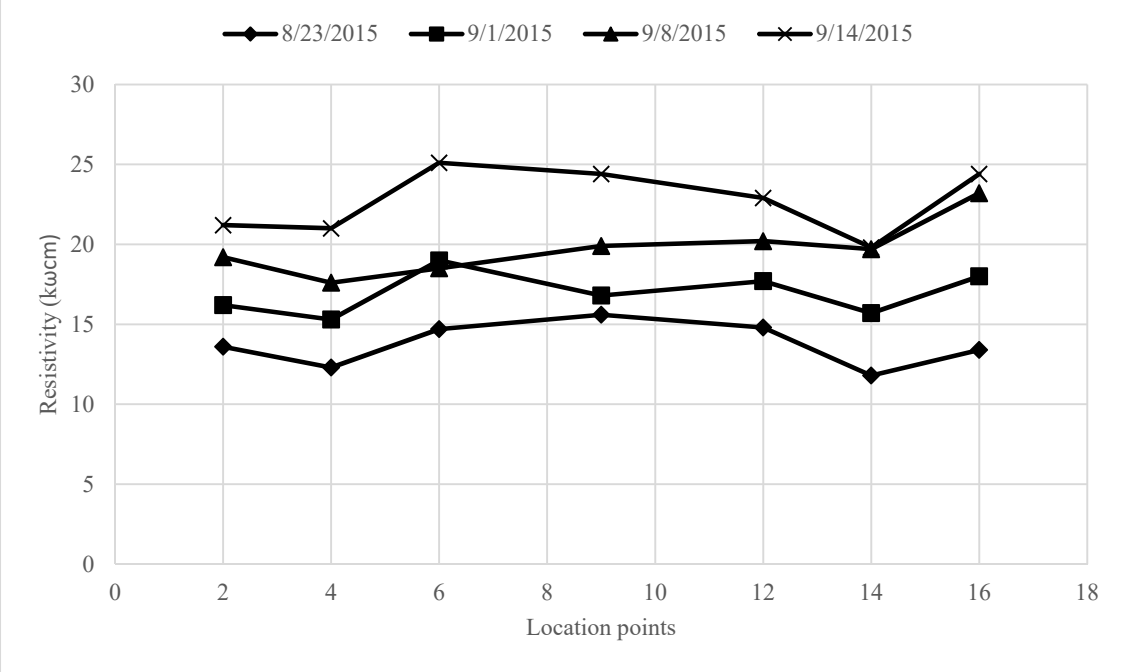

Figure 80: Center points in longitudinal direction, AFRP2

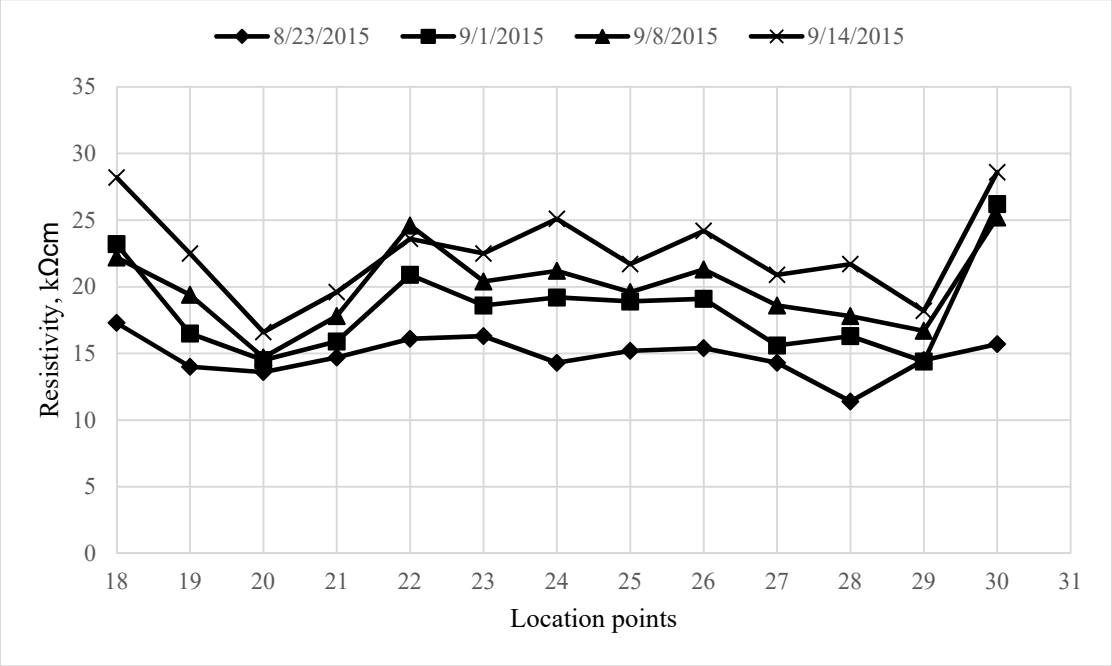

Figure 81: Transverse resistivity points, AFRP2

D.3 AFRP3

Table 22: Resistivity points for AFRP3

Location	Resistivity (kΩcm)			
	8/23/2015	9/1/2015	9/8/2015	9/14/2015
1	18.6	21.4	27.1	32
2	10.5	16.8	21.8	22.9
3	18.6	25.2	25.9	29.8
4	14.8	15.8	17.1	20.7
5	19.9	22.8	26.8	39.2
6	14.5	18	19.6	21.7
7	21.9	26	29.4	31.1
8	22.3	22.9	27.4	31.3
9	16.6	19.9	22.7	22.8
10	19.2	28.9	26.5	36.9
11	24.1	24.9	31.1	36.4
12	15.6	19.9	19.4	27.8

Table 23 Continued: Resistivity points for AFRP3

Location	Resistivity (kΩcm)			
	8/23/2015	9/1/2015	9/8/2015	9/14/2015
13	22.7	25.1	29.3	29
14	13	16.6	15	22.2
15	15.9	22.9	28.2	36.8
16	13.9	14.7	18.5	22.9
17	18.6	21.2	27.9	36.7
18	17.2	19.9	19.9	27.1
19	13.3	16.6	22.4	21.9
20	12	10.9	14.3	12.3
21	13.9	17.4	17.4	21.3
22	17.3	19.9	22.4	25.7
23	14.7	22.2	22.5	23.4
24	16.8	17.2	21.5	22.5
25	16.9	17.7	20.2	22.3
26	13.8	17.3	21.6	21.2
27	11.9	17	20.5	21.5
28	11.5	11.7	14.4	13.2
29	15.3	18	17.8	18.6
30	20.9	20.2	21.2	25.5
Average	16.54	19.63	22.33	25.89
Std Dev	3.513	4.067	4.620	6.738

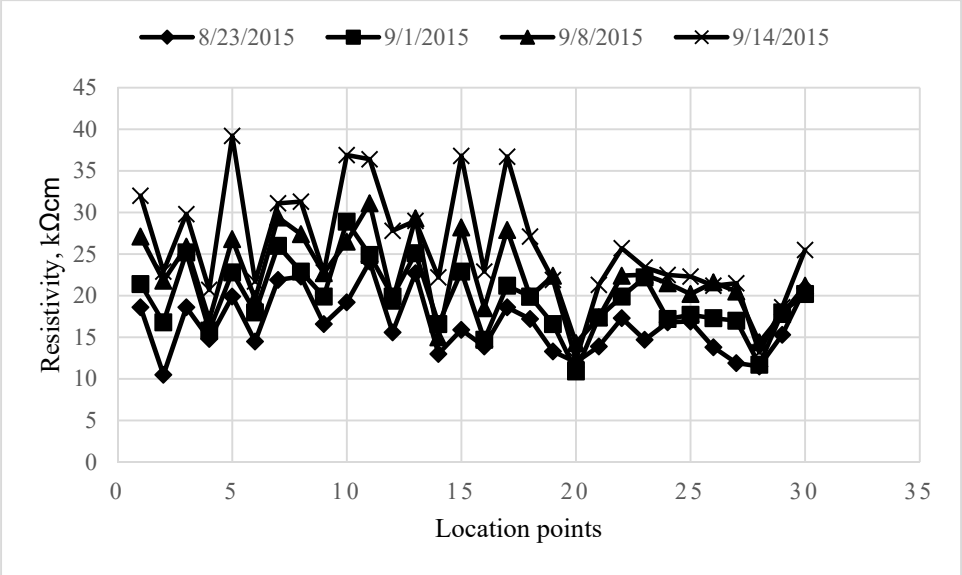

Figure 82: Overall plot of resistivity points for AFRP3

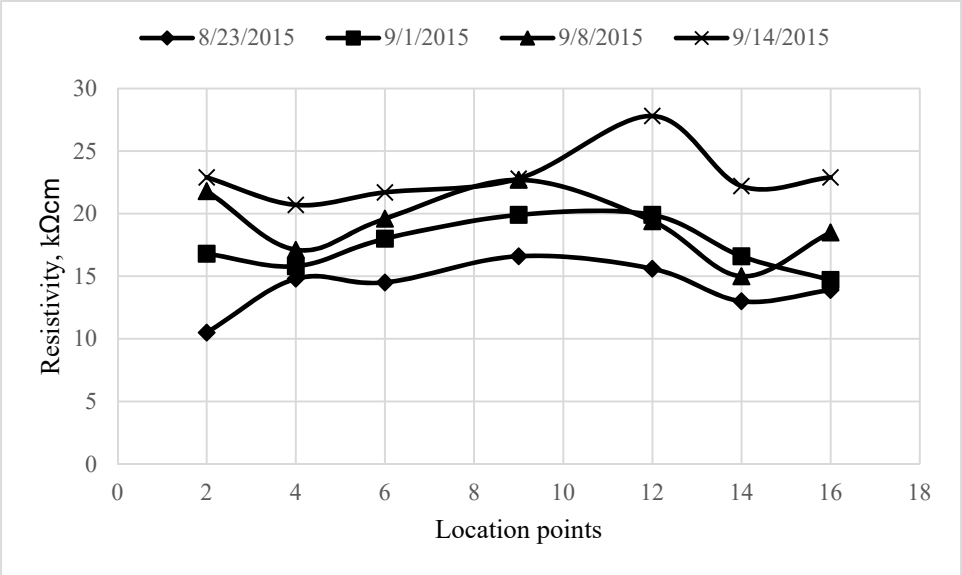

Figure 83: Resistivity points for center section in longitudinal direction, AFRP3

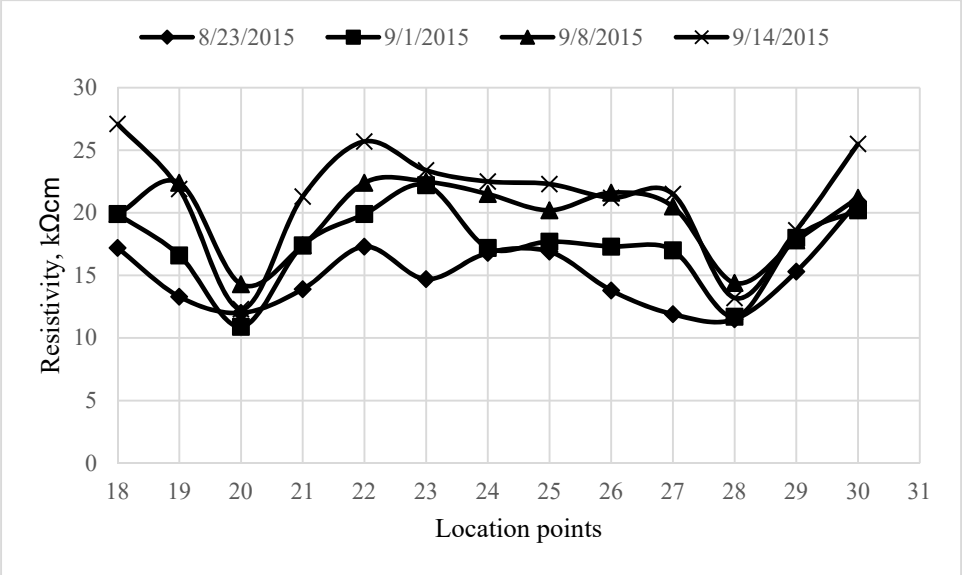

Figure 84: Transverse resistivity points, AFRP3

D.4 AFRP4

Table 24: Resistivity points for AFRP4

Location	Resistivity (kΩcm)			
	8/23/2015	9/1/2015	9/8/2015	9/14/2015
1	18.2	24.5	26.6	29.7
2	13.3	14.5	16.2	21.6
3	20.1	22.2	24.5	24.7
4	12	18.6	17.7	19.8
5	16.1	30.8	24.5	27.6
6	14.7	16.3	21.2	24.1
7	16.1	22.1	28.6	26.2
8	21.3	25.9	28.4	38.3
9	15.8	18.7	22.9	20.5
10	19	26.2	29.6	39.7
11	17.9	26.5	34.5	35.3
12	15	16.4	20.9	20.3
13	22.5	20.3	31.5	38.5
14	12	14.9	15.6	21.4
15	9.2	14.7	14.7	58.4
16	5.4	26.1	32.3	36.3

Table 25 Continued: Resistivity points for AFRP4

Location	Resistivity (kΩcm)			
	8/23/2015	9/1/2015	9/8/2015	9/14/2015
17	9.2	25.4	65.9	54.8
18	194.3	271	336	401
19	177.5	229	303	356
20	20.5	22.3	28	28.2
21	29.8	46.1	55.8	54.2
22	12.5	16.4	19.2	23.2
23	13	22.6	18.3	20.2
24	15.3	20.5	21.3	25.7
25	19	26.5	28.7	28.7
26	16	17.8	22.2	22.3
27	12.7	17.8	21	22
28	13.2	15.2	17.6	22.5
29	13.8	19.4	16.3	19.1
30	12.6	16.5	19.9	21.1
31	17.9	18.2	19.6	21.9
Average	26.64	36.24	44.60	51.72
Std Dev	42.119	56.724	73.098	86.645

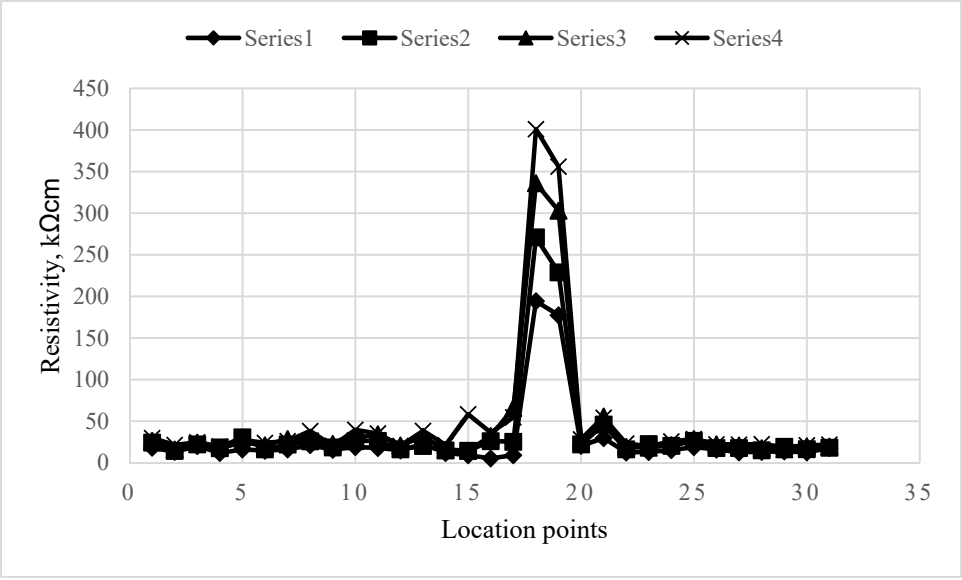

Figure 85: Overall plot of resistivity points for AFRP4

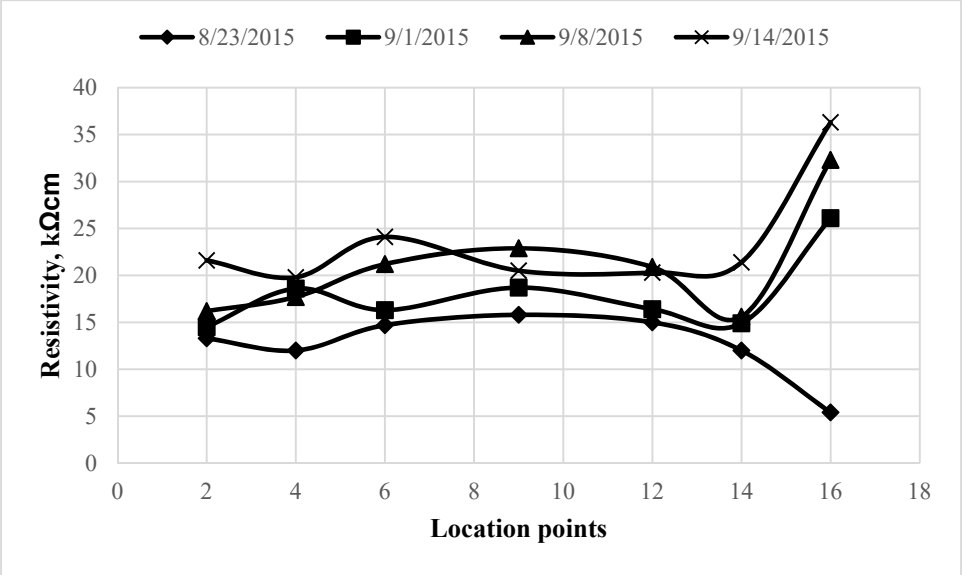

Figure 86: Resistivity points for center section in longitudinal direction, AFRP4

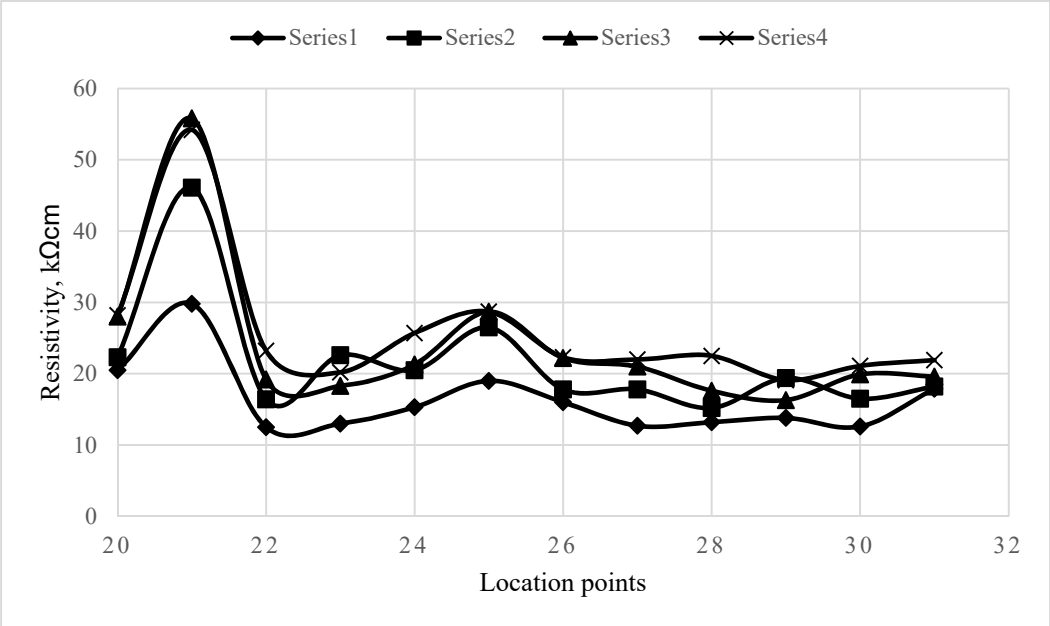

Figure 87: Transverse resistivity points, AFRP4

D.5 STEEL1

Table 26: Resistivity points for Steel1

Location	Resistivity (kΩcm)			
	9/1/2015	9/9/2015	9/10/2015	9/14/2015
1	670	641	659	797
2	424	365	412	387
3	404	626	633	854
4	393	365	342	395
5	607	599	723	717
6	403	353	350	356
7	630	640	616	697
8	620	585	595	675
9	340	279	208	312
10	871	765	696	832
11	515	532	521	552
12	381	380	356	364
13	639	611	617	742
14	398	375	363	422
15	610	584	697	623
16	375	374	384	385
17	677	690	679	749
18	602	669	591	675
19	402	422	378	402
20	486	405	410	437
21	419	488	391	374
22	431	395	396	457
23	408	435	430	404
24	407	389	392	373
25	399	428	366	376
26	402	418	408	458
27	436	457	401	426
28	444	367	326	450
29	428	425	413	373
30	484	674	631	805
Average	490.2	491.2	479.5	529.0
Std Dev	122.76	127.58	139.18	172.50

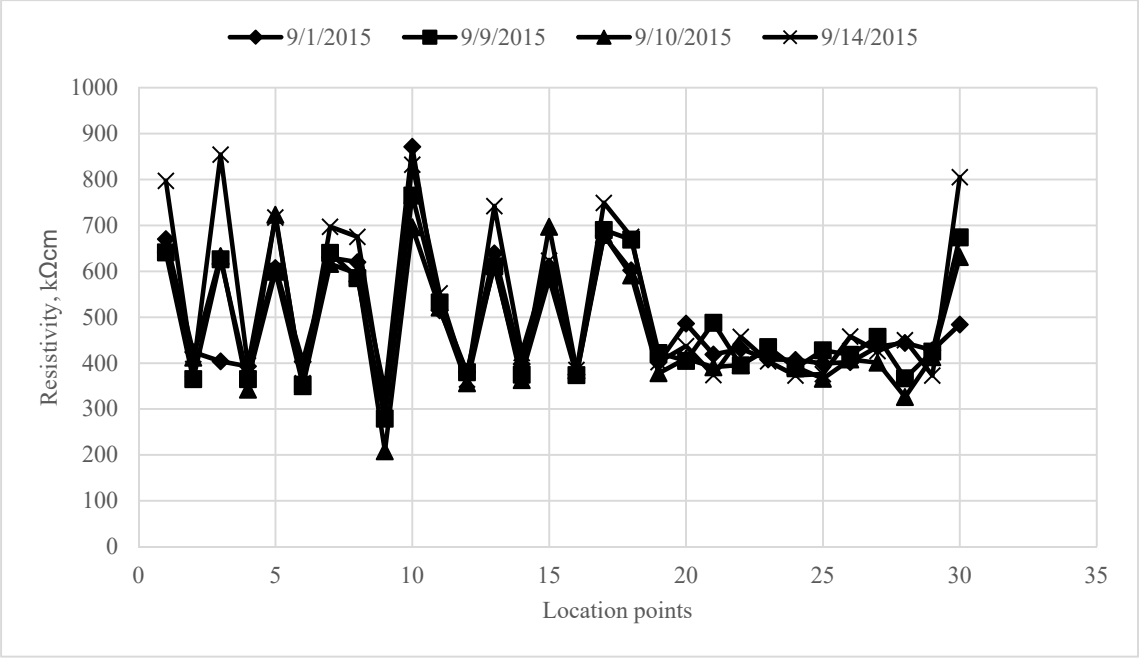

Figure 88: Overall plot of resistivity points for Steel1

D.6 STEEL2

Table 27: Resistivity points for Steel2

Location	Resistivity (kΩcm)			
	9/1/2015	9/9/2015	9/10/2015	9/14/2015
1	636	754	634	834
2	381	365	333	349
3	712	673	530	721
4	390	352	322	445
5	585	607	589	561
6	345	330	258	289
7	622	747	739	765
8	668	741	612	553
9	337	326	290	310
10	698	567	697	651
11	713	775	657	696
12	393	360	324	324
13	648	610	677	663
14	420	414	350	311

Table 28 Continued: Resistivity points for Steel2

Location	Resistivity (kΩcm)			
	9/1/2015	9/9/2015	9/10/2015	9/14/2015
15	625	631	594	567
16	378	364	318	331
17	634	559	654	691
18	508	531	510	465
19	430	406	341	310
20	427	401	329	418
21	405	477	378	378
22	416	426	358	416
23	420	361	326	369
24	407	369	341	367
25	379	402	288	360
26	356	397	326	339
27	427	405	364	393
28	394	368	308	385
29	417	396	380	389
30	530	691	637	597
Average	490.0	493.5	448.8	474.9
Std Dev	124.04	145.76	153.07	157.21

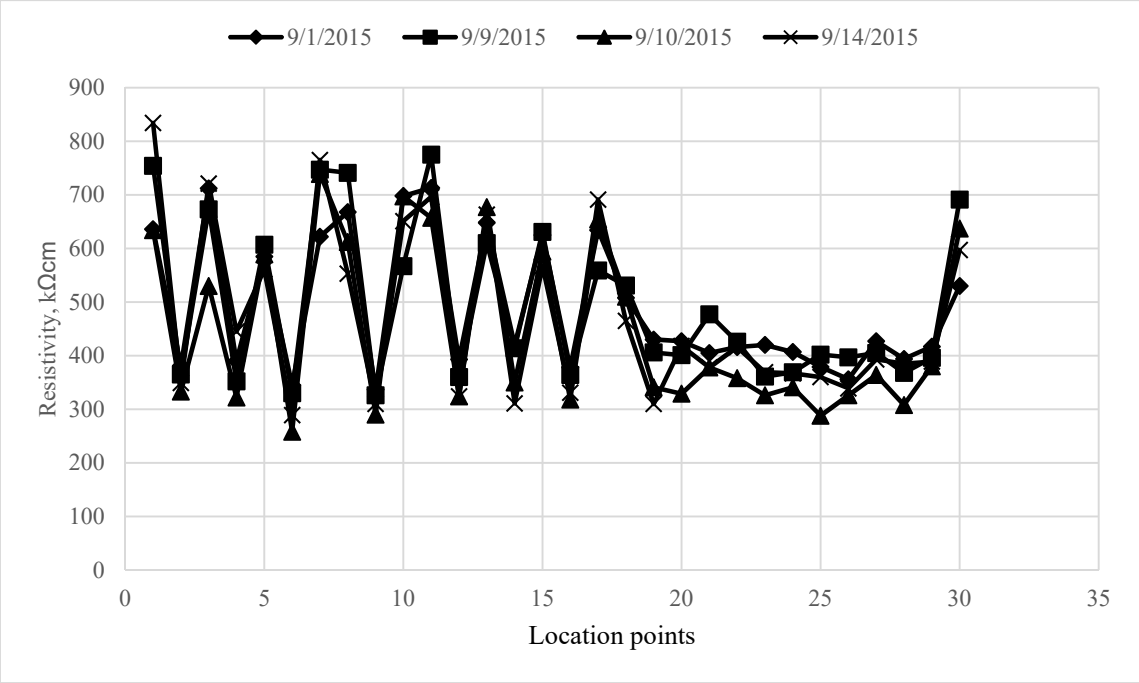

Figure 89: Overall plot of resistivity points for Steel2:

D.7 STEEL3

Table 29: Resistivity points for Steel3

Location	Resistivity (kΩcm)	
	9/1/2015	9/14/2015
1	628	723
2	348	406
3	660	738
4	396	366
5	600	658
6	311	375
7	620	768
8	589	632
9	331	329
10	678	983
11	595	713
12	370	357
13	615	757
14	313	323

Table 30 Continued: Resistivity points for Steel3

Location	Resistivity (kΩcm)	
	9/1/2015	9/14/2015
15	316	727
16	393	394
17	690	585
18	438	825
19	307	378
20	377	372
21	359	338
22	316	365
23	299	415
24	311	435
25	292	362
26	268	357
27	338	416
28	214	420
29	347	389
30	439	614
Average	425.3	517.3
Std Dev	142.65	184.46

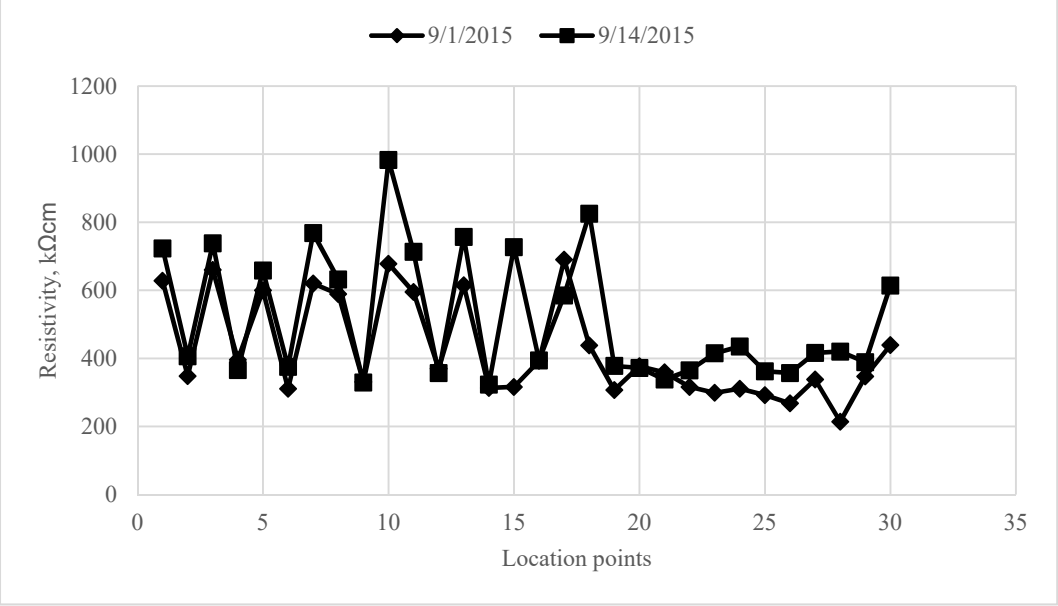

Figure 90: Overall plot of resistivity points for Steel3

D.8 STEEL4

Table 31: Resistivity points for Steel4

Location	Resistivity (kΩcm)	
	9/1/2015	9/14/2015
1	588	587
2	362	300
3	710	580
4	301	362
5	467	573
6	329	347
7	505	701
8	638	772
9	323	322
10	486	611
11	577	644
12	352	359
13	554	563
14	326	317
15	564	652
16	370	361
17	539	619
18	444	446
19	358	401
20	244	397
21	368	378
22	368	351
23	380	353
24	339	325
25	344	368
26	376	382
27	369	353
28	314	386
29	338	341
30	506	544
Average	424.6	456.5
Std Dev	113.48	134.64

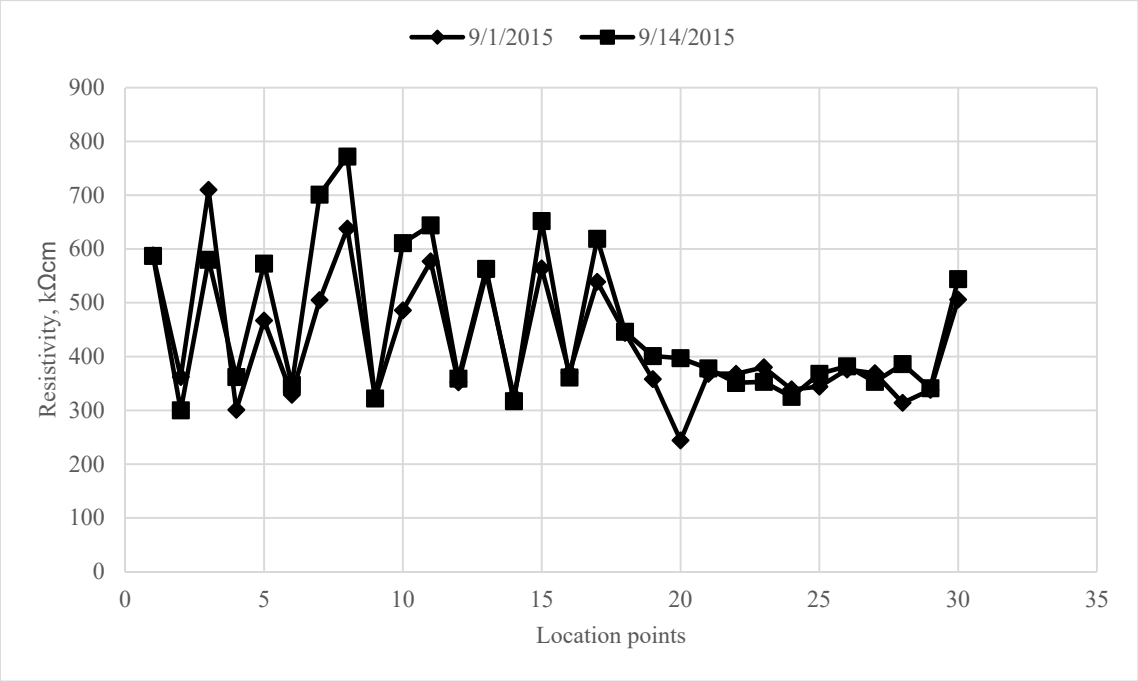

Figure 91: Overall plot of resistivity points for Steel4